

## **INFORMATION TO USERS**

This manuscript has been reproduced from the microfilm master. UMI films the text directly from the original or copy submitted. Thus, some thesis and dissertation copies are in typewriter face, while others may be from any type of computer printer.

**The quality of this reproduction is dependent upon the quality of the copy submitted.** Broken or indistinct print, colored or poor quality illustrations and photographs, print bleedthrough, substandard margins, and improper alignment can adversely affect reproduction.

In the unlikely event that the author did not send UMI a complete manuscript and there are missing pages, these will be noted. Also, if unauthorized copyright material had to be removed, a note will indicate the deletion.

Oversize materials (e.g., maps, drawings, charts) are reproduced by sectioning the original, beginning at the upper left-hand corner and continuing from left to right in equal sections with small overlaps.

Photographs included in the original manuscript have been reproduced xerographically in this copy. Higher quality 6" x 9" black and white photographic prints are available for any photographs or illustrations appearing in this copy for an additional charge. Contact UMI directly to order.

**Bell & Howell Information and Learning  
300 North Zeeb Road, Ann Arbor, MI 48106-1346 USA  
800-521-0600**

**UMI<sup>®</sup>**



**University of Alberta**

**Experimental Determination of Relative Outputs of Sr-90 Ophthalmic  
Applicators and the Anisotropy Function of the Model 6711 I-125 Seed**

by

**Geetha Vijayan Menon**



**A thesis submitted to the Faculty of Graduate Studies and Research in partial  
fulfillment of the requirements for the degree of Master of Science**

in

**Medical Physics**

**Department of Physics**

**Edmonton, Alberta**

**Fall 1999**



**National Library  
of Canada**

**Acquisitions and  
Bibliographic Services**

**395 Wellington Street  
Ottawa ON K1A 0N4  
Canada**

**Bibliothèque nationale  
du Canada**

**Acquisitions et  
services bibliographiques**

**395, rue Wellington  
Ottawa ON K1A 0N4  
Canada**

*Your file Votre référence*

*Our file Notre référence*

**The author has granted a non-exclusive licence allowing the National Library of Canada to reproduce, loan, distribute or sell copies of this thesis in microform, paper or electronic formats.**

**The author retains ownership of the copyright in this thesis. Neither the thesis nor substantial extracts from it may be printed or otherwise reproduced without the author's permission.**

**L'auteur a accordé une licence non exclusive permettant à la Bibliothèque nationale du Canada de reproduire, prêter, distribuer ou vendre des copies de cette thèse sous la forme de microfiche/film, de reproduction sur papier ou sur format électronique.**

**L'auteur conserve la propriété du droit d'auteur qui protège cette thèse. Ni la thèse ni des extraits substantiels de celle-ci ne doivent être imprimés ou autrement reproduits sans son autorisation.**

**0-612-47069-5**

**University of Alberta**

**Library Release Form**

**Name of Author:** Geetha Vijayan Menon

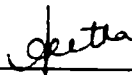
**Title of Thesis:** Experimental Determination of Relative Outputs of Sr-90  
Ophthalmic Applicators and the Anisotropy Function of the  
Model 6711 I-125 Seed

**Degree:** Master of Science

**Year this Degree Granted:** 1999

Permission is hereby granted to the University of Alberta Library to reproduce single copies of this thesis and to lend or sell such copies for private, scholarly, or scientific research purposes only.

The author reserves all other publication and other rights in association with the copyright in the thesis, and except as hereinbefore provided, neither the thesis nor any substantial portion thereof may be printed or otherwise reproduced in any material form whatever without the author's written permission.

  
\_\_\_\_\_


#202K, 5723-112 Street  
Edmonton, Alberta  
T6H 3J4

30 Aug 1999

**University of Alberta**

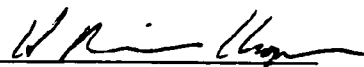
**Faculty of Graduate Studies and Research**

The undersigned certify that they have read, and recommended to the Faculty of Graduate Studies and Research for acceptance, a thesis entitled **Experimental Determination of Relative Outputs of Sr-90 Ophthalmic Applicators and the Anisotropy Function of the Model 6711 I-125 Seed** submitted by **Geetha Vijayan Menon** in partial fulfillment of the requirements for the degree of **Master of Science in Medical Physics**.

  
Dr. R. Sloboda

  
Dr. G. Greeniaus

  
Dr. A. Murtha

  
Dr. R. Hooper

  
29 July 1999

*to*  
*my parents*

## **Abstract**

One of the oldest treatment modalities in radiotherapy, brachytherapy, has recently benefited from more accurate dosimetry protocols to aid in precise treatment planning. The main purpose of this thesis is to study the dosimetry of two brachytherapy sources: Sr-90 in ophthalmic applicators and I-125 in seed form for interstitial implants. For Sr-90, particular attention was paid to using a combination of radiochromic films and a document scanner to record the relative surface dose rates from ophthalmic applicators. For the model 6711 I-125 seed, the dose rate around the source was measured using LiF TLD detectors to examine the anisotropy in the dose distribution for varying angles and at different radial distances up to 10 cm. The latter experiments were conducted using two different techniques: one incorporating a pre-read anneal and the other based on glow curve analysis. The results were compared to published Monte Carlo calculations and AAPM Task Group 43 recommended values.



## **Acknowledgements**

First, I would like to acknowledge my profound indebtedness to my supervisor, Dr. Ron Sloboda for having been a continuous source of inspiration guiding me through the project with his ingenious ideas and suggestions without which this work could never be accomplished.

I would like to thank the members of the examining committee for their valued comments for the improvement of the thesis.

Though numerous to mention by name, each and everyone in the Medical Physics Department and the Machine Shop at the Cross Cancer Institute have my special thanks for all the help they have lent me on many occasions in their own special way.

My family, to whom I am deeply indebted, deserves my appreciation and gratitude for their support and encouragement throughout the tenure of my study.

# Table of Contents

<b>CHAPTER 1 .....</b>	<b>1</b>
<b>1 INTRODUCTION .....</b>	<b>1</b>
<b>1.1 Cancer and Its Management.....</b>	<b>1</b>
<b>1.2 Radiation Therapy.....</b>	<b>2</b>
1.2.1 External Beam Therapy.....	3
1.2.2 Sealed Source Therapy (Brachytherapy) .....	4
1.2.3 Unsealed Source Therapy.....	4
<b>1.3 Brachytherapy.....</b>	<b>4</b>
1.3.1 Types of Brachytherapy.....	6
1.3.1.1 Surface Mould Applications.....	6
1.3.1.2 Interstitial Implants .....	6
1.3.1.3 Intracavitary Insertions .....	7
1.3.2 Characteristics of Brachytherapy Radionuclides .....	7
1.3.3 Physical Forms of Brachytherapy Sources.....	11
1.3.3.1 Tubes .....	11
1.3.3.2 Needles .....	11
1.3.3.3 Seeds.....	13
1.3.3.4 Fluids.....	13
1.3.3.5 Wires .....	13
1.3.3.6 Ophthalmic Applicators .....	14
<b>1.4 Brachytherapy Dosimetry .....</b>	<b>14</b>
1.4.1 General Considerations.....	15
1.4.2 Measurement of Absorbed Dose.....	17
1.4.2.1 Calorimetric Dosimetry .....	17
1.4.2.2 Photographic Dosimetry .....	17

1.4.2.3 Chemical Dosimetry .....	18
1.4.2.4 Scintillation Dosimetry .....	18
1.4.2.5 Thermoluminescent Dosimetry.....	18
<b>1.5 Phantoms .....</b>	<b>19</b>
<b>1.6 Research Objectives.....</b>	<b>20</b>
1.6.1 Relative Output of Sr-90 Applicators .....	21
1.6.2 Anisotropy of Model 6711 I-125 Seeds .....	22
<b>1.7 Thesis Overview.....</b>	<b>25</b>
References .....	26
<b>CHAPTER 2.....</b>	<b>28</b>
<b>2. BRACHYTHERAPY DOSIMETRY .....</b>	<b>28</b>
<b>2.1 Dose Specification .....</b>	<b>28</b>
2.1.1 TG-43 Formalism .....	30
2.1.1.1 Reference Point for Dose Calculations .....	30
2.1.1.2 Air Kerma Strength ( $S_k$ ).....	31
2.1.1.3 Dose Rate Constant, $\Lambda(r,\theta)$ .....	34
2.1.1.4 Geometry Factor, $G(r,\theta)$ .....	35
2.1.1.5 Radial Dose Function, $g(r)$ .....	36
2.1.1.6 Anisotropy Function, $F(r,\theta)$ .....	37
2.1.2 Dose Rate for Two Dimensional Cases.....	38
<b>2.2 Thermoluminescent Dosimetry.....</b>	<b>39</b>
2.2.1 Principle of Thermoluminescent Dosimetry .....	39
2.2.2 Mechanism of Thermoluminescence .....	40
2.2.3 Thermoluminescent Phosphors.....	42
2.2.3.1 Powder Dosimeters .....	43
2.2.3.2 Extruded and Hot Pressed Dosimeters .....	43
2.2.3.3 PTFE Based Dosimeters.....	44
2.2.3.4 Silicone-embedded Dosimeters .....	44
2.2.3.5 Sintered Dosimeters.....	44
2.2.4 Characteristics of TLD Phosphors.....	46

2.2.4.1 Sensitivity .....	46
2.2.4.2 Absorbed Dose Response .....	47
2.2.4.3 Relative Energy Response .....	50
2.2.4.4 Fading .....	51
2.2.4.5 Stability .....	52
2.2.4.6 Annealing .....	52
2.2.4.7 Glow Curve .....	53
2.2.4.8 Background Signals .....	56
2.2.5 TLD Instrumentation .....	57
2.2.6 Applications of TLDs .....	61
<b>2.3 Radiochromic Film Dosimetry .....</b>	<b>63</b>
2.3.1 Principle of Radiochromic Films .....	63
2.3.2 The GafChromic Film .....	64
<b>2.4 I-125 Seed Dosimetry .....</b>	<b>68</b>
2.4.1 Description of I-125 Seeds .....	68
2.4.2 Model 6711 I-125 Seed .....	69
<b>2.5 Ophthalmological Applicators .....</b>	<b>72</b>
2.5.1 Usage .....	72
2.5.2 Sr-90 Eye Applicator .....	72
<b>References .....</b>	<b>78</b>
<b>CHAPTER 3 .....</b>	<b>81</b>
<b>3 MATERIALS AND METHODS .....</b>	<b>81</b>
<b>3.1 Sr-90 Ophthalmic Applicator Dosimetry .....</b>	<b>81</b>
3.1.1 SIA 20 Ophthalmic Applicator .....	82
3.1.2 GafChromic Film .....	83
3.1.3 Dosimetry System Performance .....	84
3.1.3.1 Best Operating Settings .....	85
3.1.3.2 Film side dependence .....	85
3.1.3.3 Temporal Stability of scanner .....	85
3.1.3.4 Spatial Stability of Scanner .....	86

3.1.4	Applicator Dosimetry .....	87
3.1.4.1	Dose Response Curve .....	87
3.1.4.2	Relative Surface Dose Rates .....	88
<b>3.2</b>	<b><i>I-125 Seed Dosimetry</i></b> .....	<b>93</b>
3.2.1	Model 6711 Seed Description .....	93
3.2.2	TLD System Description .....	94
3.2.3	Phantom Description .....	95
3.2.4	Dosimetry System Performance .....	98
3.2.4.1	Pre-read anneal Method .....	98
3.2.4.2	Glow-Curve Deconvolution Method .....	100
3.2.4.3	Sensitization .....	101
3.2.4.4	Linearity .....	102
3.2.5	I-125 Seed Anisotropy .....	104
	<b>References</b> .....	<b>106</b>
<b>CHAPTER 4</b>	<b>.....</b>	<b>107</b>
<b>4</b>	<b>EXPERIMENTAL RESULTS</b> .....	<b>107</b>
<b>4.1</b>	<b><i>Radiochromic Film Calibration</i></b> .....	<b>108</b>
4.1.1	Dose Response Curve .....	110
4.1.1.1	Horizontal calibration .....	110
4.1.1.2	Vertical calibration .....	117
4.1.1.3	Central axis depth dose of SIA 20 .....	117
<b>4.2</b>	<b><i>Relative output of Sr-90 applicators</i></b> .....	<b>121</b>
4.2.1	Measurements using radiochromic films .....	121
4.2.2	Measurements using thermoluminescent dosimeters .....	123
<b>4.3</b>	<b><i>I-125 Model 6711 Seed Dosimetry</i></b> .....	<b>124</b>
4.3.1	ECC Determination .....	124
4.3.2	Dose Response .....	129
4.3.3	I-125 model 6711 seed anisotropy .....	132
4.3.3.1	Pre-read anneal technique .....	132
4.3.3.2	Glow Curve Deconvolution Technique .....	141

References .....	149
<b>CHAPTER 5 .....</b>	<b>150</b>
5 SUMMARY .....	150
References .....	156

## List of Tables

Table 1.1	Physical characteristics of brachytherapy sources .....	9
Table 1.2	List of ophthalmic applicators.....	21
Table 2.1	Characteristics of TL phosphors.....	45
Table 4.1	Temporal variations in optical density of film.....	109
Table 4.2a	Relative dose rates from radiochromic films (20 Gy).....	122
Table 4.2b	Relative dose rates from radiochromic films (45 Gy).....	122
Table 4.3	Relative dose rates with TLDs.....	123
Table 4.4	ECC of chips using pre-read anneal method.....	125
Table 4.5	ECC of cubes using pre-read anneal method .....	126
Table 4.6	ECC of chips using glow curve deconvolution method.....	127
Table 4.7	ECC of cubes using glow curve deconvolution method.....	128
Table 4.8	Geometry factor for line source .....	133
Table 4.9	Anisotropy function values (pre-read anneal method).....	135
Table 4.10	Anisotropy function values (glow curve deconvolution ) .....	143

## List of Figures

Figure 1.1	Time variations of dose rate for implants .....	10
Figure 1.2	Physical forms of brachytherapy sources.....	12
Figure 1.3	In-air fluence distributions of I-125 seeds.....	24
Figure 2.1	Representation of dose calculation formalism.....	32
Figure 2.2	Ionization chamber measurement setup.....	33
Figure 2.3	Mechanism of thermoluminescence.....	41
Figure 2.4	Typical dose linearity curve.....	48
Figure 2.5	Programmable heat cycle in a TLD reader.....	54
Figure 2.6	A typical TL signal.....	55
Figure 2.7	Block diagram of TLD reader.....	58
Figure 2.8	Schematic view of the structure of GafChromic MD-55-2.....	65
Figure 2.9	Models of longitudinal and transverse views of I-125 seed.....	71
Figure 2.10	Sr-90 ophthalmic applicator.....	73
Figure 2.11	Depth dose data for beta ray applicators.....	75
Figure 3.1	Lucite phantom for vertical film irradiation.....	89
Figure 3.2	Eye phantom for holding the radiochromic films.....	90
Figure 3.3	Films for relative measurement studies.....	91
Figure 3.4	Eye phantom for TLD irradiation.....	92
Figure 3.5	Solid Water phantom design.....	97
Figure 4.1	Spatial variation in optical density .....	109
Figure 4.2	Horizontally irradiated film.....	112
Figure 4.3	Film calibration curve (Horizontal).....	113
Figure 4.4	Cut radiochromic film.....	114
Figure 4.5	Cross-section of an uncut irradiated radiochromic film.....	115
Figure 4.6	Cross-section of a cut irradiated radiochromic film.....	116
Figure 4.7	Vertically irradiated film.....	118



Figure 4.8	Film calibration curve (Vertical).....	119
Figure 4.9	Depth dose curve (40 Gy).....	120
Figure 4.10	Linearity curve for chips.....	130
Figure 4.11	Linearity curve for cubes.....	131
Figure 4.12	Glow curve from pre-read anneal method.....	134
Figure 4.13	Anisotropy function for 0° angle (pre-read anneal method)..	136
Figure 4.14	Anisotropy function for 10° angle (pre-read anneal method)	137
Figure 4.15	Anisotropy function for 20° angle (pre-read anneal method)	138
Figure 4.16	Anisotropy function for 30° angle (pre-read anneal method)	139
Figure 4.17	Anisotropy function for 60° angle (pre-read anneal method)	140
Figure 4.18	Glow curve from glow curve deconvolution method.....	142
Figure 4.19	Anisotropy function for 0° angle (deconvolution method).....	144
Figure 4.20	Anisotropy function for 10° angle (deconvolution method)...	145
Figure 4.21	Anisotropy function for 20° angle (deconvolution method)...	146
Figure 4.22	Anisotropy function for 30° angle (deconvolution method)...	147
Figure 4.23	Anisotropy function for 40° angle (deconvolution method)...	148
Figure 5.1	Polar plots of 2, 3, 4 cms (pre-read anneal method).....	153
Figure 5.2	Polar plots of 2, 3, 4 cms (deconvolution method).....	154

## List of Symbols

$D$	Absorbed Dose
$\dot{D}(r,\theta)$	Two-dimensional dose rate
$F(r,\theta)$	Anisotropy function
$g(r,\theta)$	Radial dose function
$G(r,\theta)$	Geometry factor
$I$	Scanner signal of an exposed film
$I_0$	Scanner signal of an unexposed film
$k$	Proportionality constant
$K$	Kerma (Kinetic energy released in medium)
$L$	Active length of the line source
$\mu$	Linear attenuation coefficient
$P(r,\theta)$	Point of interest
$Q_j$	Charge of a single dosimeter
$\langle Q \rangle$	Average charge of a set of dosimeters
$\Lambda(r,\theta)$	Dose rate constant
$r$	Distance to the point of interest
$S_k$	Air-kerma strength
$\theta$	Angle with respect to the long axis of source

## **List of Abbreviations**

<b>AAPM</b>	<b>American Association of Physicists in Medicine</b>
<b>ECC</b>	<b>Element Correction Coefficient</b>
<b>HVL</b>	<b>Half Value Layer</b>
<b>ICWG</b>	<b>Interstitial Collaborative Working Group</b>
<b>ICRP</b>	<b>International Council for Radiation Protection</b>
<b>Kerma</b>	<b>Kinetic energy released in matter or a medium</b>
<b>LiF</b>	<b>Lithium Fluoride</b>
<b>NCRP</b>	<b>National Council on Radiation Protection and Measurements</b>
<b>NIST</b>	<b>National Institute of Standards and Technology</b>
<b>OD</b>	<b>Optical Density</b>
<b>PTFE</b>	<b>Polytetra-fluoro-ethylene</b>
<b>RCF</b>	<b>Reader Correction Factor</b>
<b>TG</b>	<b>Task Group</b>
<b>TL</b>	<b>Thermoluminescence</b>
<b>TLD</b>	<b>Thermoluminescent Dosimeter</b>
<b>TLE</b>	<b>Thermoluminescent Efficiency</b>
<b>TLR</b>	<b>Thermoluminescent Reponse</b>
<b>TTP</b>	<b>Time-Temperature Profile</b>

# **CHAPTER 1**

## **1 INTRODUCTION**

### **1.1 Cancer and Its Management**

The cancer problem is ubiquitous and rooted in the far distant past. Our present century has seen many of cancer's secrets revealed. Nevertheless, it is like peeling an onion. One removes a layer only to see another underneath it. The normal body cells grow, divide and die in an orderly fashion. During the early years of a person's life, normal cells divide more rapidly until the person becomes an adult. After that, normal cells of most tissues divide only to replace worn-out or dying cells and to repair injuries. Cancer cells, however, continue to grow and divide, and can spread to other parts of the body. These cells accumulate and form tumors that may compress, invade and destroy normal tissue. Tumor cells can proliferate readily outside the normal control mechanisms of the body. Cells that break away from such a tumor can travel through the blood stream or the lymph system to other areas of the body. Cancer therapy is concerned with the removal or killing of the cancer cells and the halting of further proliferation.

The treatment options include:

1. Surgery: the bulk removal of the tumor
2. Chemotherapy: the use of drugs for both killing and preventing the proliferation of cancer cells. The drugs enter the blood stream and reach

**RETAKES**

**SANDY McCOY**

all areas of the body, making this treatment potentially useful for cancer that has spread.

3. Immunotherapy: harnessing of the body's own defense systems to promote or support the immune system response of the body.
4. Radiation therapy: use of high-energy ionizing radiations to destroy or damage the cancer cells.
5. Hormone therapy: treatment with hormones, drugs that interfere with hormone production or hormone action, or surgical removal of hormone-producing glands to kill cancer cells or slow their growth

These modalities can be used singly or in combination.

### **1.2 Radiation Therapy**

Radiation therapy or radiotherapy uses a stream of high-energy particles or waves, such as x-rays, gamma rays, and alpha and beta particles, to destroy or damage cancer cells. The ionizing radiation deposits energy that destroys the cells in the area being treated (target tissue) by destroying their genetic material, making it impossible for these cells to continue to grow. Although radiation damages both cancer cells and normal cells, the latter are better able to repair themselves and function properly. Radiotherapy is the primary treatment for many kinds of cancers in almost any part of the body such as certain head and neck tumors, early stage Hodgkin's disease and non-Hodgkin's lymphomas, and certain localized cancers of the lung, breast, cervix, prostate, testes, bladder, thyroid and brain. Innovations in technology and technique have remarkably advanced the physics of radiation therapy. Over the past decade, the field has evolved through the introduction of state-of-the-art computers in treatment planning, the development of more sophisticated techniques for radiation measurement, and the design of more

elaborate treatments. There are three routes for the administration of radiotherapy.

### **1.2.1 External Beam Therapy**

This form of radiation therapy is performed using photons like the high-energy rays from linacs, gamma rays from Co-60 units and low energy x-rays from deep x-ray units in the orthovoltage range (50-300 kV). Megavoltage electron beams are used to treat superficial tumors. Depending on the energy of the beam, the rays can be used to destroy the tumor cells on the surface of or deeper inside the body. The higher the energy of the radiation the deeper it can penetrate inside the body to the site of the tumor. The tumor volume is defined by imaging modalities like x-ray computer tomography and magnetic resonance imaging [Williams & Thwaites, 1993]. Two upcoming methods of external beam therapy are:

- Conformal therapy: where the high dose volume is shaped using dynamic methods or multi-leaf collimators.
- Use of alternative fractionation schemes in which the treatment is given in a shorter time period but with more than one fraction delivered on each day.

Under investigation in this field of therapy is treatment using particle beams, which involves the use of fast moving subatomic particles to treat localized cancers. These radiations (neutrons, protons, pions, and heavy ions) have the drawback that they can be produced and accelerated only by very sophisticated machines.

### **1.2.2 Sealed Source Therapy (Brachytherapy)**

This mode of treatment is done using sealed radioactive sources in the form of wires or pellets, which are placed within or adjacent to the tumor volume to give a much-localized dose, thereby minimizing the dose to the surrounding normal tissues. The seal prevents the escape of radioactivity and absorbs any unwanted beta particles.

### **1.2.3 Unsealed Source Therapy**

Unsealed radioactive sources may be administered orally or by injection into the patient to localize in the tumor volume, usually with the aid of an attached pharmaceutical. They are used in liquid form for therapy and diagnosis. They are usually beta emitters so that the dose is limited to the tissues in which the source is taken up.

## **1.3 Brachytherapy**

Brachy, which in Greek means "short", is used in the context of therapy at short distances. G. Forssell coined the term for the first time in 1931 [Hilaris *et al.*, 1988]. Since then, various other terms have been used to define this treatment mode using radionuclides, such as, plesiotherapy, endotherapy, curietherapy, endocurietherapy, etc. Brachytherapy is the internal radiation treatment achieved by the placement of sealed radioactive sources into or in the proximity of the tumor, allowing the patient to receive radiation therapy from the inside out. This mode of treatment started immediately after the discovery of radium by the Curies in 1898. Dr. Danlos conducted the first



recorded treatment in 1901 by the insertion of a glass tube containing radium sulfate into a tumor [Hilaris *et al.*, 1988]. Early pioneers resorted to the method of inserting bulky radium tubes within the tumor for a certain period of time and withdrawing them. However, it was with the advent of artificial radioactivity that brachytherapy became so popular. Brachytherapy allows the delivery of a higher biologically effective dose of radiation to the tumor with less normal tissue damage in a shorter time than is possible with external radiation. By placing the radiation source or sources inside or immediately adjacent to the volume of the tissue to be treated, the dose to the other tissues can be minimized because the radiation does not have to pass through any other tissue before arriving at the treatment volume. Inside the treatment volume, the dose is non-uniform and the dose gradients are often high. There are certain systems like the Manchester technique, which are designed for dose uniformity. Brachytherapy is limited to accessible sites such as near the surface of the body or near the natural body cavities having small volumes. The dose rates in brachytherapy are usually low compared to external beam therapy.

Brachytherapy is used as a primary treatment or as a supplementation for external megavoltage radiation therapy. The advantage of brachytherapy is that it is less invasive than surgery and often has fewer side effects when compared with other procedures. Also the recovery time is very short and the patient's quality of life is not impacted much. External radiation on the other hand, though less traumatic than surgery, is extremely time consuming and requires 4-8 weeks of five-times-a-week treatments. Nevertheless, in external beam therapy, a high degree of dose uniformity can usually be achieved in the treatment volume.

### **1.3.1 Types of Brachytherapy**

The success of brachytherapy depends on the method used for delivering the effective dose of radiation and selection of the appropriate radionuclide for treatment. The technique of brachytherapy may be divided into three distinct applications: surface moulds, interstitial implants, and intracavitary insertions.

#### **1.3.1.1 Surface Mould Applications**

Surface moulds or plaques are usually employed in cases of superficial lesions, wherein the radioactive sources are arranged on the external surface of the patient, displaced slightly from the lesion. The source is then mounted on a wax or plastic piece to fill in the space between the source and the lesion. The advantage of this treatment is the rapid fall off of dose thereby saving the sensitive normal tissue below, if present. The most common use is in the treatment of ocular tumors with the help of beta and photon emitting radionuclides. Owing to the advancement in the treatments using electron beams and superficial x-rays, this mode of therapy is being slowly replaced.

#### **1.3.1.2 Interstitial Implants**

The radioactive sources used in interstitial brachytherapy are surgically inserted directly into the diseased tissue or into the tissue adjacent to the lesion but not in a body cavity. The sources usually have small diameter to allow penetration into the tissue. The commonly used radionuclides in interstitial brachytherapy are Ir-192 and I-125. They are used for treating cancers of accessible sites like the prostate, intra-oral cancers and superficial

tumors. The common dose rates prescribed range from 7-20 Gy/day over a span of 2-10 days. [Bomford *et al.*, 1993].

### **1.3.1.3 Intracavitary Insertions**

In intracavitary therapy, radioactive sources such as Co-60 or Ir-192 are introduced into the body cavity in a form-fitting applicator to irradiate the cavity walls and any lesion therein. The common cancers treated are those of the cervix, uterus, vagina, rectum, nasopharynx and esophagus. Once the applicator has been fixed in position, the radioactive sources can be loaded into it manually or remotely. High dose rate remote afterloading brachytherapy units allow treatment in a few minutes using a high activity (typically 10 Ci) radioactive source that travels through the catheters to the tumor. Since the source is moved from a shielded safe to the desired position inside the patient by remote control, the dose to the staff is insignificant.

### **1.3.2 Characteristics of Brachytherapy Radionuclides**

The suitability of a radionuclide for brachytherapy is determined by its half-life and by the type, energy, and branching ratios of its emissions. Radioisotopes emitting beta and gamma rays are usually employed in brachytherapy as they have more penetrating power than alpha rays. Although beta rays do not penetrate more than 3-4 mm, they are useful for the treatment of superficial lesions like those of the skin and eye. Gamma emitters are usually preferred in brachytherapy because of their penetrating power. Table 1.1 shows some of the radionuclides used in brachytherapy. Radium was used formerly, but has been replaced because of the hazard caused by radon gas leakage. Ir-192 and I-125 are used in the majority of

interstitial brachytherapy treatments. The radionuclides are sealed in suitable encapsulation. This covering acts as a filter to absorb any unwanted low energy radiation emitted along with the main energy, as in the case of gamma radiation being accompanied by low energy betas. The covering is usually made of titanium or an alloy of platinum and iridium. The high atomic number and density of these materials ensures the absorption of all the unwanted alpha and beta emissions. Even with the encapsulation, the sources must have a small size to ease the process of application. The problem here is that the source activity is directly proportional to the number of radioactive atoms present and inversely proportional to the half-life. For a given activity requirement, a longer half-life requires a greater number of atoms and therefore a larger source. Hence, as a compromise between the constraints, the source for a particular application is selected depending on the type of implant - temporary or permanent. The temporal dose distribution for 50 Gy delivered via temporary and permanent implants for certain radionuclides is illustrated in Figure 1.1.

Temporary implants are used for tumors that are readily accessible from opposite sides as in the neck, breast, and skin. The temporary implants mostly use Ir-192 and Cs-137 and are completed within a few hours or days.

Permanent implants use individual single seeds or seeds loaded in magazines, which can be inserted into the tumor. In permanent implants, the radioactive source remains in the patient indefinitely and hence sources having short half-lives like I-125 are preferred. This form of therapy aids in controlling fast growing tumors. Permanent implants are utilized mainly for the treatment of the tumors of the brain, prostate, lung and some gynecological sites.

**Table 1.1:** Physical characteristics of radionuclides used in brachytherapy<sup>†</sup>

Isotope	Half-life	Beta Energy (MeV)	Gamma Energy (MeV)	Exposure Rate Constant (R cm <sup>2</sup> mCi <sup>-1</sup> h <sup>-1</sup> )	Half-Value Layer (mm lead)	Clinical Uses	Source Form
Ra-226	1622 years	0.017-3.26	0.047-2.44	8.25	8.0	Temporary interstitial and intracavitary implants	Tubes, needles
Cs-137	30.18 years	0.514-1.17	0.662	3.28	6.5	Temporary interstitial and intracavitary implants	Tubes, needles
Sr-90	29.12 years	0.54-2.27	None	-	0.14	Temporary application for shallow lesions	Applicator
Co-60	5.26 years	0.313	1.17, 1.33	13.07	11.0	Temporary implants	Plaques, tubes, needles
Ir-192	74.2 days	0.24-0.67	0.136-1.062	4.69	3.0	Temporary interstitial implants of the head, neck, breast.	Wires, seeds
I-125	59.4 days	None	0.0274 avg	1.51	0.025	Permanent interstitial implants (prostate, lung); Temporary implants (eye)	Seeds
Pd-103	17.0 days	-	0.020-0.023	1.48	0.008	Permanent implants of prostate	Seeds
Au-198	2.7 days	0.96	0.412-1.088	2.327	3.3	Permanent implants	Seeds

<sup>†</sup> [Khan F.M., 1994; Hendee and Ibbott, 1996; Bomford *et al.*, 1993]

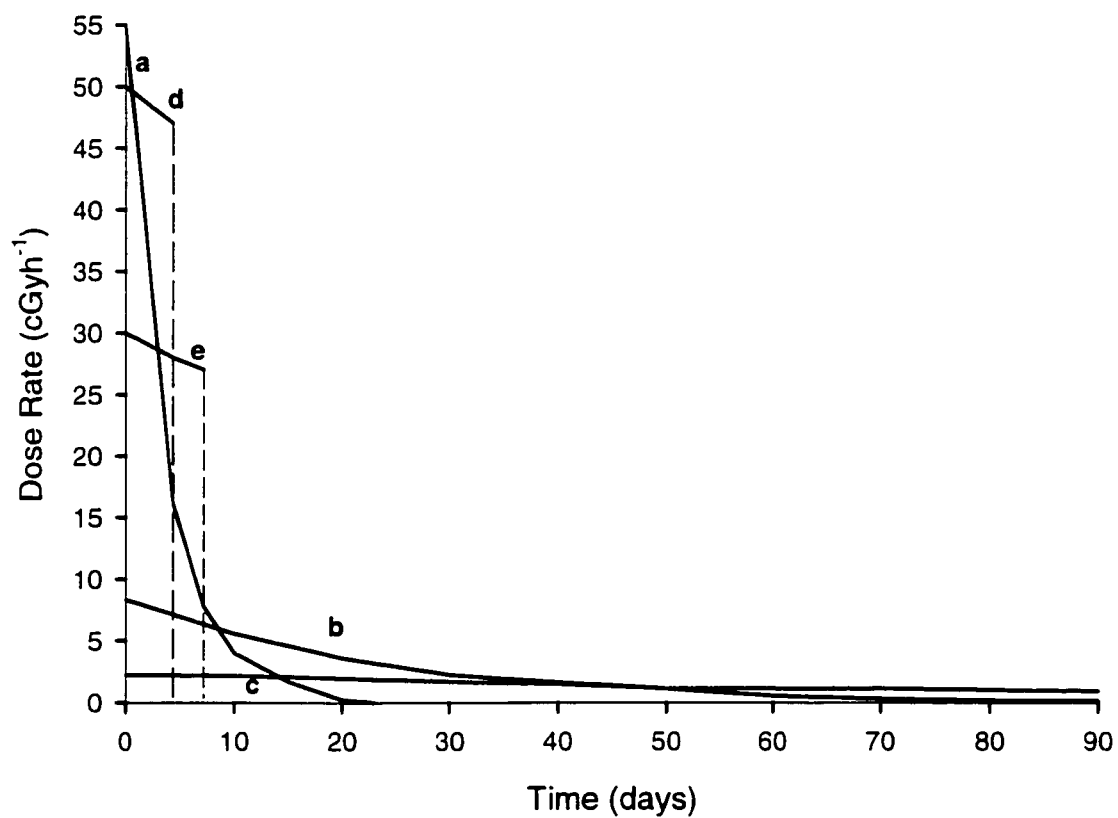


**Figure 1.1:** Time variations of dose rate for implants delivering 50 Gy: **a**, Au-198 - permanent; **b**, Pd-103 - permanent; **c**, I-125 - permanent; **d**, Ir-192 - temporary; **e**, I-125 - temporary. [Anderson *et al.*, 1990]

### **1.3.3 Physical Forms of Brachytherapy Sources**

The physical form of the source depends on the type of treatment. The radioactive sources used are specified by their (a) active length, the distance between the ends of the radioactive material; (b) physical length, the distance between the actual ends of the source; (c) activity in mCi; and (d) filtration for Ra-226 or Cs-137, transverse thickness of the capsule in millimeters of platinum or stainless steel. The sources are manufactured in the forms of tubes, needles, seeds, fluids, eye applicators, and grains.

#### **1.3.3.1 Tubes**

Radioactive tubes are used mainly in intracavitary therapy for the treatment of gynecological diseases. They are inserted into devices that are designed to fit into body cavities such as the uterine canal or cervix. The external diameter of a Cs-137 tube is typically 2.65 mm with a length of approximately 20 mm and an active length of 14 mm [Hendee and Ibbott, 1996].

#### **1.3.3.2 Needles**

Though needles are longer than tubes (typically 15-45 mm active length), they have a smaller diameter and therefore carry less activity. The reduced diameter allows for easier insertion directly into tissue. One end of the needle is sharp for entering the tumor and the other end has an eyelet for attaching a thread used to suture the needle in place and to withdraw it. Needles have an outer casing of platinum-iridium alloy, silver or stainless steel.

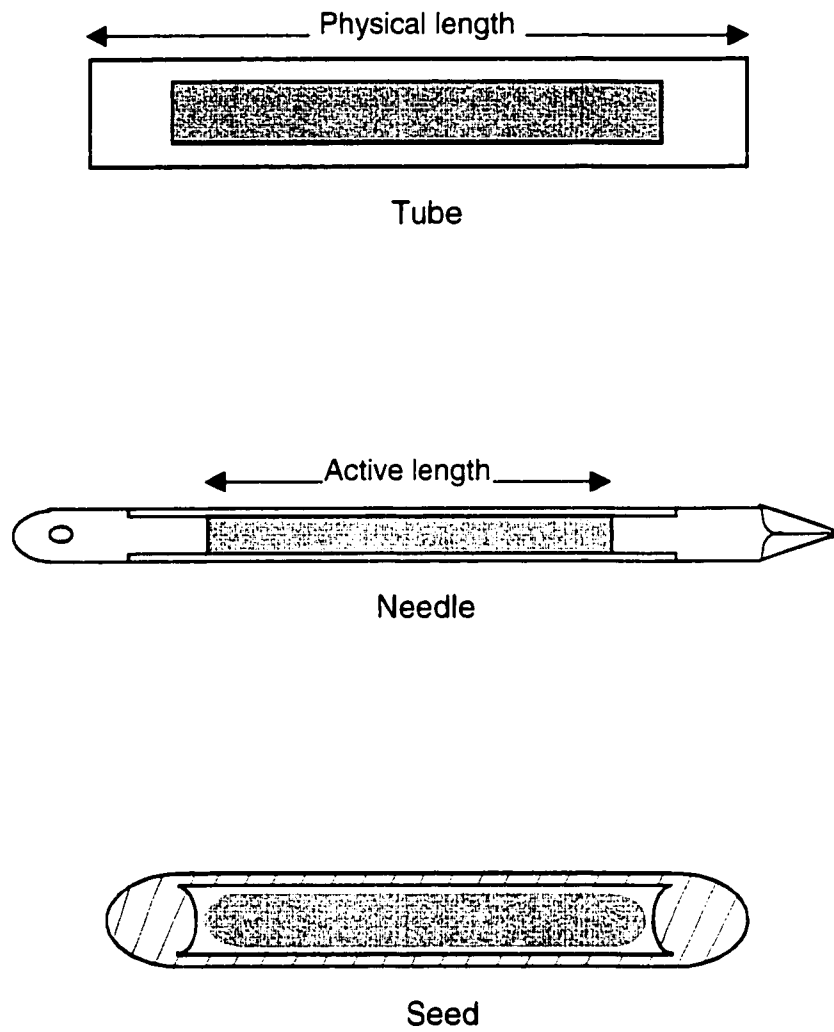


**Figure 1.2:** Physical forms of brachytherapy sources



### **1.3.3.3 Seeds**

Seeds find use in temporary and permanent implants. Radioactive seeds containing I-125 and Au-198 are mostly used for permanent implants. However, seeds of Ir-192, which have a longer half-life, are usually supplied in nylon ribbons that can be removed after the required dose has been delivered. Ir-192 seeds are encapsulated using platinum to filter out the low energy beta component. The activity per seed ranges from 0.1-40.9 mCi for I-125 and 0.35-17.6 mCi [Anderson *et al.*, 1990] for Ir-192. The seeds have active lengths of about 3-3.5 mm.

### **1.3.3.4 Fluids**

Short-lived radioactive fluids are unsealed sources employed for the treatment of various diseases, such as the use of I-131 and Au-198 for thyroid carcinoma and P-32 for the treatment of diffuse microscopic disease in the peritoneal space [Williams and Thwaites, 1993].

### **1.3.3.5 Wires**

Outside North America, Ir-192 is mainly available in the form of wires. These are thin, flexible and can be easily cut to the desired length. The iridium wires are made from an Ir-Pt core surrounded by a cladding of platinum, and are used for interstitial treatments. The typical outer diameters of the wires vary from 0.3-0.6 mm [Anderson *et al.*, 1990].

### **1.3.3.6 Ophthalmic Applicators**

Tumors of the eye have to be treated without injuring the lens and optic nerve to preserve function. Pterygium, the vascularization or ulceration of the cornea, is treated with a small radioactive applicator positioned on or near the cornea for a short period of time. Present day applicators use Y-90 ( $T_{1/2}=64$  hours) in secular equilibrium with its parent Sr-90 ( $T_{1/2}=28$  years). The front surface of the applicator absorbs most of the low energy beta particles from Sr-90 (0.54 MeV), but permits the high energy beta from Y-90 (2.27 MeV) to enter the eye. The dose rate at the center of an applicator surface may be as high as  $100 \text{ cGy.s}^{-1}$ . The dose rate near the applicator decreases to about 50% at a depth of 1 mm in tissue and becomes 5% of the surface dose rate at a depth of 4 mm, which is the average depth of the lens below the cornea [Hendee and Ibbott, 1996].

## **1.4 Brachytherapy Dosimetry**

Brachytherapy is considered a primary tool in radiation oncology, and standardized dosimetric protocols have been instituted to support this application of ionizing radiation in cancer treatment. The dose to the tumor and surrounding tissue and also the spatial geometry of the treatment delivery must be known very accurately and precisely. Brachytherapy dose calculation requires a knowledge of the distance and orientation of the source with respect to the point of interest, together with the source strength and a factor incorporating the dose per unit source strength and corrections for attenuation in the capsule and body tissues.

### 1.4.1 General Considerations

When electromagnetic radiation gets attenuated in a medium, the energy released in the interaction processes that follow partly gives rise to scatter and partly produces fast electrons, which in turn produce ionization leading to energy deposition. This energy deposition in the tissue from the incident radiation causes chemical and biological changes and can be quantified in terms of absorbed dose and kerma. The kerma (*kinetic energy released in matter*) is the sum of the initial kinetic energies of all interacting particles liberated in a volume element of matter divided by the mass of matter in the volume element [Khan, 1994]. Hence the kerma is

$$K = \frac{\Delta E_{tr}}{\Delta m}, \quad (1.1)$$

where  $\Delta E_{tr}$  is the sum of the initial kinetic energies of all the charged particles liberated by the uncharged ionizing particles in a material of mass  $\Delta m$ . The energy released by the photons in a mass need not be totally absorbed in that mass. It can be carried away by energetic electrons to be deposited elsewhere. The energy actually deposited in the mass of interest is given by the absorbed dose. The absorbed dose (D) is the energy absorbed per unit mass in the volume element:

$$D = \frac{\Delta E_d}{\Delta m}, \quad (1.2)$$

where  $\Delta E_d$  is the energy imparted by ionizing radiation to the matter in a volume element of mass  $\Delta m$ . The unit for both kerma and absorbed dose is  $J.kg^{-1}$  or Gray. ( $1Gy = 1J.kg^{-1} = 100 \text{ cGy} = 100 \text{ rads}$ )

For an isolated point source, the gamma rays are emitted isotropically in all directions. The intensity of the radiation will decrease with the inverse

square of the distance from the source and the intensity will be uniform over a spherical surface centered on it. Therefore, the dose rate will be directly proportional to the activity of the source and inversely proportional to the square of the distance from the source. Brachytherapy sources are specified in terms of their air-kerma strength [AAPM Report No. 21, 1987]. The air-kerma strength ( $S_k$ ) expressed in terms of  $\mu\text{Gy m}^2 \text{ hr}^{-1}$ , is defined as the product of the air kerma rate ( $\dot{K}_d$ ) at a specific distance  $d$  and the square of this reference distance (usually 1m) taken along the perpendicular bisector of the source longitudinal axis to the point of measurement,

$$S_k = \dot{K}_d d^2. \quad (1.3)$$

The air kerma rate  $\dot{K}$ , is related to the exposure rate  $\dot{X}$  ( $\text{R hr}^{-1}$ ) at a reference point in free space as

$$\dot{K} = \dot{X} \left( \frac{\overline{W}}{e} \right), \quad (1.4)$$

where  $\frac{\overline{W}}{e} = 0.876 \text{ cGy R}^{-1}$  is the average energy absorbed per unit of ionization in air.

The determination of the dose absorbed is necessary for the prescription of the treatment. A device that can provide a measurable response to the energy absorbed in a medium due to the incident radiation is known as a radiation dosimeter. The most important characteristic of a good dosimeter is to indicate the energy that would be absorbed in the medium it displaces, irrespective of the fluence rate and energy spectrum of the incident radiation.

### 1.4.2 Measurement of Absorbed Dose

The clinical application of ionizing radiation for therapy is based on a foundation of dosimetric concepts and instrumentation.

#### 1.4.2.1 Calorimetric Dosimetry

Calorimetric dosimetry uses an instrument known as the calorimeter, which measures the absorbed dose by detecting the temperature rise in a medium. The absorbing medium is thermally insulated from the environment and hence the rise in temperature is proportional to the absorbed energy.

#### 1.4.2.2 Photographic Dosimetry

On developing a radiographic film, the metallic silver in the emulsion is deposited in regions that have been exposed to the radiation. The light transmitted through a region of the processed film varies with the amount of the deposited silver and hence with the energy absorbed from the radiation. The transmittance (T) is given in terms of the optical density (OD) of the film as

$$OD = \log_{10} \left( \frac{1}{T} \right) = \log_{10} \left( \frac{I_0}{I} \right), \quad (1.5)$$

where I and  $I_0$  are the light intensities measured with and without the film in place [Hendee and Ibbott, 1996; Khan, 1994]. This dosimetry tool has the drawback of not being tissue equivalent and being energy dependent.

Another form of film dosimetry employs the radiochromic films. Radiochromic films are thin film chemical sensors consisting of colorless

leuco dyes that turn blue without the need for development when exposed to ionizing radiation [Muench *et al.*, 1991]. The intensity of this blue color keeps increasing with the radiation dose. Since radiochromic films have low atomic number constituents, they can be employed for dosimetric studies in tissue equivalent phantoms. They can record the dose distribution very close to a source with very fine spatial resolution and hence are desirable in regions of steep dose gradient. The greatest advantages of these films are that they are self-developing and are insensitive to visible light.

### **1.4.2.3 Chemical Dosimetry**

Chemical dosimetry is based on the measurement of the oxidation and reduction of chemical solutions exposed to radiation. The Fricke dosimeter using ferrous sulfate solution is the most widely used chemical dosimeter [Bomford *et al.*, 1993].

### **1.4.2.4 Scintillation Dosimetry**

Scintillation detectors use materials that fluoresce during exposure to ionizing radiation. The intensity of the light emitted depends on the rate of absorption of energy. A commonly used scintillator is thallium-activated sodium iodide (NaI(Tl)). These scintillators are also energy dependent.

### **1.4.2.5 Thermoluminescent Dosimetry**

Thermoluminescent dosimeters (TLDs) are crystalline materials that release light when heated following exposure to ionizing radiation [Oberhofer

and Scharmann, 1981]. A very small portion of the absorbed energy is stored in the crystal when electrons are raised from the valence band to the conduction band. Some of the electrons return to the valence band, but others are trapped in the intermediate energy levels created due to the crystal impurities. On heating the crystals, the trapped electrons are released and return to the conduction band. They then return to the valence band releasing energy in the form of light (Section 2.2.2) that is used to generate an electrical signal in a photomultiplier tube. This signal is proportional to the energy deposited, i.e. to the absorbed dose. Thermoluminescent materials like LiF and  $\text{Li}_2\text{B}_4\text{O}_7$  are tissue equivalent [McKinlay, 1981]. Thermoluminescent dosimeters find use as personnel monitors and in patient dose measurements.

### 1.5 Phantoms

As it is not possible to conduct dose measurements in a patient on every occasion, it is necessary to devise a reference material that can simulate the human body. Water is an ideal phantom material simulating tissue and has the advantage of being homogeneous, and allowing free movement of the radiation detectors in it. The dose measurements required for brachytherapy treatment planning need to be very accurate. However, when the measurements are conducted in water there arise positioning uncertainties. For example, to achieve  $\pm 2\%$  accuracy at 1 cm from a point source, the position of the detector needs to be known to  $\leq 0.01$  cm. Hence, the need for other tissue equivalent phantom materials becomes evident. These materials should behave in the same manner as the body tissues on irradiation. From an analysis of the absorption processes, the phantom material must have: (1) an effective atomic number very close to that of the tissue it simulates because of the dependence of the photoelectric absorption

and pair production processes on that atomic number, (2) an electron density close to that of the tissue simulated because of the dependence of the Compton scattering process on the number of electrons per gram and, (3) a density or specific gravity close to that of the tissue simulated [Bomford *et al.*, 1993]. For measurements where the distance has to be accurate, it is necessary to use solid phantoms. These materials may not simulate the tissue as closely as water does. Hence, they are used for relative measurements. Some of the non-water phantoms include Mix D [Khan, 1994], Temex rubber, PMMA (Perspex, Plexiglass, Lucite) and polystyrene. A commercially available solid substitute for water made from an epoxy resin called Solid Water<sup>†</sup> is a commonly used phantom material [Khan, 1994].

### 1.6 Research Objectives

The International Collaborative Working Group has observed that, although the potential benefits of brachytherapy to a cancer patient are well established, there is still uncertainty regarding the dose calculations and lack of agreement on the dose specification conventions [Anderson *et al.*, 1990]. In brachytherapy, the source dosimetry has to be specified with good accuracy for the success of the treatment. The overall objectives of this thesis are to study,

- the relative output of different models of Sr-90 applicators.
- the anisotropic properties of model 6711 I-125 seeds.

---

<sup>†</sup> Gammex RMI, Middleton, WI



### 1.6.1 Relative Output of Sr-90 Applicators

The treatment of diseases like pterygia and other benign conditions on the surface of the eye can be effected using ophthalmic applicators containing beta ray sources. Most ophthalmic applicators employ a Sr-90/Y-90 compound in secular equilibrium that is incorporated in a rolled silver foil. This source features emission of beta rays of end-point energies of 0.546 and 2.283 MeV with only a small accompaniment of gamma radiation [Goetsch and Sunderland, 1991]. Even then, the dosimetry of Sr-90 applicators is quite complex because the low penetration of the emitted radiation, the high dose rate, and the shape and size of the source complicates the accurate determination of the surface dose from the applicator [Ali & Khan, 1990]. The surface dose rate of an ophthalmic applicator is used to determine the lens and sclera dose and to specify, for comparative purposes, the clinical effectiveness of the applicator. Most of the applicators available at our institution (Table 1.2) are about 30 years old and needed to be recalibrated. The relative calibration measurements carried out in this thesis employed radiochromic films and thermoluminescent dosimeters.

**Table 1.2:** List of Ophthalmic Applicators Used

	SOURCE			
Code number	SIA K964	SIA K610	SIA K965	SIA 20
Radionuclide	Sr-90 – Y-90	Sr-90 – Y-90	Sr-90 – Y-90	Sr-90
Present activity <sup>†</sup> (mCi)	7.96	26.54	53.08	52.29
Diameter	7x4 mm	12 mm	18 mm	9 mm
Surface dose rate <sup>†</sup> (cGy/sec)	17.14	13.06	11.15	61.61

<sup>†</sup> Values on 12<sup>th</sup> June, 1998 obtained from data originally supplied by the manufacturer

Before radiochromic film could be used for dosimetry measurements, a device to read the exposed films had to be selected. Modern desktop scanners offer high resolution images and represent one possible choice. However, before a document scanner is used for this purpose, its

effectiveness in such measurements must be validated. The significant questions in its performance that were analyzed are:

- Which is the best imaging mode of the scanner?
- Which are the best operating parameters?
- Does the scanner have temporal and spatial stability?
- Does the scanner show consistency in the reading?

The relative output study of the four Sr-90 ophthalmic applicators was then conducted with radiochromic films. A comparison study was also done using thermoluminescent dosimeters.

### **1.6.2 Anisotropy of Model 6711 I-125 Seeds**

Model 6711 I-125 seeds are used primarily for permanent implants in interstitial brachytherapy where relatively low dose rates are required. The Model 6711 has the disadvantage of having a highly anisotropic photon emission spectrum (Figure 1.3). This property, due in part to non-uniform activity distribution, leads to inaccurate dosimetry and uncertainty in treatment planning when the source orientation is not known [Nath & Melillo, 1993]. In addition, the plasma arc welding at the ends of the source results in a glob of molten titanium at each end. This causes more attenuation along the natural axis of the seed. A point source approximation is reasonable for a multi-source implant where about 50-100 sources are randomly oriented in the tumor volume. However, when the sources are regularly arranged in a catheter, as in the case of prostate implants where the seeds are oriented preferentially in the direction of the needles, the point source approximation is inadequate. Therefore, for the accurate representation of dose rates in tissue a more realistic dose calculation formalism is required.

The two dimensional dose distribution around a cylindrically symmetric source can be expressed as

$$\dot{D}(r, \theta) = S_k \Lambda \left[ \frac{G(r, \theta)}{G(r_0, \theta_0)} \right] g(r) F(r, \theta), \quad (1.6)$$

where  $S_k$  is the air kerma strength in  $\mu\text{Gy m}^2 \text{h}^{-1}$  (this unit is often denoted by the symbol  $U$ , where  $1U = 1 \mu\text{Gy m}^2 \text{h}^{-1} = \text{cGy cm}^2 \text{h}^{-1}$ ),  $\Lambda$  is the specific dose rate constant expressed in  $\text{cGy h}^{-1} U^{-1}$ ,  $G(r, \theta)$  is the geometry factor ( $\text{cm}^{-2}$ ),  $g(r)$  is the radial dose function and  $F(r, \theta)$  is the dimensionless anisotropy function [Anderson *et al.*, 1990].

All cylindrical sources exhibit significant anisotropy in the emitted radiation pattern, specifically a reduction in emission near the source axis. This is described by the anisotropy function  $F(r, \theta)$  which describes the polar angle dependence of the dose distribution around a single source. For I-125, the reference data available is that from AAPM Task Group 43 [Nath *et al.*, 1995]. Some of the anisotropy values appear to have large experimental errors and unrealistic spatial variations (up to 10%), especially for  $F(r=3\text{cm}, \theta)$ . This could be attributed to the fact that this data, which is difficult to measure accurately, is from a single laboratory. Hence, the accuracy of this dosimetric parameter is of concern.

In practice, relative dose rate distributions can be measured as a function of angle for distances up to 10 cm from the source using lithium fluoride thermoluminescent detectors in a solid water phantom. The data obtained is then combined with the geometry factor according to Equation 1.7 to give the anisotropy factor

$$F(r, \theta) = \frac{\dot{D}(r, \theta)G(r, \theta_0)}{\dot{D}(r, \theta_0)G(r, \theta)}. \quad (1.7)$$

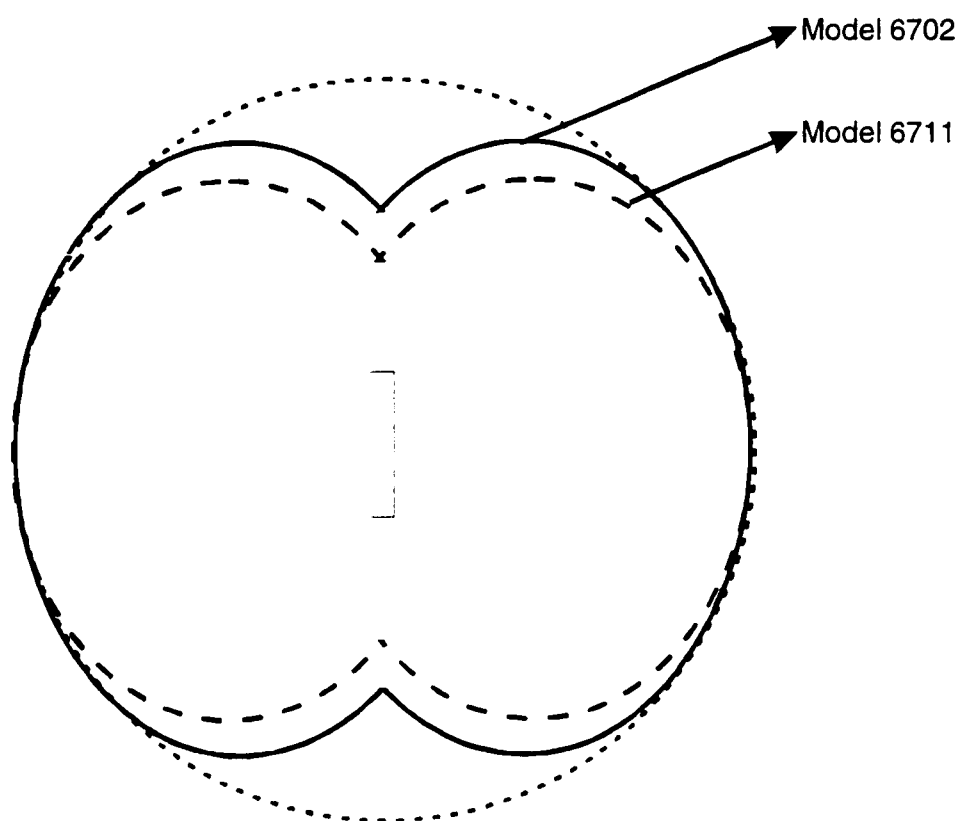


**Figure 1.3:** In-air fluence distributions of models 6702 and 6711 I-125 seeds [Anderson *et al*, 1990]

Validation of the anisotropy values recommended by Task Group 43 (TG-43), set up by the American Association of Physicists in Medicine (AAPM), is definitely warranted for the correct specification of the dose delivered by the implant.

### **1.7 Thesis Overview**

In view of the need for accuracy in brachytherapy, treatment dosimetry becomes very important. Of the numerous dosimetric tools available, the experiments in this thesis were conducted using thermoluminescent dosimeters and radiochromic film. The advantage and the relevance of these tools have been discussed earlier in this introductory chapter. The thesis is logically organized in five chapters. Chapter 2 contains a synopsis of the basic knowledge and theories applied in the following chapters. It discusses in greater length the ideas put forward in this first chapter. Chapter 3 exhaustively examines the materials used such as the thermoluminescent dosimeters, radiochromic films, I-125 seeds, the ophthalmic applicators and the instrumentation. It also describes the methods employed for the various studies. The aim of Chapter 4 is to present the experimental results and to analyze all the data obtained. Finally, Chapter 5 summarizes the whole thesis, giving an assessment of the practical problems and the success of the work.

## References

1. AAPM Report No. 21, "Specification of brachytherapy sources - Task Group No. 32", American Institute of Physics, New York, (1987)
2. Ali M.M., Khan F.M., Determination of surface dose rate from a Sr-90 ophthalmic applicator, *Medical Physics*, 17(3), 416-421, (1990)
3. Anderson L.L., Nath R., Weaver K.A., Nori D., Phillips T.L., Son Y.H., Chiu Tsao S., Meigooni A.S., Meli J.A., Smith V., "Interstitial Brachytherapy - Physical, Biological, and Clinical Considerations", Interstitial Collaborative Working Group, Raven Press, New York, (1990)
4. Bomford C.K., Kunkler I.H., Sherriff S.B., "Textbook of Radiotherapy", Churchill Livingstone, (1993)
5. Goetsch S.J., Sunderland K.S., Surface dose rate calibration of Sr-90 plane ophthalmic applicators, *Medical Physics*, 18(2), 161-166, (1991)
6. Hendee W.R., Ibbott G.S., "Radiation Therapy Physics", Mosby, Missouri, (1996)
7. Hilaris, Nori, Anderson, "An Atlas of Brachytherapy", Macmillan Publishing Co., New York, (1998)
8. Khan F.M., "The Physics of Radiation Therapy", Williams & Wilkins, Maryland, (1994)
9. McKinlay A.F., "Thermoluminescence Dosimetry - Medical Physics Handbooks 5", Adam Hilger, Bristol, (1981)
10. Muench P.J., Meigooni A.S., Nath R., McLaughlin W.L., Photon energy dependence of the sensitivity of the radiochromic film and comparison with silver halide film and LiF TLDs used for brachytherapy dosimetry, *Medical Physics*, 18(4), 769-775 (1991)
11. Nath R., Anderson L.L., Luxton G., Weaver K.A., Williamson J.F., Meigooni A.S., Dosimetry of interstitial brachytherapy sources: Recommendations of AAPM Radiation Therapy Committee Task Group No. 43, *Medical Physics*, 22(2), 209-234 (1995)

12. Nath R., Melillo A., Dosimetric characteristics of a double wall I-125 source for interstitial brachytherapy, *Medical Physics*, 20(5), 1475-1483 (1993)
13. Oberhofer M., Scharmann A., "Applied Thermoluminescence Dosimetry", Adam Hilger, Bristol, (1981)
14. Williams J.R., Thwaites D.I., "Radiotherapy Physics in Practice", Oxford Medical Publications, Oxford, (1993)

## **CHAPTER 2**

### **2. BRACHYTHERAPY DOSIMETRY**

This chapter begins with a discussion of dose specification in brachytherapy. The experiments conducted for this thesis used mainly two types of radiation detectors - thermoluminescent dosimeters and radiochromic films. There are some interesting characteristics of TLDs that make them suitable for dose measurements in low energy, low fluence radiation fields which are presented in detail. Chemical radiation sensors such as radiochromic films that need no post-irradiation processing have the advantage of greater spatial resolution and were selected for the ophthalmic applicator dosimetry. The chapter concludes with an account of the dosimetric characteristics of Sr-90 ophthalmic applicators and I-125 seeds.

#### **2.1 Dose Specification**

A nuclide suitable for brachytherapy must have an adequate photon yield so that a small source can produce a clinically acceptable dose rate. The strength of brachytherapy sources was traditionally expressed in terms of equivalent mass of radium or the apparent activity in mCi. Equivalent mass of radium is the amount of radium in 0.5mm Pt encapsulation that produces the same exposure rate in air at a large distance from the source center along the transverse axis. Similarly, the apparent activity is the activity of a point hypothetical bare source that produces the same exposure rate in air as the actual source. These recommendations were made in the National Council for



Radiation Protection Report #41 [NCRP Report #41, 1974], which also suggested the use of exposure rate at 1 m from the source to specify the  $\gamma$  ray brachytherapy sources.

The older dosimetry protocols worked with the photon fluence around the source in free space, while clinical applications required the dose distribution in a scattering medium such as a patient. Since a brachytherapy source can have a considerable anisotropy, it is not always easy to determine accurately the dose distribution in the scattering medium from the photon fluence in free space. This method also had another disadvantage that it was strictly applicable only to point isotropic sources. Therefore in 1988, the Radiation Therapy Committee of the American Association of Physicists in Medicine (AAPM) formed the Task Group 43 which recommended the use of quantities derived directly from dose rates in a water medium near the actual source [Nath *et al.*, 1995].

The formalism clearly defines the physical quantities necessary for dose specification: air kerma strength, dose rate constant, geometry factor, radial dose function and anisotropy function. Specification of the source by these factors will eventually replace the use of the old parameters: exposure rate constant, gamma ray constant, tissue attenuation factors, apparent activity and exposure to dose conversion factors. The new formalism also helps to compare theoretical and measured values using the absolute dose rate, which is the dose rate in  $\text{cGy hr}^{-1}$  per unit source strength and is used experimentally to standardize source strength. The relative dose, which implies that the relative dose distribution has been normalized to unity at a reference point near the source. The new quantities replaced the old ones as follows (AAPM TG-43):

Apparent activity, ( $A_{\text{app}}$ )	—————→	Air Kerma Strength, $S_k$
Exposure rate constant, ( $T_\delta$ )	—————→	Dose rate constant, $\Lambda$
Inverse square distance, ( $1/r^2$ )	—————→	Geometry factor, $G(r, \theta)$ (For 2D calculations only)
Tissue attenuation factor, $T(r)$	—————→	Radial dose function, $g(r)$

Anisotropy constant,  $\bar{\phi}_{an}$   $\longrightarrow$  Anisotropy function,  $F(r,\theta)$

The air kerma is related to the exposure by the relation

$$K = \left( \frac{\bar{W}}{e} \right) X, \quad (2.1)$$

where  $\frac{\bar{W}}{e}$  is the average energy required to produce an ion pair in dry air and has a value of  $33.97 \text{ J C}^{-1} = 0.876 \text{ cGy R}^{-1}$ . This new protocol allowed for two-dimensional  $(r,\theta)$  calculations around cylindrically symmetric sources thus overcoming the limitation of point isotropic sources.

## 2.1.1 TG-43 Formalism

### 2.1.1.1 Reference Point for Dose Calculations

The reference point for dose calculations is chosen to lie on the transverse bisector of the source at a distance of 1 cm from its center, i.e.  $r_0 = 1 \text{ cm}$  and  $\theta_0 = \pi/2$ . In this consideration,  $r$  is the radial distance in cm of a point from the source center and  $\theta$  is the polar angle formed by the longitudinal axis of the source and the ray from the source center to the point of interest. This choice for reference point can be compared with the use of the 1 cm distance from the source, which is the reference point in traditional methods.

To describe the formalism, a cylindrical source as shown in Figure 2.1. is considered. The dose distribution of such a source is two-dimensional and is given in terms of a polar coordinate system with its origin at the source center where  $r$  is the distance to the point of interest,  $P(r,\theta)$ , and  $\theta$  is the angle with respect to the long axis of the source.

The two angles  $\theta_1$  and  $\theta_2$  from the ends of the source are

$$\theta_1 = \tan^{-1} \left( \frac{r \sin \theta}{r \cos \theta + \frac{L}{2}} \right), \quad (2.2a)$$

and

$$\theta_2 = \tan^{-1} \left( \frac{r \sin \theta}{r \cos \theta - \frac{L}{2}} \right). \quad (2.2b)$$

### 2.1.1.2 Air Kerma Strength ( $S_k$ )

The source strength quantities can be categorized either as a measure of the source output or as a measure of the radioactivity actually contained in the source. The source output quantities are the equivalent mass of radium, apparent activity, reference exposure rate, reference air kerma rate and reference air kerma strength.

The quantities mentioned above are equivalent to a measurement of the source output in free space along the perpendicular bisector of the source at a large distance relative to the dimensions of the source and detector (Figure 2.2). Since the measurements are said to be done in "free space", it necessitates the use of corrections for absorption and scattering in any medium like air, present in the calibration geometry.

The source strength is specified in terms of the air kerma strength and defined as the product of the kerma rate ( $\dot{K}_d$ ) in air at a large calibration distance,  $d$ , from the source center along the transverse axis and the square of that distance,  $d^2$ .

$$S_k = \dot{K}_d d^2 = \dot{X} \left( \frac{\overline{W}}{e} \right) d^2. \quad (2.3)$$

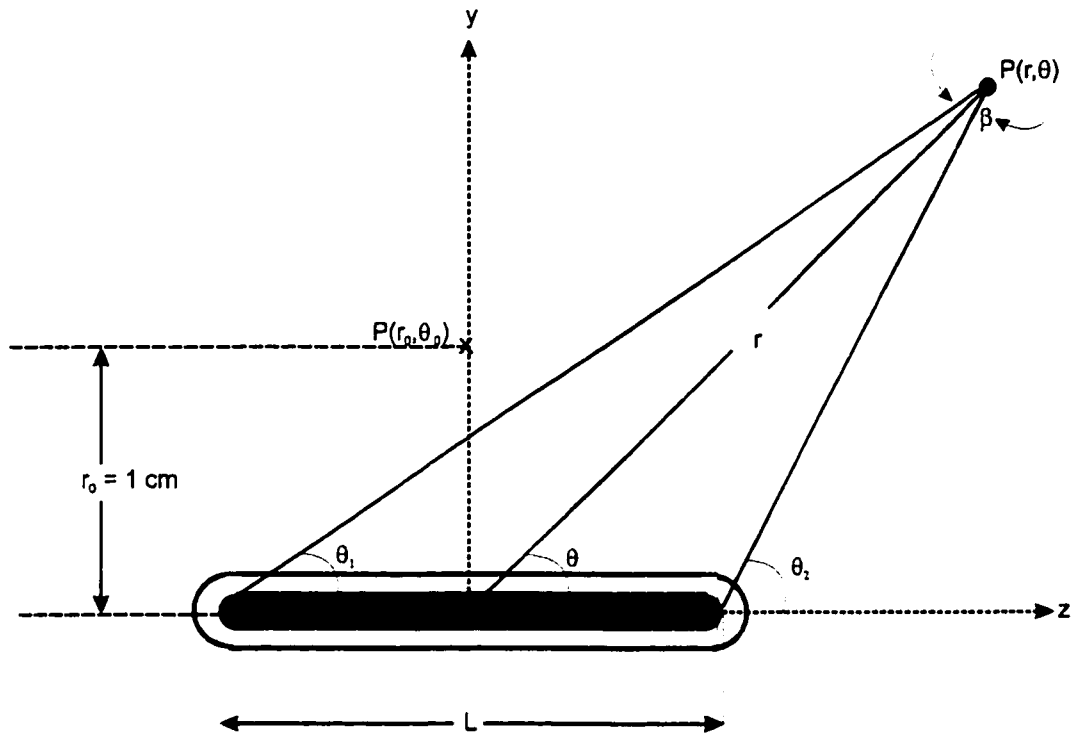


**Figure 2.1:** The coordinate system and angles used in the dose calculation formalism for a line source of active length  $L$  with the reference point at  $P(r, \theta)$

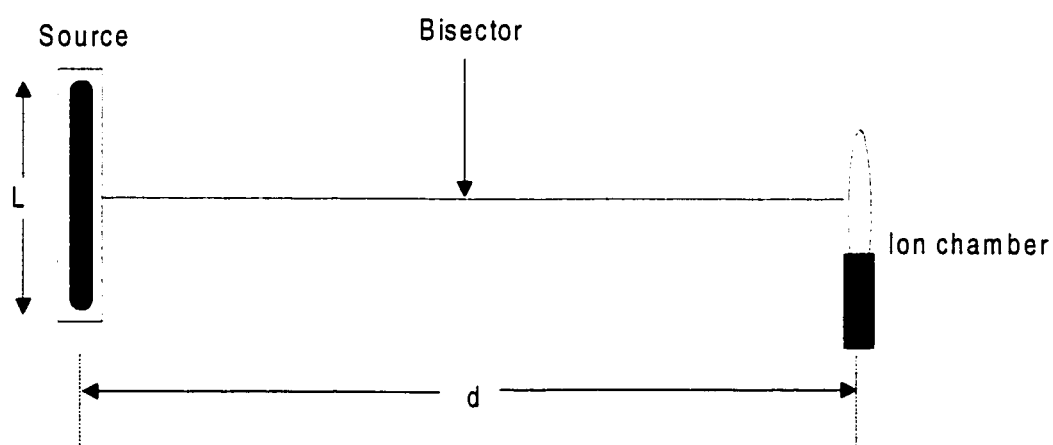


**Figure 2.2:** A cylindrical source kept at a distance  $d$  from an ionization chamber.

The distance  $d$  is made large so that the inverse square law holds to acceptable accuracy and the source can be treated as a mathematical point. If kerma, time, and distance are assigned units of  $\mu\text{Gy}$ ,  $\text{h}$  and  $\text{m}$ , respectively,  $S_k$  will have units of  $\mu\text{Gy m}^2 \text{h}^{-1}$  [AAPM TG-32] and can be represented by the symbol  $U$ .

$$1U = 1 \text{ Unit of air kerma strength}$$

$$1U = 1 \mu\text{Gy m}^2 \text{h}^{-1}$$

$$1U = 1 \text{ cGy cm}^2 \text{h}^{-1}$$

Although source calibration measurements can be performed at any large distance  $d$ , the air kerma strength is specified at a reference distance chosen as 1 m.

#### 2.1.1.3 Dose Rate Constant, $\Lambda(r,\theta)$

Dose rate distributions have many manifestations in clinical practice: published dose rate tables for sources of radium or its substitutes, and the output per unit strength of computerized treatment planning algorithms such as the Sievert integral [John and Cunningham, 1983]. The dose rate constant is defined as the dose rate to water at a distance of 1 cm on the transverse axis of a unit air kerma strength source in a water phantom. It is an absolute quantity, unlike all the other quantities in the TG-43 formalism.

The dose rate constant is written as

$$\Lambda = \dot{D}(r_0, \theta_0) / S_k . \quad (2.4)$$

$\Lambda(r,\theta)$  has units of  $\text{cGy h}^{-1}$  per unit of  $S_k$ .

The constant includes the effects of spatial geometry, the spatial distribution of radioactivity within the source, encapsulation and self-filtration within the source, and scattering in water surrounding the source.  $\Lambda$  is not a fundamental property of the radionuclide but is a contingent property of a particular source design. The numerical value of the dose rate constant is dependent on the source calibration geometry to which the air kerma strength  $S_k$  is traceable. Thus the dose rate constant applies to real physical sources and any change in the distribution of the isotope or in the thickness, length, or material of the encapsulation will result in a different dose rate at 1 cm for the same air kerma strength, and hence a different value of  $\Lambda$ .

#### 2.1.1.4 Geometry Factor, $G(r,\theta)$

The geometry factor describes the 2-D distribution of primary photon fluence around the source due only to the spatial distribution of radioactivity within the source, ignoring photon absorption and scattering in the source or the surrounding medium.

In general, the geometry factor can be written as

$$G(r,\theta) = \frac{\int_V \rho(r') dV' / |r' - r|^2}{\int_V \rho(r') dV'} , \quad (2.5)$$

where  $\rho(r')$  is the fraction of the contained activity per unit volume, that is the activity density ( $\text{cm}^{-3}$ ) at the point  $r' = (x', y', z')$  within the source, and  $V$  is the volume of the active source cavity.  $dV'$  is a volume element located at  $r'$  in the source and  $r$  denotes the point of interest located outside the source. Dividing the dose by this quantity helps to reduce the variability of the measured dose

with respect to position so that one can interpolate more accurately between sparsely distributed measured dose values.

When the distribution of radioactivity is approximated by a point source,  $G(r, \theta)$  reduces to

$$G(r, \theta) = \frac{1}{r^2}. \quad (2.6)$$

Now assuming that the radioactivity is uniformly distributed over a line source of active length  $L$  positioned along the axis of the seed, then  $G(r, \theta)$  is given by

$$G(r, \theta) = \frac{\beta}{L r \sin \theta}, \quad (2.7)$$

where  $\beta$  is the angle subtended by the active source with respect to the point  $(r, \theta)$  i.e.  $\beta = \theta_2 - \theta_1$ . The two angles  $\theta_1$  and  $\theta_2$  are given by equations 2.2a and 2.2b.

#### 2.1.1.5 Radial Dose Function, $g(r)$

The radial dose function accounts for the radial dependence of photon absorption and scatter in the medium surrounding the source.

It is defined as

$$g(r) = \frac{\dot{D}(r, \theta_0) G(r_0, \theta_0)}{\dot{D}(r_0, \theta_0) G(r, \theta_0)}, \quad (2.8)$$

and has a value of unity at  $r=r_0=1\text{cm}$ .



Since the radial dose function is measured only along the transverse axis, it applies to those points that have an angle  $\theta_0=\pi/2$ . Besides absorption and scattering in the medium, it is also influenced by the filtration of photons by encapsulation and source materials [Nath *et al.*, 1995].

For a point source, the radial dose function reduces to

$$g(r) = \frac{\dot{D}(r) r^2}{\dot{D}(r_0) r_0^2}. \quad (2.9)$$

So the radial dose function for a point source is essentially the ratio of the dose rates at two distances with the inverse square factors removed.

#### 2.1.1.6 Anisotropy Function, $F(r,\theta)$

The anisotropy function accounts for the anisotropy of the dose distribution around the source, including the effects of absorption and scatter in the medium for polar angles off the transverse bisector ( $\theta \neq \pi/2$ ). The anisotropy function is defined as

$$F(r, \theta) = \frac{\dot{D}(r, \theta) G(r, \theta_0)}{\dot{D}(r, \theta_0) G(r, \theta)}, \quad (1.7)$$

and gives the angular variation of dose about the source at each distance due to activity self-filtration, oblique filtration of primary photons through the encapsulation and scattering of photons in the medium. The dose anisotropy function is normalized at  $\theta=\theta_0=\pi/2$ ,

$$F(r, \pi/2) = \frac{\dot{D}(r, \pi/2) G(r, \pi/2)}{\dot{D}(r, \pi/2) G(r, \pi/2)} = 1 \quad (2.10)$$

### 2.1.2 Dose Rate for Two Dimensional Cases

The two-dimensional dose distribution around a cylindrically symmetric source can be represented using the TG-43 dose calculation formalism [Nath *et al.*, 1995]. If  $r$  is the distance from the source center to the point of interest and  $\theta$ , the angle with respect to the long axis of the source, then the dose rate at a point with coordinates  $(r, \theta)$  from the center of a source of air kerma strength  $S_k$  can be shown to be

$$\dot{D}(r, \theta) = S_k \Lambda \left[ \frac{G(r, \theta)}{G(r_0, \theta_0)} \right] g(r) F(r, \theta), \quad (2.11)$$

where  $\Lambda$  is the specific dose rate constant ( $\text{cGy h}^{-1} \text{U}^{-1}$ ),  $G(r, \theta)$  is the geometry factor ( $\text{cm}^{-2}$ ) that accounts for the spatial distribution of the radioactive material,  $g(r)$  is the radial dose function which is dimensionless and accounts for the radial dependence of photon absorption and scatter in the source and medium along the transverse axis ( $\theta = \pi/2$ ), and  $F(r, \theta)$  is the dimensionless anisotropy function that accounts for the angular dependence of photon absorption and scatter in the source and the medium.

For points along the transverse axis ( $F(r, \pi/2) = 1$ ) at a distance of  $r > 4h$ ,  $h$  being the active core length [Wang & Sloboda, 1998], the above equation simplifies to the approximation

$$\dot{D}(r, \pi/2) \approx \Lambda S_k \frac{g(r)}{r^2}. \quad (2.12)$$

## **2.2 Thermoluminescent Dosimetry**

### **2.2.1 Principle of Thermoluminescent Dosimetry**

Luminescence results when electrons trapped in the defects in a crystal lattice are released from these metastable states giving off energy in the form of light. The process can be brought about by heating the crystal to excite the electrons (or holes) into the conduction (valence) band. This is called *thermoluminescence*. A photomultiplier tube detects the optical photons and the light output can be measured. Dosimeters can be reused once they have been annealed to eliminate any residual thermoluminescent signal.

Thermoluminescent dosimeters (TLDs) cannot be used as absolute radiation detectors as there is no direct method to relate the thermoluminescence released from an irradiated sample to the amount of radiation received by the dosimeter material. Hence, all TLD systems must be calibrated by exposing the dosimeter to known amounts of radiation. For accuracy of calibration, the same irradiation source should be used for experiments as well as calibration. As absolute dose measurements are usually only made in standards laboratories, secondary standards must be used. However, for many clinical measurements, it is often only necessary to have a comparison of the radiation exposures at different spatial locations at different times, and hence relative measurements are adequate. Relative dose measurements have many advantages. They eliminate the need for having a calibrated radiation source, of correcting for the difference in energies between the calibrated irradiation facilities and the experimental irradiation, and of reading the many dosimeters often necessary for a complete calibration curve.

The advantage of using TLDs is that being small they have good spatial resolution, and can be used over a large dosimetric range from 1mR to

$10^5$  R [DeWerd L.A, 1996]. These materials have high precision and many are tissue equivalent. After annealing they can be reused and will retain the information after irradiation for a long time. Rapid retrieval of this information is possible using on-site readers. TLDs are also found to have good environmental stability.

### **2.2.2 Mechanism of Thermoluminescence**

Perfect halide lattices have two interpenetrating cubic lattices of alkali and halogen ions. All real crystals have one or more of the following lattice defects:

- i. Thermal or intrinsic
- ii. Substitutional or extrinsic
- iii. Radiation induced.

The intrinsic defects help in thermoluminescence. A negative ion vacancy is a region of excess positive charge and a potential trap for electrons. Similarly, a positive ion vacancy is a potential trap for holes. An ideal crystal has all electrons in the valence band and the conduction band is completely empty. The forbidden gap of this crystal with defects present has additional electron trap and hole trap sites and luminescence centers. A divalent impurity doped into a phosphor, for example LiF (TLD 100), acts as an activator or a recombination center. Since the impurities do not go into the crystal uniformly, the TL response is not uniform throughout the crystal. To overcome this non-uniformity the crystal is crushed, uniformly mixed and used (1) in powder form, (2) hot pressed, (3) sintered, (4) extruded as solids, or (5) embedded in teflon. The higher the temperature of the lattice, the greater is the number of defects.

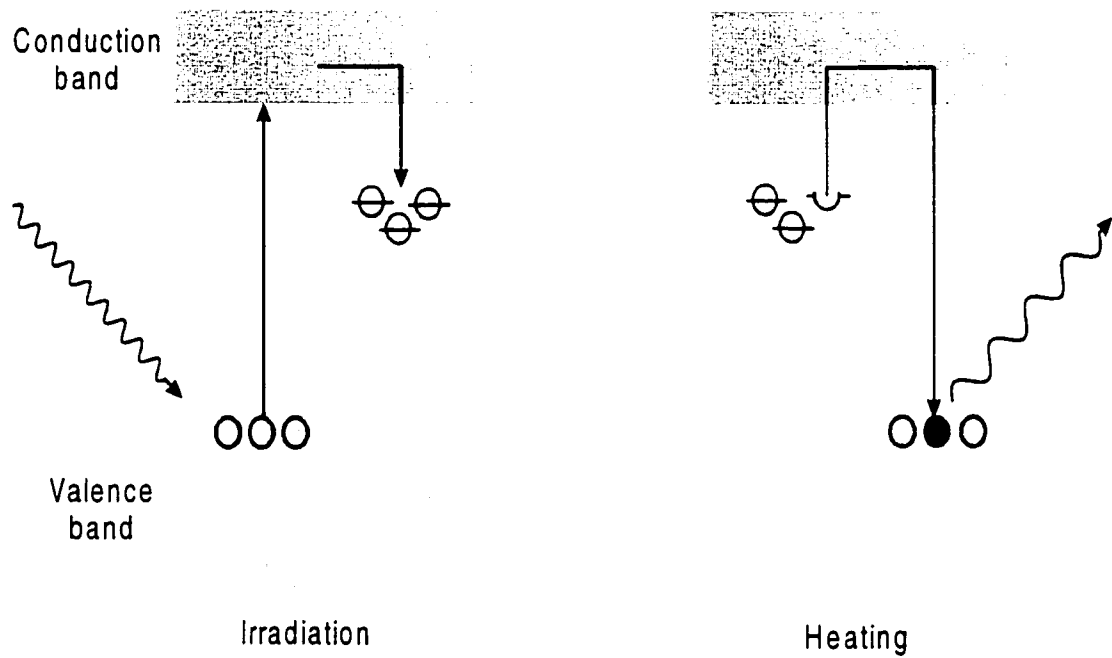


**Figure 2.3:** Electron transitions occurring when a thermoluminescent material is irradiated and heated. [Hendee, 1996]

The production of thermoluminescence in a material is mainly by the following three steps (Figure 2.3):

- *Ionization*: Free electrons and holes are produced when ionizing radiation is incident on the material.
- *Trapping of electrons and holes*: Some of the free carriers become trapped in the field potential of certain defects and impurities in the material. The stronger the field, the tighter is the trapping and more energy is required for the release of the electrons. The carriers are lost easily from shallow traps, resulting in decreased stability and greater fading. For good thermoluminescent characteristics, traps should be deeper inside the forbidden gap, though the higher temperatures needed for their release will result in infrared emission, a process that contributes to the signal background.
- *Recombination of electrons and holes*: As the crystal is heated the traps are emptied – first the shallow traps (nearer in energy to the conduction band) and then the deeper traps. The escape energy depends on the trap depth and material temperature. Some of the electrons thus released from the trapping centers during this readout process recombine with the holes, releasing excess energy in the form of a characteristic luminescence. This produces a number of thermoluminescent peaks. The amount of light emitted is proportional to the number of electrons trapped, which in turn is proportional to the amount of energy absorbed from the radiation.

### **2.2.3 Thermoluminescent Phosphors**

Thermoluminescent phosphors are used mainly in two different forms: either as loose powder or solid dosimeters. The solid form of TLDs are mostly composed of a single crystal of the phosphor and polycrystalline extrusions,

or as a homogeneous composite of the phosphor powder and a binding material such as polytetrafluoroethylene (PTFE) [McKinlay A.F, 1981]. The thermoluminescent sensitivity of a dosimeter is dependent on the amount of phosphor present and the self-absorption of the thermoluminescence signal.

#### **2.2.3.1 Powder Dosimeters**

Though single crystals are a sensitive form of dosimeter, their TL sensitivity distribution is very non-uniform. On the other hand, a powder form of this single crystal gives a uniform TL sensitivity. The material is powdered and sieved to have a grain size between 75-200  $\mu\text{m}$ , whereby the grains adhere to each other and give a uniform distribution. The advantage of powder dosimeters is that they can assume the shape of the planchet. The sample is dispensed using a vibrating volume dispenser, which can dispense equal volumes of the powder. The powder has to be weighed each time before readout to confirm that no loss of material has occurred. There is also an uncertainty in the uniformity of the distribution and positioning of the powder. Since the ratio of the surface area to the volume is high with respect to solid dosimeters, surface related effects like triboluminescence and chemiluminescence [McKinlay A.F, 1981] are important. These can be reduced by using an inert gas of fixed flow rate like oxygen-free nitrogen that has been passed through a filter located between the storage cylinder and TLD reader to remove dust.

#### **2.2.3.2 Extruded and Hot Pressed Dosimeters**

The extruded and hot pressed forms are available as ribbons (chips) or rods. They have good thermal conductivity and are produced by the compression of normal phosphor ingredients at an elevated temperature. Extruding fused polycrystalline material through an appropriately shaped die

produces the extruded forms. They are then cut and polished in the required shape. The advantage of the hot pressed forms is that they have more sensitivity and can be annealed at high temperatures, washed and handled.

#### **2.2.3.3 PTFE Based Dosimeters**

PTFE dosimeters are produced by heating a homogeneous mixture of fine grain phosphor powder (10 $\mu$ m) and PTFE powder to a temperature above the softening temperature of PTFE in a mould to form an intimate matrix. These dosimeters have low conductivity and cannot be annealed at temperatures above 300°C. They are available as discs and micro-rods. LiF: PTFE discs are widely used for personal dosimetry and micro-rods for clinical applications.

#### **2.2.3.4 Silicone-embedded Dosimeters**

Silicone-embedded dosimeters have phosphor powder incorporated in silicone rubber. A limitation here is that some silicone rubbers are thermoluminescent when exposed to ultraviolet radiation and cannot be reused, as they cannot be heated above 280°C.

#### **2.2.3.5 Sintered Dosimeters**

Compressing the phosphor powder in a press mould followed by high temperature sintering produces sintered dosimeters. Owing to their large diameter and thin form, they are very fragile.



**Table2.1:** Characteristics of certain TL phosphors [McKinlay A.F, 1981]

Phosphor Characteristics	LiF	CaF <sub>2</sub> :Dy	Li <sub>2</sub> B <sub>4</sub> O <sub>7</sub> :Mn	CaSO <sub>4</sub> :Mn
Density (g cm <sup>-3</sup> )	2.64	3.18	2.30	2.61
Photon effective atomic number	8.2	16.3	7.4	15.3
Main glow peak temperature (°C)	190-210	200, 240	200-220	110
Spectrum emission peaks (nm)	400	480, 577	600	500
Fading of peak at ambient temperature	5% in 3-12 months	25% in 4 weeks	5-10% in 3 hours	35% in 24 hours
Useful range of absorbed dose (Gy)	5x10 <sup>-5</sup> -10 <sup>3</sup>	10 <sup>-6</sup> -10 <sup>-3</sup>	10 <sup>-4</sup> -10 <sup>4</sup>	10 <sup>-7</sup> -10 <sup>2</sup>
Physical forms	Crystals, powders, chips, micro-rods, cubes, PTFE discs	Powders, chips, micro-rods	Powder, chips, PTFE based micro-rods	Powder
Principal applications	Personal, accident and radiotherapy dosimetry	High or low absorbed dose measurement	Radiotherapy and diagnostic radiology dosimetry	Environmental and short term dosimetry

## 2.2.4 Characteristics of TLD Phosphors

Thermoluminescent dosimeters have found wide application in personal, clinical and environmental dosimetry. The phosphors used for TL dosimetry are selected for each application after studying their physical characteristics. The properties studied are absorbed dose response, glow curves, fading, supralinearity, sensitivity, energy response and stability.

### 2.2.4.1 Sensitivity

Thermoluminescent sensitivity is the amount of light or the thermoluminescent yield released by the phosphor per unit mass of phosphor per unit exposure of radiation. The thermoluminescent yield (Y) is calculated as the ratio of the energy emitted as light (TL) to the mass of the detector (m) and the absorbed dose (D),

$$Y = \frac{TL}{mD}. \quad (2.13)$$

Sensitivity changes with the form of the phosphor, with the photon energy, and with the LET (linear energy transfer) of the radiation. LET is the rate of energy loss per unit path length in collisions in which energy is absorbed locally rather than being carried away by energetic secondary electrons. As TLD sensitivity is proportional to the total phosphor mass present, the matrix in which the phosphor is located will to some extent determine the TLD sensitivity. Therefore, dosimeters containing only the active phosphor (such as powder, extruded ribbons and rods) are more sensitive than the PTFE-based materials, where the active phosphor is mixed with a matrix material. When employed for diagnostic applications, the TLD

used must have good sensitivity, as absorbed doses are smaller than in radiation therapy. The magnitude of the doses delivered in radiotherapy also affects the sensitivity of the dosimeter. When doses falling in the region of supralinearity and saturation are given (Section 2.2.4.2), the sensitivity of the material increases by a factor of up to 5 even after annealing for a short time. This is called sensitization. The increase in sensitivity can be reduced by a 1-2 hour anneal at 400°C [Mckinlay, 1981]. The cooling rate (from 400°C) also affects sensitivity. TLD readers and phosphors are made to be sensitive over a large dynamic exposure range. A reader correction must be applied to account for the spectral match of the TL emission and peak sensitivity.

#### **2.2.4.2 Absorbed Dose Response**

For simplification in calibration, it is useful to have a TLD phosphor whose TL-absorbed dose response over measurement and calibration ranges is linear. But TLD phosphors do not respond linearly in the dose range of interest. They are linear at low absorbed doses and then become supralinear at higher values. The responses of the TLDs are independent of the absorbed dose rate over a very wide range.

A plot of the TL signal against the dose gives the linearity of the TL phosphor as shown in Figure 2.4. The background TL signal from an unirradiated phosphor is depicted as B.  $D_m$  is the dose up to which the linearity holds. Beyond this dose supralinearity starts, saturating at  $D_s$ . If there are several maxima in the glow curve at different temperatures, then either the integrated light or peak intensity emitted by a selected peak, or the complete integral of the light emitted by the phosphor from all the different peaks represents the TL signal.

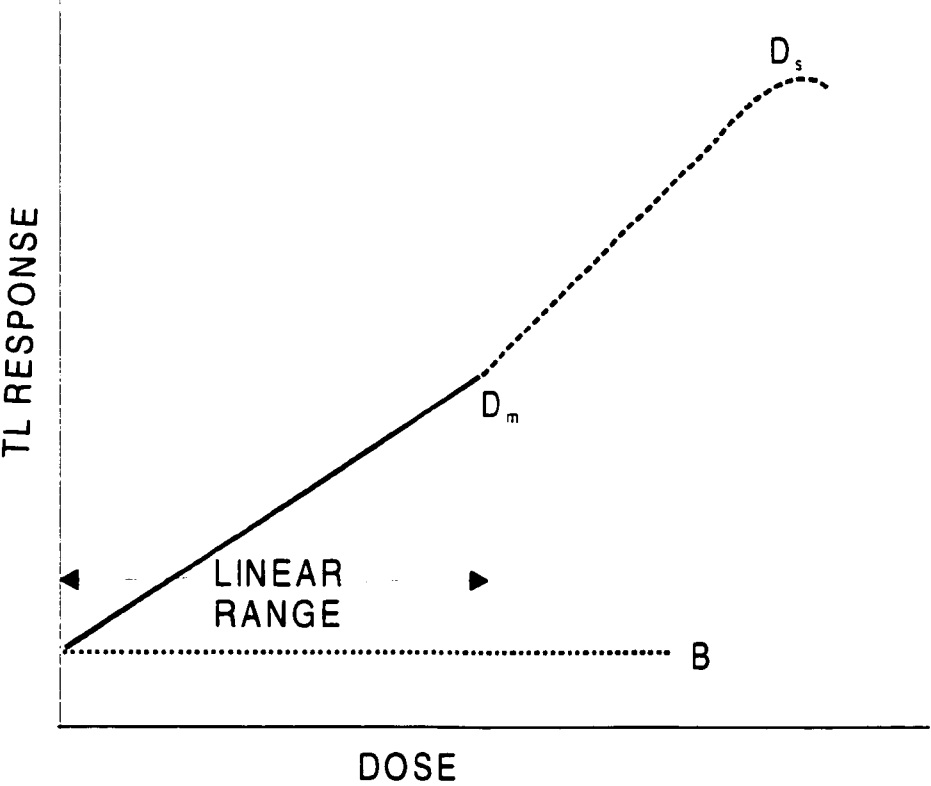


**Figure 2.4:** A typical dose linearity curve

The response is linear at relatively low absorbed doses. The TL signal for an absorbed dose  $D$  is

$$TL = fD + B, \quad (2.14)$$

where  $f$  is the TL emitted per unit absorbed dose and  $B$  is the background signal from the unirradiated phosphor.

For LiF, the linear portion extends up to approximately 100R (1R=1cGy) and at higher exposures becomes supralinear. Beyond the supralinear region, saturation sets in at about  $10^4$  R [Oberhofer & Scharmann, 1981], as there is a decrease in the number of available traps. To compensate for the supralinearity, new correction factors have to be introduced. Even though the sensitivity increases in this region, measurement accuracy decreases. Factors like the quality and type of radiation are also found to affect this non-linearity. Supralinearity is supposed to be caused because of either:

- the creation of additional trapping sites as a result of irradiation,
- the creation of new recombination centers,
- an increase in intrinsic efficiency.

A model was proposed by N. Suntharlingam [Suntharlingam & Cameron, 1969], which explains the existence of competing non-luminescent traps that have a higher capture cross-section for electrons but are fewer in number than TL traps. As the dose is increased, the non-luminescent traps saturate first, leading to enhanced activity at the TL traps. It is seen that for any particular phosphor, the supralinearity increases as the energy of the radiation becomes higher. The higher saturation levels accompanying this phenomenon may be due to less radiation damage. The upper dose limit for a detector is taken as 20% below the saturation value. Once the supralinear region is reached, the TL detector maintains the new sensitivity even after the readout process. A complete annealing of the detector has to be performed to

restore its initial sensitivity. Even then a complete restoration to the original state may not be possible due to the amount of damage suffered. This increased sensitivity of the supralinear region varies with annealing temperature.

A useful empirical formula for the correcting of supralinearity for LiF detectors is

$$C_{\text{supralin}} = [1 + aD + bD^2]^{-1}, \quad (2.15)$$

where D is the dose in Grays and the factors a and b are the regression values.  $C_{\text{supralin}}$  is the factor by which the reading is multiplied to correct for supralinearity [Williams and Thwaites, 1993]. This formula is found to work fairly well for doses up to 20 Gy.

### 2.2.4.3 Relative Energy Response

The relative energy response,  $S(E)$ , is a measure of the energy absorbed in a TL material in comparison to the energy absorbed in a reference material, when irradiated at the same exposure. For photons the energy response of a TL material is calculated as the ratio of the mass energy absorption coefficient of the dosimeter to that of air in the energy range up to 3 MeV,

$$S(E) = \frac{(\mu_{\text{en}}/\rho)_{\text{dosimeter}}}{(\mu_{\text{en}}/\rho)_{\text{air}}}. \quad (2.16)$$

Usually a single value for Co-60 gamma rays is specified. As the dosimeter can be made up of a mixture of different elements, its mass energy absorption coefficient is given as

$$(\mu_{en}/\rho)_{\text{dosimeter}} = \sum_i (\mu_{en}/\rho)_i w_i, \quad (2.17)$$

where  $(\mu_{en}/\rho)_i$  is the mass energy absorption coefficient of the  $i^{\text{th}}$  element and  $w_i$  is the fraction by weight of the  $i^{\text{th}}$  element in the phosphor. The mass energy absorption coefficient is a function of the photon energy and is dependent on the photon absorption and major interaction processes, photoelectric effect, Compton scattering, and pair production.

The energy response of a dosimeter is said to be good if its response per unit of exposure changes very little with photon energy. Since the photoelectric effect is the major interaction mechanism at low energies and is dependent on the atomic number  $Z$ , it is seen that phosphors with high atomic numbers show higher response at low photon energies up to several hundred keV. In the energy range of 20-10<sup>4</sup> keV in tissues, the Compton effect is most important.

#### 2.2.4.4 Fading

In a TL phosphor that has been irradiated with an ionizing radiation, there are electrons trapped in the various trapping levels. The release of these electrons on heating and the subsequent light emission when they combine with holes gives a measure of the absorbed dose. The release of the electrons may take place even in the absence of heating, and so a fraction of the original TL signal may be lost. This unintentional loss of electrons before readout is called fading. Fading is actually the decrease in the TL signal between irradiation and readout, and is caused by the electrons in the shallow traps moving into the stable state. There can be either thermal or optical (uv radiation or visible) fading.

Fading occurs mainly with electrons in shallow traps, hence it is always useful to eliminate these low temperature contributions. This is done by giving

a pre-irradiation anneal which reduces the magnitude of the low temperature peaks, and a pre-read anneal which fades away any filled low temperature traps. Another alternative is to process the glow curve to remove the contributions from the low temperature peaks [Pla & Podgorsak, 1983].

#### **2.2.4.5 Stability**

A phosphor selected for TL dosimetry must have good physicochemical stability. This calls for no changes during repeated irradiation and annealing. For this the glow curve and hence the TL yield must not change with time. The non-heating induced light emission causing fading at low temperatures must be insignificant, so that it does not change the output. In short, a TL phosphor is said to be stable if the glow curve, the fading rate and the TL yield do not change appreciably during extended storage of the material.

#### **2.2.4.6 Annealing**

The TL phosphor is annealed to remove all residual TL signal that may be stored even after readout. Heating for specified times and specified temperatures can change the number and configuration of traps in the phosphor. Also, heating can change the number of charge carriers (electrons and holes) in the traps. Annealing helps out in two ways in TL dosimetry. Firstly, it helps to completely empty out the electrons in the electron traps after an irradiation and readout cycle. Secondly, it helps to stabilize the electron traps so as to obtain the same glow curve even after repeated irradiation and thermal treatments. Annealing thus restores the initial



conditions after each TLD use. A typical sequence of events is as follows (Figure 2.5):

- low temperature anneal to empty shallow traps (pre-heat)
- TLD readout
- high temperature anneal to “reset” TLD
- irradiation.

Automated readers can often be set up to perform the annealing and readout operations concurrently.

#### **2.2.4.7 Glow Curve**

The luminescence or glow intensity from the electrons from a single trapping level, when plotted against the temperature gives the *glow curve* (Figure 2.6). At low temperatures the curve rises exponentially to a series of maxima known as the glow peaks, and then falls to zero. Either the main peak height (peak 5 for LiF) or the area under the curve can be taken as the relevant signal. As the height of the main glow peak depends on the heating rate of the dosimeter, it is required that extremely reproducible heat cycles be maintained. The low temperature peaks, which are subject to fading, are omitted in the glow curve analysis. The area and the height of each glow peak depend on the number of associated electron traps present. The amount of light released by the phosphor per unit of radiation exposure gives the thermoluminescent sensitivity.

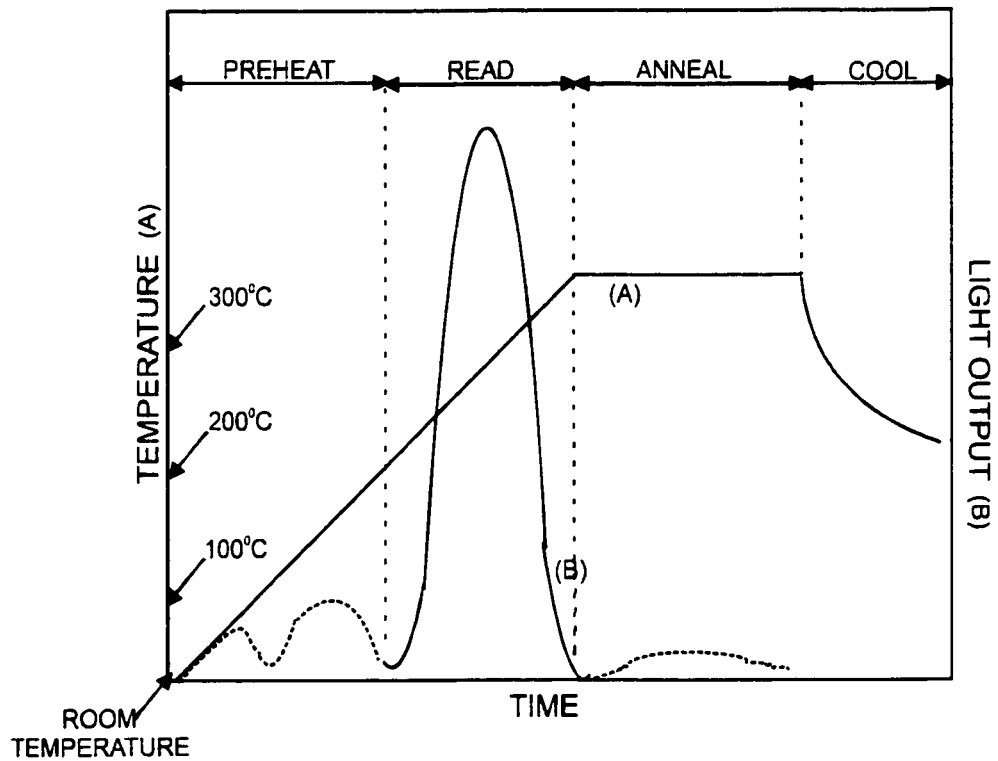


**Figure 2.5:** Programmable heat cycle showing pre-read, read and anneal. (A) Temperature, (B) Light output

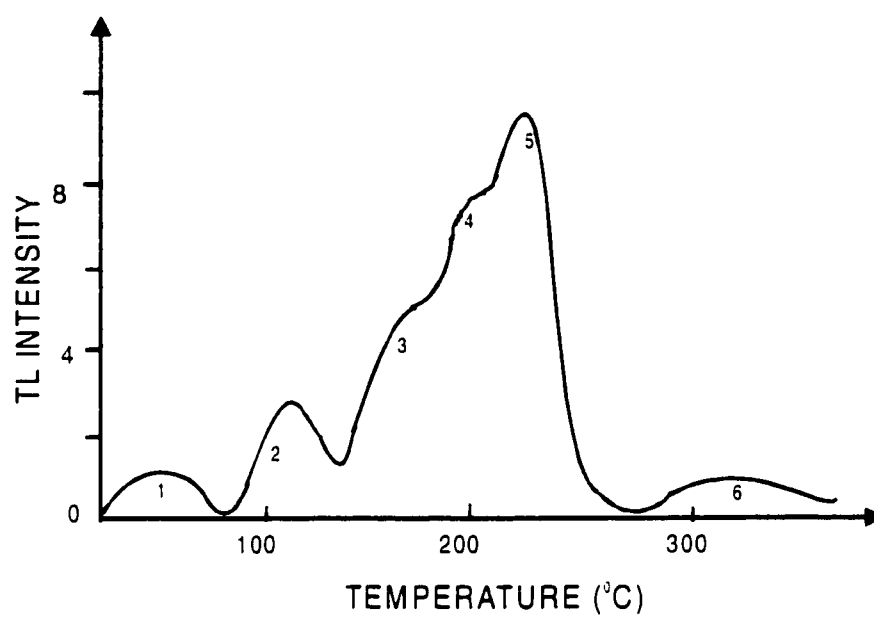


**Figure 2.6:** A typical TL signal obtained by heating a previously irradiated LiF (TLD-100) crystal.

#### **2.2.4.8 Background Signals**

Even under ideal conditions, there is some signal recorded from unirradiated dosimeters. This affects the sensitivity and the signal to noise ratio. The background signal is affected by a number of sources.

- **Dark current of the PMT:**

Dark current is the signal generated by the photomultiplier tube in the absence of light and ranges from  $10^{-10}$  amp to  $10^{-8}$  amp depending on the operating voltage. This phenomenon is due to the thermal emission of electrons from the cathode layer. Thus, the magnitude of the dark current can be reduced by operating the tube at low temperatures. Since changes in temperature affect the sensitivity, the tube should be kept at a constant temperature.

- **Residual signals from previous irradiations:**

Even after readout, some electrons may be trapped in very deep traps. Often they are removed by annealing the dosimeter. If they still persist, they may be released during a subsequent readout and contribute to the signal.

- **Background luminescence:**

Very slight luminescence can be produced by unirradiated dosimeters, arising from the movement of the crystal lattice (triboluminescence) or chemical interactions on the surface of the dosimeters (chemiluminescence). Any form of mechanical friction among the crystals induces triboluminescence. The surface tensions release their energy as light during the heating process, thereby introducing spurious signals in the readout. Chemiluminescence is due to the oxidation of contaminants on the surface during heating and can be reduced by clean handling or by performing the read-out in the presence of an inert gas like nitrogen, with no traces of oxygen

and water vapor. Both processes are related to the surface area and increase as the surface area increases, as for powder dosimeters and single crystals.

### 2.2.5 TLD Instrumentation

The irradiated TLDs are read for the information stored in them using a TLD reader. The different types of readers available in the market have essentially the same features (Figure 2.7).

- (a) A phosphor heating system
- (b) A light collection and detecting system
- (c) A signal-measuring system
- (d) A display and recording system

The precision of the TLD dose measurement is affected by the following factors [Pla & Podgorsak, 1983]:

- (a) physical properties of the TL material (dosimeter),
- (b) design of the analyzer (reader),
- (c) thermal treatment of the dosimeter (various combinations of pre- and post-irradiation annealing), and
- (d) the handling of the dosimeters during the full readout cycle by the user.

As a dosimeter is heated, it gives off light due to the recombination of electrons and holes. This TL light is collected by the photomultiplier tube and converted into an electrical current. The current is then integrated over the acquisition time to produce a charge integral, which is expressed in nC. Charge samples are also recorded in time channels and displayed as a glow curve. Charge values can be converted to dosimetric units through a reader calibration factor (RCF) expressed in  $\text{nC cGy}^{-1}$ . Thus, the RCF expresses in one variable the ability of the reader to convert stored thermoluminescent information characterizing a TLD exposure to measurable dose.

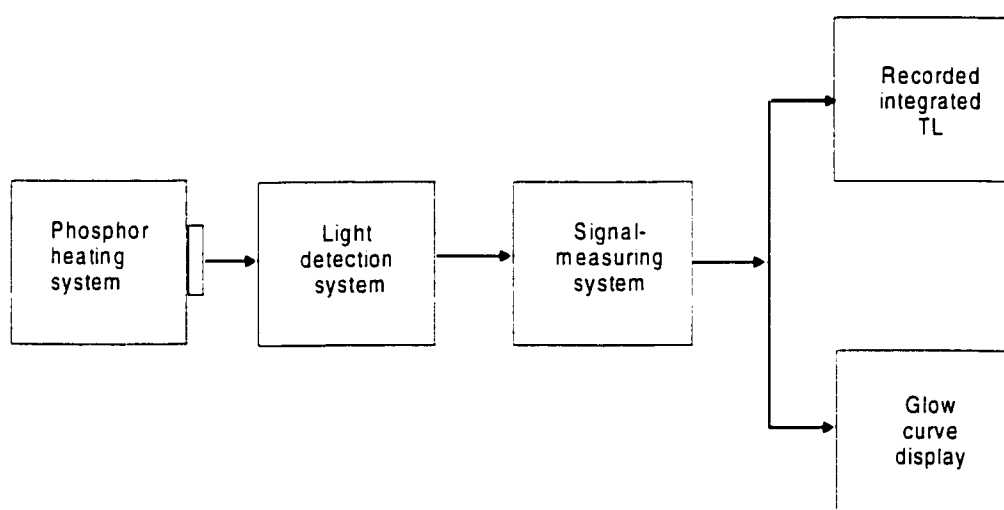


**Figure 2.7:** Block diagram of the TLD reader.

The RCF can be represented as

$$RCF = \frac{\langle Q \rangle}{D_{cal}}, \quad (2.18)$$

where  $\langle Q \rangle$  is the average reported charge of a set of calibration dosimeters exposed to a known dose,  $D_{cal}$ .

Another calibration factor is also needed because the TL efficiency is not the same for all the TL dosimeters. This dimensionless parameter is called the element correction coefficient (ECC). ECCs correct the sensitivity of each dosimeter in a population to the average sensitivity of the set. A variation of 10-15% in efficiency in a batch of TLDs can be reduced to 1-2% using ECC correction. The TL response (TLR) of a particular dosimeter, which is the measurement resulting from giving it one unit of ionizing radiation, is proportional to the TL efficiency.

$$TLR = k \times TLE, \quad (2.19)$$

where  $k$  is a common proportionality constant.

If  $Q_j$  is the charge reported by the reader for dosimeter  $j$  after being irradiated to  $n$  units, then the TLR of dosimeter  $j$  ( $j=1,2,\dots,m$ , where  $m$  is the number of dosimeters) is

$$TLR_j = \frac{Q_j}{n}, \quad (2.20)$$

The average TLR is

$$\langle TLR \rangle = \frac{\langle Q \rangle}{n}, \quad (2.21)$$

where

$$\langle Q \rangle = \frac{1}{m} \sum_{j=1}^{j=m} Q_j. \quad (2.22)$$

If  $ECC_j$  is the element correction coefficient for dosimeter  $j$  and  $TLE_j$  and  $TLR_j$  are the TL efficiency and TL response of dosimeter  $j$ , then

$$ECC_j = \frac{\langle TLE \rangle}{TLE_j}, \quad (2.23)$$

where

$$\langle TLE \rangle = \frac{1}{m} \sum_{j=1}^{j=m} TLE_j$$

This leads to

$$ECC_j = \frac{\langle TLR \rangle}{TLR_j}, \quad (2.24)$$

where

$$\langle TLR \rangle = \frac{1}{m} \sum_{j=1}^{j=m} TLR_j$$

Hence using equations (2.20), (2.21) and (2.24),

$$ECC_j = \frac{\langle Q \rangle}{Q_j}. \quad (2.25)$$

Since

$$\begin{aligned} RCF &= \frac{\langle Q \rangle}{D_{cal}}, \\ ECC_j &= \frac{RCF \times D_{cal}}{Q_j}. \end{aligned} \quad (2.26)$$



From this relation,

$$D_{cal} = \frac{Q_i \times ECC_i}{RCF}. \quad (2.27)$$

The proportionality constant k is

$$k = \frac{D_{cal}}{D_i}.$$

Thus the dose given is

$$D_i = \frac{Q_i \times ECC_i}{RCF \times k}. \quad (2.28)$$

## 2.2.6 Applications of TLDs

TLDs find application in many areas for the measurement of ionizing radiation because of their small size and ability to store information for quite a period of time.

### 1. Environmental applications:

TLDs are used near nuclear installations to find the radiation level as they have high reproducibility and low fading rate. Flight exposure levels can be measured using TLDs in aircraft.

### 2. Geological Activity:

The dating of ancient pottery, lava and lunar materials can be done since the amount of thermoluminescence emitted increases with age. After a piece of pottery is shaped, it is fired which removes any previously accumulated thermoluminescence in the quartz crystals that get mixed with

the clay used in making the pottery. The natural radioactivity irradiates the quartz crystals which acts as TLDs. The amount of thermoluminescence in the crystals helps to determine the date of firing and hence the age of the pottery. Similarly when a volcano erupts, the hot lava removes any past thermoluminescence. The TL phosphor (lava) which gets irradiated over a period of time shows the age of the lava when studied. The greater the thermoluminescence, the older the lava. [DeWerd & Stoebe, 1972]

### 3. Personnel monitoring:

TLDs, being tissue equivalent and convenient to wear, are used in personnel monitoring badges.

### 4. Medical applications:

TLDs find usage in diagnostic radiology and radiation therapy. In the former case, they are used for the measurement of radiation exposure to the staff mainly in mammography and fluoroscopy. In computer tomography (CT), they are used to study the spread of the x-ray beam and exposure received. The half value layer (HVL) of diagnostic x-ray machines can also be found using these dosimeters.

In radiation therapy, they are used to measure the doses to internal organs such as the uterus and outer organs like the eye to confirm accumulated and individual doses during a certain treatment period. In the area of quality assurance, they can be employed to perform beam uniformity checks, and to measure therapy machine output and absorbed doses in phantom.

## **2.3 Radiochromic Film Dosimetry**

### **2.3.1 Principle of Radiochromic Films**

Radiochromic systems are chemical radiation sensors consisting of solid or liquid solutions of colorless leuco dyes that become colored without the need for development when exposed to ionizing radiation [Muench, Meigooni & Nath, 1991]. They are available in various forms: thin films, thick films and gels, liquid solutions and liquid-core waveguides. Radiochromic film is a thin, high resolution 2D planar dosimeter, finding many applications in radiation oncology.

The concept of radiochromic films was successful because the silver halide films used conventionally for film dosimetry had a non-linear photon energy response at low energies, and radiation interaction properties different from those of tissues [Stevens, Turner, Hugtenburg & Butler, 1996]. Another disadvantage of silver halide film was that the post irradiation processing (e.g. chemical processing) of these films introduced a lot of variation in output. On the other hand, radiochromic films have a broad energy response up to a few hundred Gy, making them ideal for dose measurement in high dose gradient regions such as near a radioactive source, where the fall off is extreme and doses cover a wide range [Meigooni, Sanders, Ibbott, Szeglin, 1996]. The use of silver halide films and ionization chambers in these regions is limited because of their low useful dose range, energy dependence or large collecting volume.

The idea of the traditional radiochromic film was proposed by McLaughlin and Chalkey in 1965. These films had low sensitivity in the radiation therapy dose range, however their response to surface dose rates of a few  $\text{cGy sec}^{-1}$  was adequate and hence they could be used for measurements of Sr-90  $\beta$ -ray ophthalmic applicators.

Modern radiochromic film is much more versatile and convenient to use than its predecessors. The film is insensitive to visible light above 300nm

and hence there is ease of handling. It is about a hundred times more sensitive than traditional films. Saylor *et al.* observed a dose-dependent shift of visual absorbance versus absorbed dose for fixed wavelengths of 596-650nm (which are the two principal peaks of GafChromic film) [Saylor *et al.*, 1988]. The radiochromic film is made from low atomic number constituents such that it does not perturb the radiation beam as much as a silver halide film [Sayeg and Gregory, 1991]. The response of the film is independent of the dose rate.

### 2.3.2 The GafChromic Film

The GafChromic film employed for the experiments reported here is a high-resolution image-forming film indicating the dose in two dimensions. The thin radiosensitive layers of the film are made of a colorless gel containing microcrystals of polycrystalline substituted diacetylene monomer about 15  $\mu\text{m}$  in size and coated on an inner mylar base about 25  $\mu\text{m}$  thick.

The GafChromic film is composed of seven layers<sup>†</sup> [Klassen, Zwan, Cygler, 1997]. The two outer mylar layers which are 67  $\mu\text{m}$  thick, are stuck to the centerpiece with a layer of glue, which is a pressure sensitive adhesive, having a thickness of 44.5  $\mu\text{m}$ . The radiosensitive gel is sandwiched between the outer mylar layer and the glue. The mylar layers are clear, the glue is grayish and the radiosensitive gel is light blue when unirradiated and darker when irradiated. The gel undergoes partial polymerization that produces a blue dye polymer on irradiation with any ionizing radiation. The reaction is initiated by single events in which energy is transferred from an energetic photon or particle to the receptive part of the photomonomer molecule. Thus, here the single event producing a polymerization process is in fact creating changes in many molecules, leading to an amplification or gain.

---

<sup>†</sup> GAF Chemicals Corp., Wayne, New Jersey

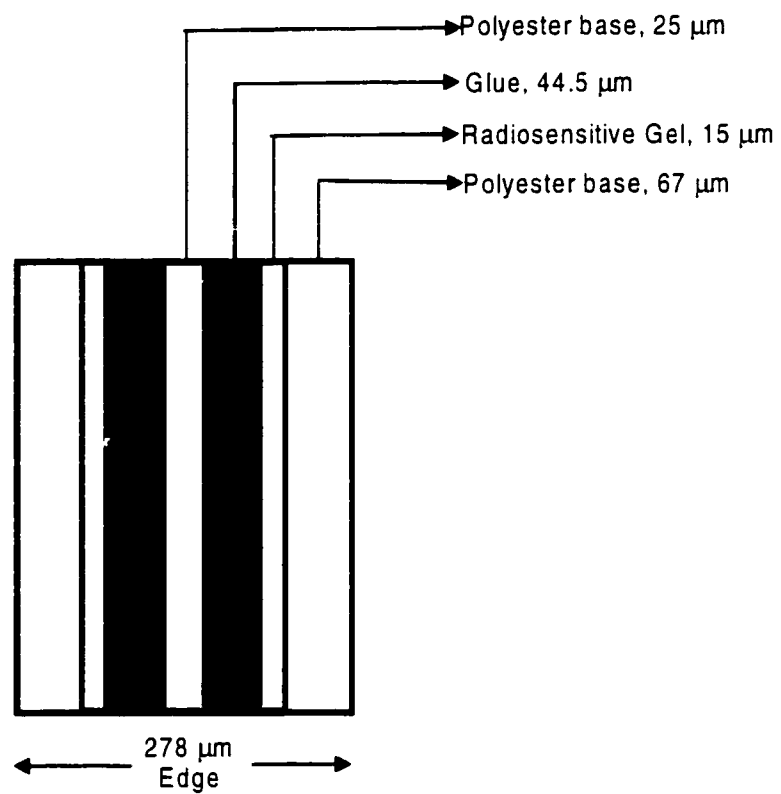


**Figure 2.8:** Schematic view of the structure of GafChromic MD-55-2 (not to scale)

The transparent radiochromic film has a light blue hue. It turns more bluish as soon as it is exposed and this blue tint increases with the amount of radiation exposure. The optical density due to the polymer increases with the absorbed dose without any physical, chemical, or thermal treatment. This blue coloration means that the broad band light source of a conventional densitometer is only attenuated in the red part of the spectrum, and the varying degree of blue color in the resultant image formed on the film indicates the dose in two dimensions. It takes a while for the emulsion sensor to stabilize and hence the film should be read at least two days after irradiation [Chiu Tsao, Zerda, Lin, Kim, 1994]. The optical density can change by 16% in the 24 hours immediately after irradiation.

The film can register radiation fluence with fine spatial resolution and low spectral sensitivity, and hence is useful for dosimetry in regions with a steep dose gradient, such as the penumbra. These features of a 2D dosimeter are put to use in stereotactic radiosurgery [McLaughlin *et al.*, 1994]. Radiochromic films also help in the mapping of dose distributions around brachytherapy sources, as they can record the incident radiation at closely spaced points simultaneously, and close to the source.

The irradiated films can be scanned using densitometers or document scanners. The sensitivity or the net optical density of the film per unit absorbed dose can be measured over a wide dose range. If  $I_0$  is the scanner signal for an unexposed film, that is the “dark current”, and  $I$  the scanner signal for the film at the point of interest, then the net optical density of the film is

$$OD = \log_{10} \left( \frac{I_0}{I} \right). \quad (1.5)$$

The optical density is reported to have a power law relation to the dose D.

$$\log_{10}\left(\frac{I_0}{I}\right) = aD^\alpha, \quad (2.29)$$

where  $a$  and  $\alpha$  are constants.

To find the constants, take the logarithm of this equation,

$$\ln\left[\log_{10}\left(\frac{I_0}{I}\right)\right] = \ln(a) + \alpha\ln(D).$$

If a plot is made of  $\ln[\log_{10}(I_0/I)]$  against  $\ln(D)$ , then the result is a straight line with slope  $\alpha$ , intercept  $\ln(a)$  and a linear regression coefficient  $r$ . A linear fit to the calibration data gives the constants  $\alpha$  and  $a$ .

Solving for D:

$$D = \left[\frac{1}{a}\log_{10}\left(\frac{I_0}{I}\right)\right]^{1/\alpha}. \quad (2.30)$$

On applying this relation to each element of the scanner signal data matrix, the measured scanner signal is converted to a dose matrix [Stevens, Turner, Hugtenburg & Butler, 1996]. Though an ideal 2D dosimeter yields a uniform response on being exposed to a uniform irradiation field, non-uniformities up to 15% have been reported. [Meigooni, Sanders, Ibott, 1996]. The films have to be kept clean as they have a tendency to pick up dust because of the static charges on the outer mylar layers.

## 2.4 I-125 Seed Dosimetry

### 2.4.1 Description of I-125 Seeds

Sealed sources of radioactive I-125 are widely used in temporary and permanent brachytherapy implants to manage localized cancers at a variety of anatomical sites. This approach is used in transperineal permanent implants of cancer of the prostate and the treatment of apical lung and pancreatic carcinoma. This radiation modality has been also employed in the treatment of glioblastoma multiforme, ocular tumors, and head and neck tumors in the form of temporary implants.

I-125 is produced in a nuclear reactor when Xe-124 absorbs a neutron to become Xe-125, which then undergoes electron capture (half-life 18 hours) to form I-125. I-125 decays by electron capture to an excited state of Te-125, which de-excites by internal conversion. The electron capture and internal conversion results in the removal of atomic electrons, leading on average to the emission of 1.47 characteristic x-rays per decay with energies from 27.4 to 31.4 keV, and 0.07 gamma rays per decay with an energy of 35.5 keV [Ahmad *et al.*, 1992]. The mean energy hence is about 28.33 keV. The half-life of I-125 is 59.4 days. The exposure rate and air kerma rate constants for an ideal point I-125 source are  $1.51 \text{ R cm}^2 \text{ mCi}^{-1} \text{ hr}^{-1}$  and  $1.0 \text{ cGy cm}^2 \text{ mCi}^{-1} \text{ hr}^{-1}$  [Nath *et al.*, 1995]. Because of the low energy of the I-125 and Te-125 x and  $\gamma$  rays and the associated ease in radiation shielding, I-125 finds use as a substitute for Cs-137 and Ir-192 in temporary implants. Its small half-value layer (0.025-mm Pb), assists in the shielding of medical personnel, visitors, and radiosensitive healthy tissue distant from the implanted area (HVL in water is 20mm) [Ahmed *et al.*, 1992].

The major drawback of the radionuclide in clinical applications is a complex dosimetry and corresponding dose rate uncertainty caused by a



severe anisotropy when encapsulated as a cylindrical seed, loss of back scatter and tissue-type dependence [Luxton *et al.*, 1990].

Lawrence Soft X-ray Corporation clinically introduced I-125 seeds in the 1970s and the first clinical applications were pioneered at the Memorial-Kettering Institute in New York. There are several types of encapsulated sources currently available in North America. The three models available from the leading supplier, Nycomed-Amersham<sup>†</sup>, are designated as models 6702, 6711, 6712. They are identical in size and encapsulation, the only difference being in the internal design. The model 6702 seed consists of I-125 adsorbed on the surface of three resin ion-exchange spheres encapsulated within a titanium tube. Model 6702 is not easily visible on a radiograph, though the titanium end welds can be seen if the surrounding tissue is not thick. These higher activity seeds have been used as temporary interstitial implants in the brain and in eye plaques. The seed strengths usually range from 6.4 to 51.9  $\mu\text{Gy m}^2 \text{h}^{-1}$  (5-40.9 mCi) [Chiu-Tsao, 1990].

#### **2.4.2 Model 6711 I-125 Seed**

A model 6711 seed consists of I-125 adsorbed as silver iodide onto the surface of a radiopaque silver wire 0.5 mm in diameter and 3 mm long. This source is primarily used in permanent implants where a relatively low dose rate is required. This distribution of AgI could be non-uniform enough to cause ~20% variation in the radiation intensity in the equatorial plane of the seed. The encapsulation made of titanium is 0.05 mm thick with both ends welded. The electrons and gamma rays liberated with energies below 5 keV are absorbed by the titanium shell. The overall outer dimensions are 4.5 mm long x 0.8 mm in diameter.

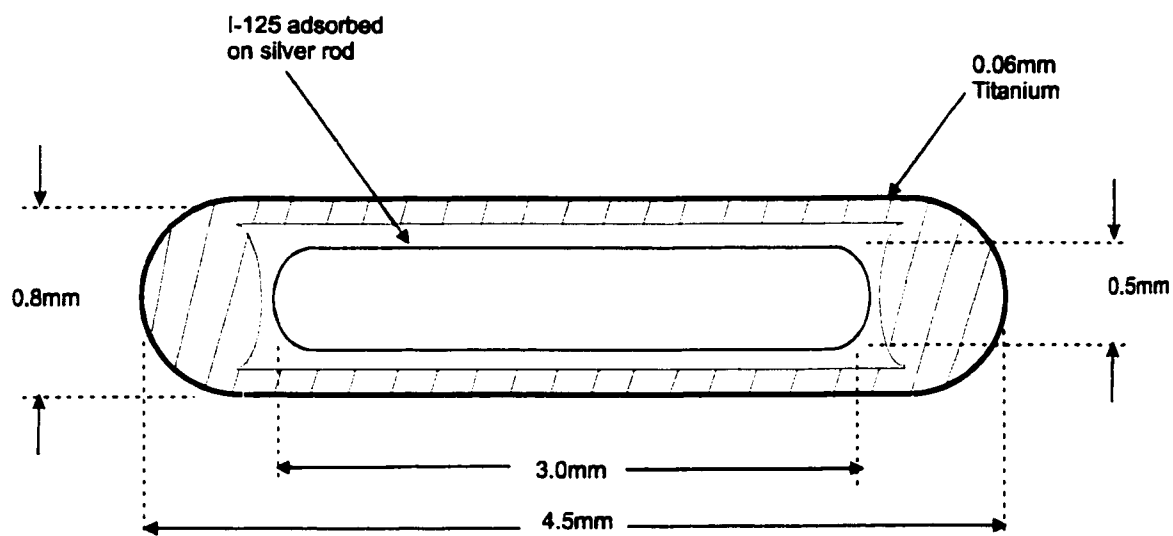
---

<sup>†</sup> Nycomed-Amersham, Oakville, Ontario

The photon spectrum of model 6711 seeds contains mainly three peaks, the 27.4 keV  $k_{\alpha}$ , the 31.4 keV  $k_{\beta}$  and the 35.5 keV gamma, with two additional peaks at 22.1 keV and 25.2 keV. These two peaks are due to fluorescent photons resulting from the interaction of I-125 photons with the silver wire, which absorbs about half of the photons emitted by the I-125. This lowers the average energy to 27.4 keV from 28.4 keV for the original spectrum. Because of the photon interaction in the seed, the manufacturer states the source strength as the "compensated" activity based on the exposure rate measured in the transverse plane. These seeds are available at air kerma strengths in the range of 0.13 to 7.58  $\mu\text{Gy m}^2 \text{h}^{-1}$  (0.1 - 5.99 mCi).

The model 6711 seed offers some advantages over the model 6702. As a result of the increased mass of the silver wire, the radiopacity is increased so that the seed orientation within the implant is readily visible from orthogonal radiographs. This makes easier the identification and localization of I-125 seeds in deep-seated implants. It is found that the movement of the silver wire inside the titanium encapsulation is less compared to the models having resin spheres, thus making the dosimetry more reliable. As the seed orientation can be determined, the anisotropic dose distribution pattern of individual seeds can be included in the dosimetric computations. The end welds cause the photon fluence around the seeds to be quite anisotropic. The model 6712 is 38% thinner than the 6711 so as to match the diameter of Ir-192 seeds [Ahmad *et al.*, 1992].

Longitudinal view of Model 6711 I-125 seed:



Transverse view of Model 6711 I-125 seed:

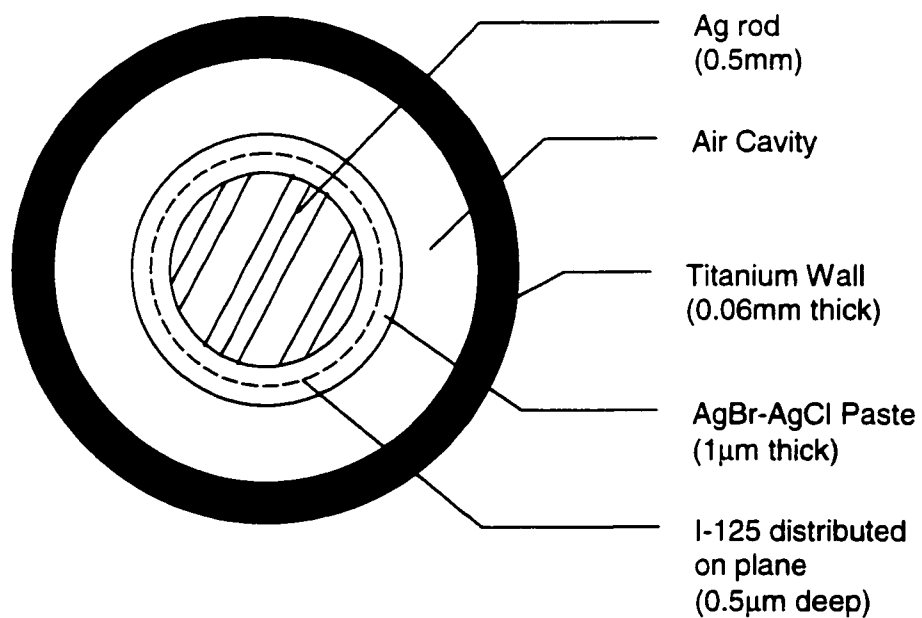


**Figure 2.9:** Geometric models of the longitudinal and transverse views of the interstitial I-125 seeds [Williamson, 1991].

## **2.5 Ophthalmological Applicators**

### **2.5.1 Usage**

Encapsulated radioactive sources have, for many years, found application in the treatment of superficial lesions. Postoperative treatment of certain diseases of the eye by contact radiotherapy utilizing beta-emitting isotopes has been found successful in preventing recurrence of the lesion [Goetsch & Sunderland, 1991]. Some of the ophthalmological conditions thus treated are pterygium, the vascularisation or ulceration of the cornea, and certain intraorbital malignancies like ocular melanoma. Pterygia are wing-shaped fibrovascular proliferations of the bulbar conjunctiva onto the sclera of the human eye. Though benign, they grow onto the cornea and can lead to the obstruction of vision. They often recur after surgical removal. This potential is reduced effectively by postoperative beta irradiation using brachytherapy techniques, by which high doses are delivered to the affected area [Glecker, Valentine, Silberstein, 1998]. This is done by positioning small radioactive applicators on or near the sclera for a short period of time. The beta rays penetrate only the superficial layers of the body tissues. In such a treatment the important clinical parameters to be specified are the surface dose, depth dose, field uniformity and protocols for dose delivery.

### **2.5.2 Sr-90 Eye Applicator**

Strontium-90, a long-lived fission fragment, was first used clinically by Friedell in 1950 as a beta-ray applicator for radiotherapy of the eye, and was then marketed by Tracerlab (model RA-1) [Goetsch & Sunderland, 1991]. It replaced radium as a means of treatment for eye diseases.

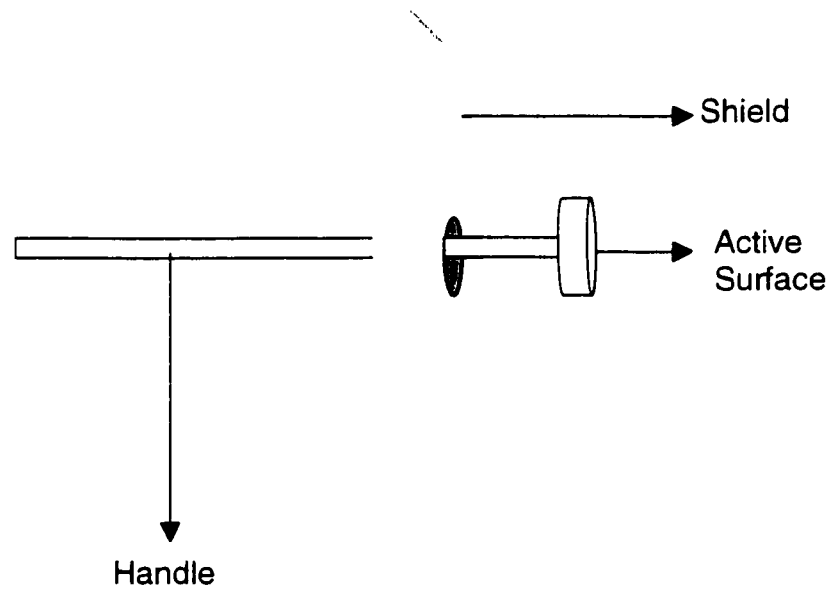


**Figure 2.10:** A Sr-90 ophthalmic applicator

The applicator often has a standard shape: a cylindrical metallic rod on one end of which is mounted a distributed source of Sr-90 in equilibrium with Y-90, bonded in a silver foil. The source is protected by covering it with 0.08 mm of monel and sealed by a double hermetic seal [Ali & Khan, 1990]. The main advantages of these applicators over Ra-226 applicators are the very low gamma ray contamination and an absence of gaseous decay products. Another advantage is that the betas coming from the Sr-90/Y-90 decay scheme have very short range. The problem with the previously used radon applicators was that they were sealed in glass bulbs, whose shapes were not replicated exactly thereby causing changes in dosimetry. In addition, the fluence of gamma rays escaping from the bulb was unacceptable.

Sr-90 applicators have either a flat or a concave active surface so as to fit the contour of the eye. The concave shape also gives a focussing effect so that the depth dose along the axis is higher. Sr-90 has a half-life of 28 years and decays by beta emission with a maximum energy of 0.546 MeV to the radioactive daughter Y-90. Y-90 also decays by beta emission with a half-life of 64 hours and a highly penetrating beta of maximum energy 2.283 MeV to form Zr-90 [Reft *et al.*, 1990]. The half value thickness in tissue is about 1mm. This decay scheme is accompanied by a negligible amount of gamma radiation. The steel encapsulation filters out the low energy beta radiation from the Sr-90/Y-90 source.

Figure 2.11 shows the depth dose measurements for various beta applicators. The percent depth dose is given along the vertical axis and the positions of the various parts of the eye along the horizontal axis. The curve for radium is seen to drop to 10% at 1 mm and 1% at 2 mm. The relative dose for radon drops to 30% at 1 mm and 5% at 3 mm. The averaged curve for the Sr-90 applicators shows that the dose falls to 43% at 1 mm, 19% at 2 mm and to 5% at 4 mm.

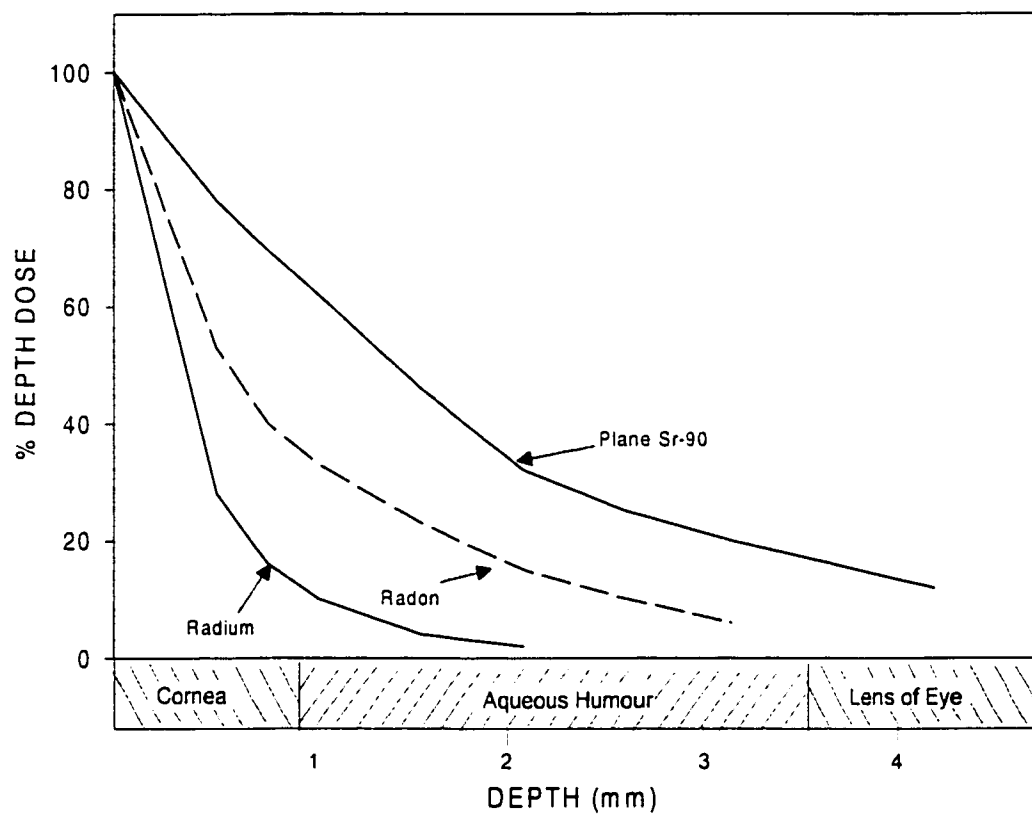


**Figure 2.11:** Depth dose data for beta ray applicators [Johns & Cunningham, 1983].

The dose rate at the center of an applicator surface may be as high as  $100 \text{ cGy s}^{-1}$ . The dose rate may vary greatly across the surface of an applicator and can be made more uniform by constructing a compensating filter designed to fit over the end of the applicator. The dose rate from a beta ray applicator decreases to about 5% of the surface dose rate at a depth of about 4 mm, the average depth of the lens below the cornea. The surface dose rate was previously expressed as REB  $\text{s}^{-1}$  or Roentgen-Equivalent-Beta per sec. It corresponds to a beta ray energy deposition of  $87 \text{ ergs g}^{-1}$  of air [Sayeg, Gregory, 1991]. The correction factor to Gy in water is

$$\begin{aligned} \text{REB} &= 87 \times 10^{-4} \text{ J/Kg} \times 1.0\text{Gy}/(\text{J/Kg}) \times 1.12 \\ &= 9.7 \times 10^{-3} \text{ Gy (H}_2\text{O)} \end{aligned} \quad (2.31)$$

where 1.12 is the mass collision stopping power of water relative to air for an effective energy of 0.78 MeV. The surface dose rate for an ophthalmic applicator is used to determine the lens and sclera dose. The National Institute of Standards and Technology (NIST) has presently defined the surface dose rate as "the dose rate to an infinitesimal layer of water at the exact surface of the applicator" [Pruitt, Soares, Ehrlich, 1988]. Hence the dose to the sclera can be estimated knowing the surface dose rate and duration of irradiation. The accurate estimation of the lens dose is made complicated due to various factors: (1) the variability in the placement of the applicator; (2) the uncertainty in the percent depth dose for the particular applicator which is usually not provided by the manufacturer; (3) variability in the duration of exposure; (4) inconsistent applicator characterization and calibration; (5) insufficient follow-up times after the complete treatment; and (6) depth of the lens in a particular patient which is usually not measured, leading to uncertainty in the spatial distribution of the dose throughout the eye. Hence individual eye treatments in different institutions typically result



in different lens doses in the range between 1000-7200 cGy [Glecker, Valentine, Silberstein, 1998].

## References

1. American Association of Physicists in Medicine(AAPM) Report No.21: "Recommendations of AAPM Task Group 32: Specification of Brachytherapy Source Strength" (American Institute of Physics, New York, 1987)
2. Ahmad M., Fontenia D.P., Chiu-Tsao S., Chui C.S., Reiff J.E., Anderson L. L., Huang D.Y.C., Schell M.C., Diode dosimetry of models 6711 and 6712  $^{125}\text{I}$  seeds in a water phantom , *Medical Physics*, 19(2), 391-398 (1992)
3. Ali M.M., Khan F.M., Determination of surface dose rate from a  $^{90}\text{Sr}$  ophthalmic applicator, *Medical Physics*, 17(3), 416-421 (1990)
4. Anderson L.L, Nath R., Weaver K.A., Nori D., Phillips T.L., Son Y.H., Chiu Tsao S., Meigooni A.S., Meli J.A., Smith V., "Interstitial Brachytherapy - Physical, Biological, and Clinical Considerations", Interstitial Collaborative Working Group, Raven Press, New York, (1990)
5. Chiu-Tsao S., Anderson L.L., O'Brien K., Sanna R., Dose rate determination for I-125 seeds, *Medical Physics*, 17(5), 815-825 (1990)
6. Chiu-Tsao S., Zerda A., Lin J., Kim J.H., High-sensitivity GafChromic film dosimetry for  $^{125}\text{I}$  seeds, *Medical Physics*, 21(5), 651-657 (1994)
7. DeWerd L.A., "Applications of Clinical Thermoluminescent Dosimetry", Refresher Course Material TH-B5-01.T, (1996)
8. DeWerd L.A., Stoebe T.G., Thermoluminescent properties of solids and their applications, *American Scientist*, 60, 303-310 (1972)
9. Glecker M., Valentine J.D., Silberstein E.B., Calculating lens dose and surface dose rates from Sr-90 ophthalmic applicators using Monte Carlo modeling, *Medical Physics*, 25(1), 29-36 (1998)
10. Goetsch S.J., Sunderland K.S., Surface dose rate calibration of Sr-90 plane ophthalmic applicators, *Medical Physics*, 18(2), 161-166 (1991)

11. Johns H.E. and Cunningham J.R., "The Physics of Radiology", 4<sup>th</sup> Edition, Springfield, Illinois (1983)
12. Klassen N.V., Zwan L., Cygler J., GafChromic MD-55: Investigated as a precision dosimeter, *Medical Physics*, 24(2), 1924-1934 (1997)
13. Luxton G., Astrahan M.A., Findley D.O., Petrovich Z., Measurement of dose rate from exposure-calibrated <sup>125</sup>I seeds, *International Journal of Radiation Oncology, Biology and Physics*, 18, 1199-1207 (1990)
14. McKinlay A.F., "Thermoluminescent Dosimetry: Medical Physics Handbook 5", Adam Hilger Ltd, Bristol(1981)
15. McLaughlin W.L., Soares C.G., Sayeg J.A., McCullough E.C., Kline R.W., Andrew Wu, Maitz R.W., The use of a radiochromic detector for the determination of stereotactic radiosurgery dose characteristics, *Medical Physics*, 21(3), 379-388 (1994)
16. Meigooni A.S., Sanders M.F., Ibbott G.S., Szeglin S.R., Dosimetric characteristics of an improved radiochromic film, *Medical Physics*, 23(11), 1883-1888 (1996)
17. Muench P.J., Meigooni A.S., Nath R., McLaughlin W.L., Photon energy dependence of the sensitivity of the radiochromic film and comparison with silver halide film and LiF TLDs used for brachytherapy dosimetry, *Medical Physics*, 18(4), 769-775 (1991)
18. Nath R., Anderson L.L., Luxton G., Weaver K.A., Williamson J.F., Meigooni A.S., Dosimetry of interstitial brachytherapy sources: Recommendations of AAPM Radiation Therapy Committee Task Group No. 43, *Medical Physics*, 22(2), 209-234 (1995)
19. NCRP Report No. 41, "Specification of gamma ray brachytherapy sources", Washington DC, (1974)
20. Oberhofer M., Scharmann A., "Applied thermoluminescent dosimetry", Adam Hilger Ltd, Bristol (1981)
21. Pla C., Podgorsak E.B., A computerized TLD system, *Medical Physics*, 10(4), 462-466 (1983)

22. Pruitt J.S., Soares C.G., Ehrlich M., "Calibration of beta particle radiation instrumentation and sources", NBS special publication, 250(21), (April 1988)
23. Reft C.S., Kuchnir F.T., Rosenberg I., Myrianthopoulos L.C., Dosimetry of  $^{90}\text{Sr}$  ophthalmic applicators, *Medical Physics*, 17(4), 641-646 (1990)
24. Sayeg J.A., Gregory R.C., A new method for characterizing beta-ray ophthalmic applicator sources, *Medical Physics*, 18(3), 453-461 (1991)
25. Saylor M.C., Tamargo T.T., McLaughlin W.L., Khan H.M., Lewis D.F., Schenfele R.D., "A thin film recording medium for use in food irradiation", *Radiation in Physics and Chemistry*, 31, 529-536 (1988)
26. Stevens M.A., Turner J.R., Hugtenburg R.P., Butler P.H., High resolution dosimetry using radiochromic film and a document scanner, *Physics in Medicine and Biology*, 41, 2357-2365 (1996)
27. Suntharlingam N., Cameron J.R., *Physics in Medicine and Biology*, 14, 394, (1969)
28. Wang R., Sloboda R.S., Influence of source geometry and materials on the transverse axis geometry of Ir-192 brachytherapy sources, *Physics in Medicine and Biology*, 43, 37-48, (1998)
29. Williams J.R., Thwaites D.I., "Radiotherapy Physics in Practice", Oxford Medical Publications, (1993)
30. Williamson J.F., Comparison of measured and calculated dose rates in water near I-125 and Ir-192 seeds, *Medical Physics*, 18(4), 776-785 (1991)

## **CHAPTER 3**

### **3 MATERIALS AND METHODS**

This chapter provides details about the materials and the methods used in the experimental work. Information is given about the Sr-90 applicators and the model 6711 I-125 seed and the instrumentation employed. The preliminary experiments conducted, the dosimetric considerations for data collection and the calculation methodology are described.

#### **3.1 Sr-90 Ophthalmic Applicator Dosimetry**

Superficial lesions have long been treated using sealed radioactive sources. Certain diseases of the eye are treated using Sr-90 applicators. These beta-emitting isotopes have to be calibrated accurately as the dose distribution around the source will be quite complex. The four applicators used in this study were the SIA K964, SIA K610, SIA K965, and SIA 20<sup>†</sup>. The detector chosen to study the surface dose rates of these sources was radiochromic film. The exposed films were imaged using a document scanner. The performance of the film and the scanner was assessed prior to their use.

---

<sup>†</sup> Amersham Healthcare, Arlington Heights, IL

### 3.1.1 SIA 20 Ophthalmic Applicator

An SIA 20 Sr-90 pterygium applicator, serial # 0960ML, from Amersham International was used to make most of the measurements. The surface dose rate quoted by the manufacturer was  $64.8 \text{ rads s}^{-1}$  as on 26<sup>th</sup> April 1996. This dose rate is quite high and hence the applicator is capable of delivering a therapeutic dose in a very short time.

The SIA 20 applicator contains an insoluble Sr-90 compound incorporated in a rolled silver disc with a face thickness of 0.05 mm and fabricated into a stainless steel cylinder having a window thickness of 0.05 mm. This steel holder is attached to a 15 cm long stainless steel shaft onto which is mounted a plastic shield, for shielding the operator (see Figure 2.10). It has a diameter of 9 cm and thickness about 0.95 cm. The shaft allows the active head to be rotated through  $180^\circ$ . The nominal active diameter is 8.5 mm. The inactive back of the cylinder is thick enough to absorb the beta particles. Although the beta radiation is emitted only from the front face of the applicator, x-rays are produced in all directions by the interaction of beta particles with the metal of the device. The source is supplied with a stainless steel cap for safety during storage and is removed for treatment. The entire source assembly is stored in a shielded housing fitted inside a wooden box. The energy spectrum and spatial distribution of the beta rays from the applicator are complex. The inner aluminum and outer stainless steel filters, separating the source and irradiated object, serve to make the surface dose rate more uniform and also attenuate the higher energy beta rays.

### 3.1.2 GafChromic Film

The films employed here were the GafChromic dosimetry media from Nuclear Associates<sup>‡</sup>, type MD-55-2, model no: 37-041, Lot #90116 and 37051. A black light-tight envelope contains 10 films each of size 5" x 5" and 278  $\mu\text{m}$  in thickness. Non-uniformity arises due to local fluctuations of the film response with respect to the mean response. Factors affecting this change are the pixel size, pixel depth, film grain size, and spatial and signal resolution of the film scanner and electronic noise. Non-uniformity is also affected by regional variations arising from any scanner problem or any non-uniformity in the emulsion layers of the film [Niroomand-Rad *et al.*, 1998]. The film is quite insensitive to ordinary room light and hence these films can be irradiated in normal lighting conditions. The dose on the film is known from the varying amount of bluish color that it acquires after irradiation. It takes about two days for the emulsion on the film to stabilize and hence it is not read immediately after being irradiated. This film is found to give very good spatial resolution and can be used in regions where the dose gradient is steep. For this reason, the films have to be read using a high-resolution device. The suitability of using a document scanner [Stevens *et al.*, 1996] for this purpose was ratified in this work.

The scanner used was a flatbed type Hewlett Packard Scanjet 5p<sup>†</sup>, which offers a resolution of 600 dots per inch (dpi). The light source in the scanner is a single xenon lamp. The scanner was operated using the software package Hewlett Packard Desk Scan II for windows. Various parameters were set in the scanning software so as to provide optimum operating conditions. Stevens *et al.* in 1996 reported that the variation of intensity with dose for the red component is more when using the color mode and that the dose-intensity relationship was much smoother when using the

---

<sup>‡</sup> Nuclear Associates, Carle Place, New York

<sup>†</sup> Hewlett-Packard Company, Boise, Idaho

black and white mode. The choice of the picture type is important as it influences the quality of the final image and size of the scanned file. Hence, the picture type was set to be in the *black and white photograph* mode. The black and white photograph imaging mode had shades of gray in addition to the black and white areas. The scans are presented in a gray-scale of 256 elements where a white object takes the value of 256 and a black object that of one. The scanning parameters such as contrast and brightness were selected so as to include a wide range of scan values for the different parts of the irradiated film.

### 3.1.3 Dosimetry System Performance

A single 5" x 5" sheet of GafChromic film was cut into smaller pieces of area 3 x 2 cm<sup>2</sup>. The top surface of each strip was marked. After irradiation with a dose of 30 Gy using the SIA 20 ophthalmic applicator, the films were stored away from ambient fluorescent light to reduce any potential errors due to post-irradiation coloration. These films were handled delicately as any scratch on the surface could alter the optical density. Each set of experiments had a control group of two filmstrips cut in the same dimension. They were stored unirradiated at room temperature to provide a background optical density. The radiochromic films were read with the HP Scanjet 5p scanner, as high resolution is required. Published data shows that fluorescent light from devices like document scanners can produce distinct scans with no significant additional coloration of the GafChromic film [Butson *et al.*, 1998].

Diverse experiments were conducted to verify the validity of using the document scanner for the read-out of the radiochromic films. The following studies were made on the HP Scanjet 5p.



### **3.1.3.1 Best Operating Settings**

Some small filmstrips irradiated to 30 Gy using the SIA 20 applicator were used for setting the operating parameters of the scanner. Since optical density changes considerably in the first 24 hours following irradiation, a waiting period of 48 hours was chosen. The filmstrips were then scanned at the same time. The films were read several times with different functioning values set in the scanner. An optimal “path” was obtained when the black and white photograph mode was set at a resolution of 600 dots per inch (dpi). Brightness and contrast values of 170 and 180 were selected.

### **3.1.3.2 Film side dependence**

The film's dependence on the side of irradiation was evaluated before its performance study. Two filmstrips were irradiated with 20 Gy and 45 Gy and another two with the same doses but on the opposite side. The films were read after the delay time using the same set parameters.

### **3.1.3.3 Temporal Stability of scanner**

It is advantageous if the scanner gives the same measurement when reading the same film at different times. Two filmstrips cut into 3 x 2 cm<sup>2</sup> pieces were placed on a lucite block and irradiated one at a time, using an SIA 20 Sr-90 source at the center to a dose of 30 Gy. Two more strips were cut for measuring the background optical density. These strips, the irradiated and the controls, were stored at room temperature away from light for 48 hours. The scanned images were analyzed using the MATLAB software

package<sup>†</sup> (version 5.2.0.3084). The processed images are stored by MATLAB in the form of matrices, each element of the matrix corresponding to a single pixel in the image. The image processing toolbox accompanying the package supports a number of operations: image display, filtering, analysis of image data and image transformation. A small portion in the center of the image of the Sr-90 source was signal averaged to find the mean scanner signal corresponding to the given dose. The films serving as background monitors were read using the same brightness and contrast parameters at the same spatial locations on the scanner bed.

The net optical density was then calculated as

$$OD = \log_{10} \left( \frac{I_0}{I} \right), \quad (1.5)$$

where  $I_0$  is the background signal and  $I$  is the scanner signal from the irradiated film. The films were scanned daily for a period of 2 weeks to check temporal stability.

### 3.1.3.4 Spatial Stability of Scanner

The spatial variance of the scanner bed was investigated to decide on an optimal position during readout. As before, the 3 x 2 cm<sup>2</sup> strips were irradiated to 30 Gy and placed at different positions on the scanner. A cardboard mask was made to station the films at various locations. A number of cutouts of the same dimension as that of the films were made on the 22 x 27 cm<sup>2</sup> cardboard piece which covered a major portion of the scanner bed. The films were read after being positioned in all the cutouts in the template.

---

<sup>†</sup> The Mathworks Inc., Natick, MA

The background filmstrips were also read in all the locations. The evaluation of optical density was done using Equation 1.5.

### **3.1.4 Applicator Dosimetry**

The dose gradient near a brachytherapy source is complicated due to the presence of high dose gradients and severe hot spots. Unlike other dosimetry tools, radiochromic films have a broad response range that helps in the measurement of the steep dose fall off near the radioactive source.

#### **3.1.4.1 Dose Response Curve**

Several filmstrips were irradiated with increasing doses from 10 Gy to 50 Gy using the SIA 20 Sr-90 pterygium ophthalmic applicator. The films were placed horizontally on a lucite block to provide sufficient backscatter. The scanning of the films was done after two days, to allow for the stabilizing of the film response to irradiation.

The response of the film was also determined along the vertical axis by giving doses from 10 Gy to 45 Gy. The film was held between two 4 x 4 x 2 cm<sup>3</sup> lucite pieces (Figure 3.1) with one of its edges parallel to the corresponding faces of the lucite blocks. A calibration curve of the optical density versus applied dose was obtained from the measurements.

### **3.1.4.2 Relative Surface Dose Rates**

The GafChromic film was cut into thin strips of 1 cm width and held using elastoplast onto the dome of a lucite eye phantom (Figure 3.2). The filmstrips were irradiated using the four ophthalmic applicators described in Table 1.2. The filmstrips were given two doses of 20 Gy and 45 Gy using each applicator (Figure 3.3). The relative surface dose rates were compared relative to the SIA K610 applicator. The experiment was repeated with TLD cubes as the detection media. They were dropped in the hole on top of the eye phantom (Figure 3.4). Doses of 10 Gy and 12.7 Gy (for SIA 20 only) were given and relative measurements with SIA K610 done.

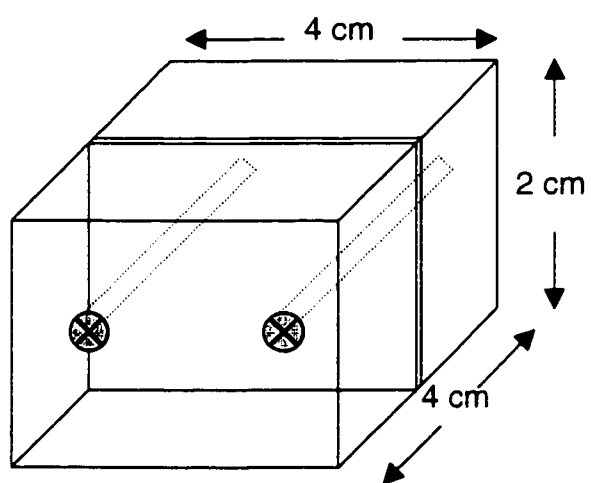


**Figure 3.1:** Lucite phantom for vertical film irradiation

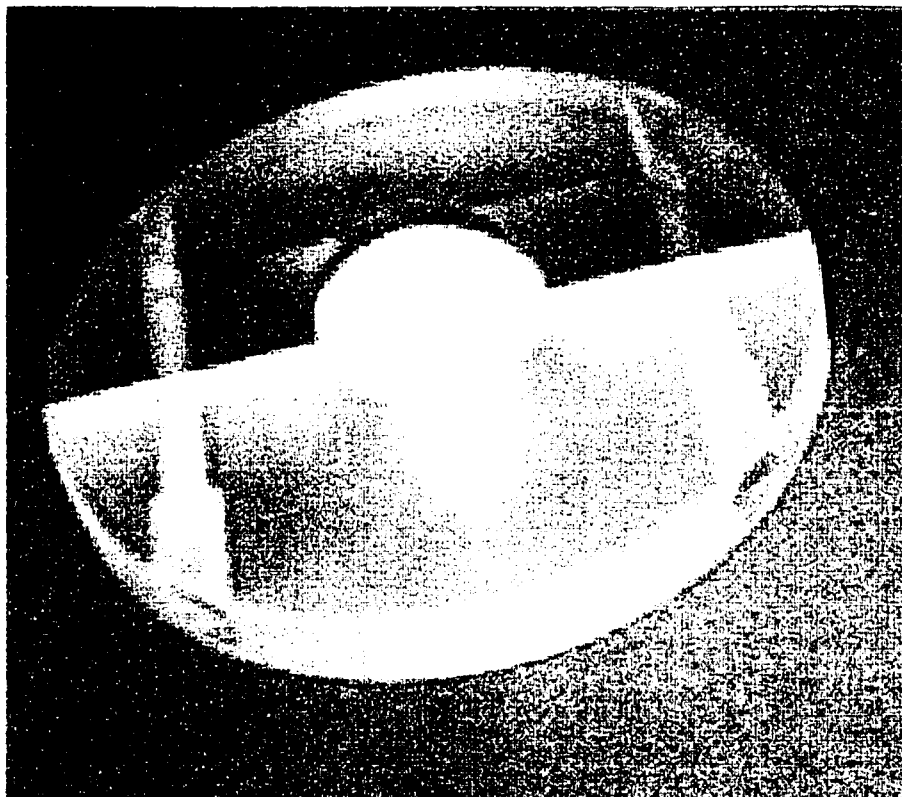


**Figure 3.2:** Eye phantom for holding the radiochromic films.

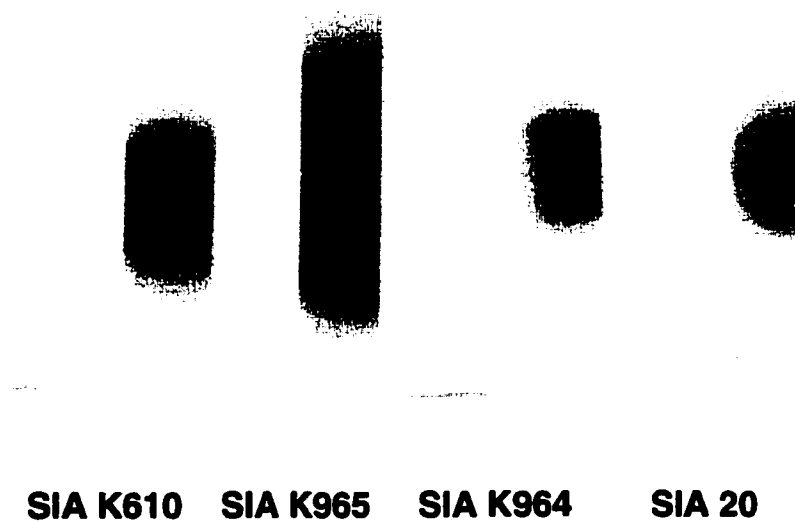


**Figure 3.3:** Films irradiated with a dose of 45 Gy using the four applicators.

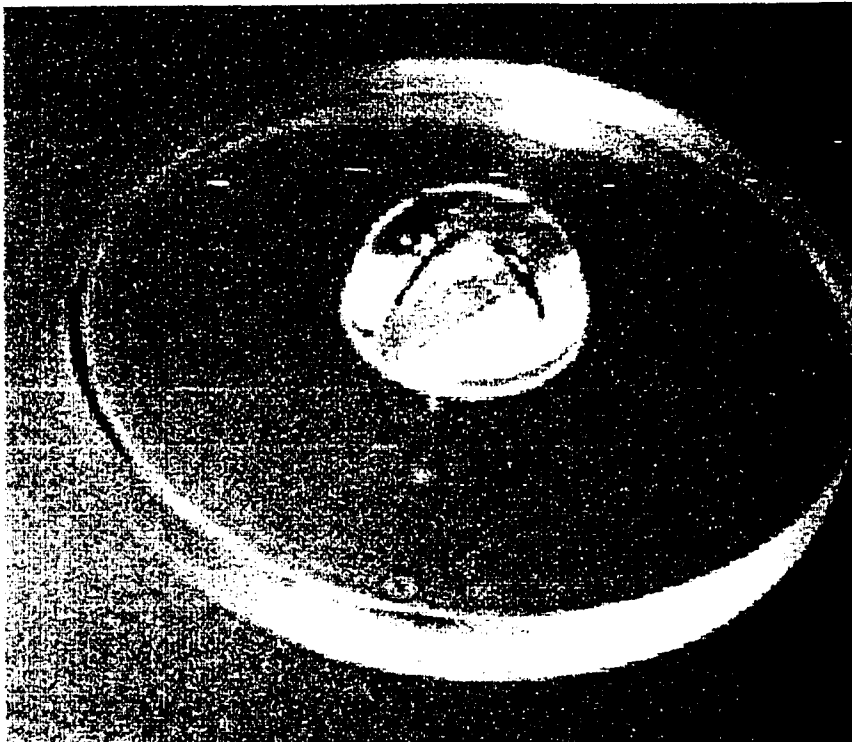


**Figure 3.4:** Eye phantom for TLD irradiation.



### 3.2 I-125 Seed Dosimetry

Interstitial brachytherapy calls for knowledge of the exact dose distribution around the radioactive source for effective treatment and management of the cancer. A point source gives an isotropic dose distribution unlike a cylindrical one, which can be very anisotropic. Certain corrections have to be incorporated in the dosimetric calculations to account for this dose reduction due to the end welds of the cylindrical seed. The measurements around the I-125 seed source were done using thermoluminescent dosimeters (TLDs) arranged in a water-equivalent solid water phantom. The TLDs were conditioned before use for the dosimetry. Correction factors were determined for each TLD to account for the variations in their individual response. These TLDs were then used to determine the anisotropy function using (see discussion in Section 2.1.1.6)

$$F(r, \theta) = \frac{\dot{D}(r, \theta)G(r, \theta_0)}{\dot{D}(r, \theta_0)G(r, \theta)}. \quad (1.7)$$

#### 3.2.1 Model 6711 Seed Description

The I-125 seeds used for the experiments recorded in this thesis work were obtained from Nycomed-Amersham Canada, Oakville, ON. As mentioned earlier, I-125 is available in three forms of which the low activity model 6711 was used for the study. In this model, I-125 is adsorbed onto a silver rod (which acts as a x-ray marker) and encapsulated in a welded titanium capsule. Usually these seeds are available with air kerma rates in the range  $0.13\text{-}7.58 \mu\text{Gy h}^{-1}$  (equivalent activities in the range  $0.10\text{-}5.99 \text{ mCi}$ ) at 1m.

### 3.2.2 TLD System Description

Since low dose rates are involved here, it is quite complicated to measure exactly the dose rate around the sources. Because of the steep dose gradient, a small volume ionization chamber cannot be used, as the ionization current will be very low compared to the leakage current and background noise. On the other hand, larger ionization chambers have good signal to noise but poor spatial resolution near the sources. Hence for our experiments we have made use of thermoluminescent dosimeters (TLDs), which are small solid state detectors. The doses around the I-125 seed were measured by placing the LiF TLDs in shallow holes machined precisely in a slab of a solid water phantom (see Section 3.2.3). The experiments made use of TLD 100 cubes and chips<sup>†</sup>. For distances less than 3 cm from the center of the source TLD cubes having dimensions of 1 x 1 x 1 mm<sup>3</sup> were used. For the larger distances from 4-10 cm, TLD chips of dimensions 3.1 x 3.1 x 0.89 mm<sup>3</sup> were used. Two batches each of the cubes and chips were used as the experiments were conducted employing two different techniques, to be discussed in sections 3.2.4.1 and 3.2.4.2, and each treated cubes and chips differently.

The TLDs have to be conditioned and their element correction coefficients (see Section 2.2.5) determined before they are used for calibration studies. The TLDs were irradiated in the previously-calibrated high dose rate photon beam of Co-60 (Theratron 780 unit) to deliver a dose of 100 cGy. The irradiated TLDs from both methods were then read using a Harshaw 5500 TLD reader. It is a PC-driven, table-top instrument for thermoluminescent measurement designed in such a way so as to provide both high performance and high reliability. It includes an automatic sample changer and carrier disk for unattended processing. The reader is capable of reading 50 dosimeters per loading and can accommodate TL chips, rods and

---

<sup>†</sup> Harshaw-Bicron, Solon, Ohio

cubes of various sizes on different carrier disks. The disks can be placed in the drawer assembly using the dosimeter load/unload push button. The main functions of the reader are dosimeter transport, dosimeter conditioning (heating and cooling), and signal acquisition. The reader is connected to a DOS-based IBM compatible computer, providing the user interface and the applications software to perform dosimetric data storage, instrument control and operator input. The TLDs in the reader are heated by a linearly programmable heating system using hot nitrogen gas in a closed loop. The advantage of hot gas heating is that the transfer of heat to the dosimeters is fast and avoids the necessity for good thermal contact with the tray. The instrument can produce linearly-ramped temperatures accurate to within  $\pm 1^\circ\text{C}$  up to  $400^\circ\text{C}$ . The time-temperature profile (TTP) has three parts called the pre-heat, acquire and anneal, and each part has independently set times and temperatures (Figure 2.5.). The acquire temperature usually spans a broad range for the LiF TLDs. A cooled photomultiplier with its associated electronics is used to measure the light emitted from the dosimeters during heating. To prevent the photomultiplier tube from becoming overheated, nitrogen gas is circulated around it. The linear time-temperature profile thus obtained, which includes the pre-read and post-read anneal, gives the glow curve. The reader has good TTP reproducibility, linearity and high voltage stability [Harshaw 5500 TLD reader operating manual].

### **3.2.3 Phantom Description**

As there is a high dose gradient near the I-125 source, the source to detector distance is very critical. Hence, water phantoms are replaced by solid phantoms such that the TLDs can be positioned precisely and the distances determined accurately. The radiation characteristics of solid water are very close to that of water for radiotherapy beams as well as for

diagnostic x-rays and hence this material can be used as phantoms for calibrations in both cases [Constantinou, 1982]. The solid water material used for our experiments was obtained from Radiation Measurement Inc (RMI)<sup>†</sup>. The components of the solid water are epoxy CB4 (80.48%), polyethylene (10.00%), calcium carbonate (5.77%) and phenol microspheres (PMS) (3.75%). The elemental composition is H(8.09%), C(67.22%), N(2.40%), O(19.84%), Ca(2.32%) and Cl(0.13%). The specific gravity of the material is  $1.015 \pm 0.002 \text{ kg m}^{-3}$  [Constantinou, 1982]. The advantage of solid water is that it makes dosimetric measurements easier, overcoming the question of uncertainties in the positioning of the TLDs and eliminating the problem of waterproofing the radiation detectors. The solid water material was bought as slabs of dimensions  $25 \times 25 \times 2 \text{ cm}^3$ . Twelve circular slabs were machined from the square pieces, each with a diameter of 25 cm.

On one of the circular slabs, a slot was machined at the center to hold the I-125 seed with cross-sectional length of 4.8 mm and width of 0.8 mm. Concentric holes were drilled at distances of 0.5, 1, 2, 3, 4, 6, 8 and 10 cm from the center in two opposing quadrants, along six diverging lines as shown in Figure 3.5. The short distance measurements were done using TLD cubes that could be dropped into holes of diameter 1.5 mm and a depth of 1 mm. For distances from 4-10 cm, TLD chips were used in holes having a diameter of 4.7 mm and depth 1 mm drilled at 2 cm intervals. Solid water plugs were made to serve as spacers to fill the holes that were unoccupied by the TLD chips. Water droplets were used to fill the empty cube holes. The centers of the TLDs were positioned in a plane containing the seed's longitudinal axis with an accuracy  $\leq 0.1 \text{ mm}$ . This slab of solid water was sandwiched by 12 cm of solid water on the top and 10 cm on the bottom (which including the 2 cm thickness of the drilled slab makes 12 cm at the bottom).

---

<sup>†</sup> Gammex RMI, Middleton, WI

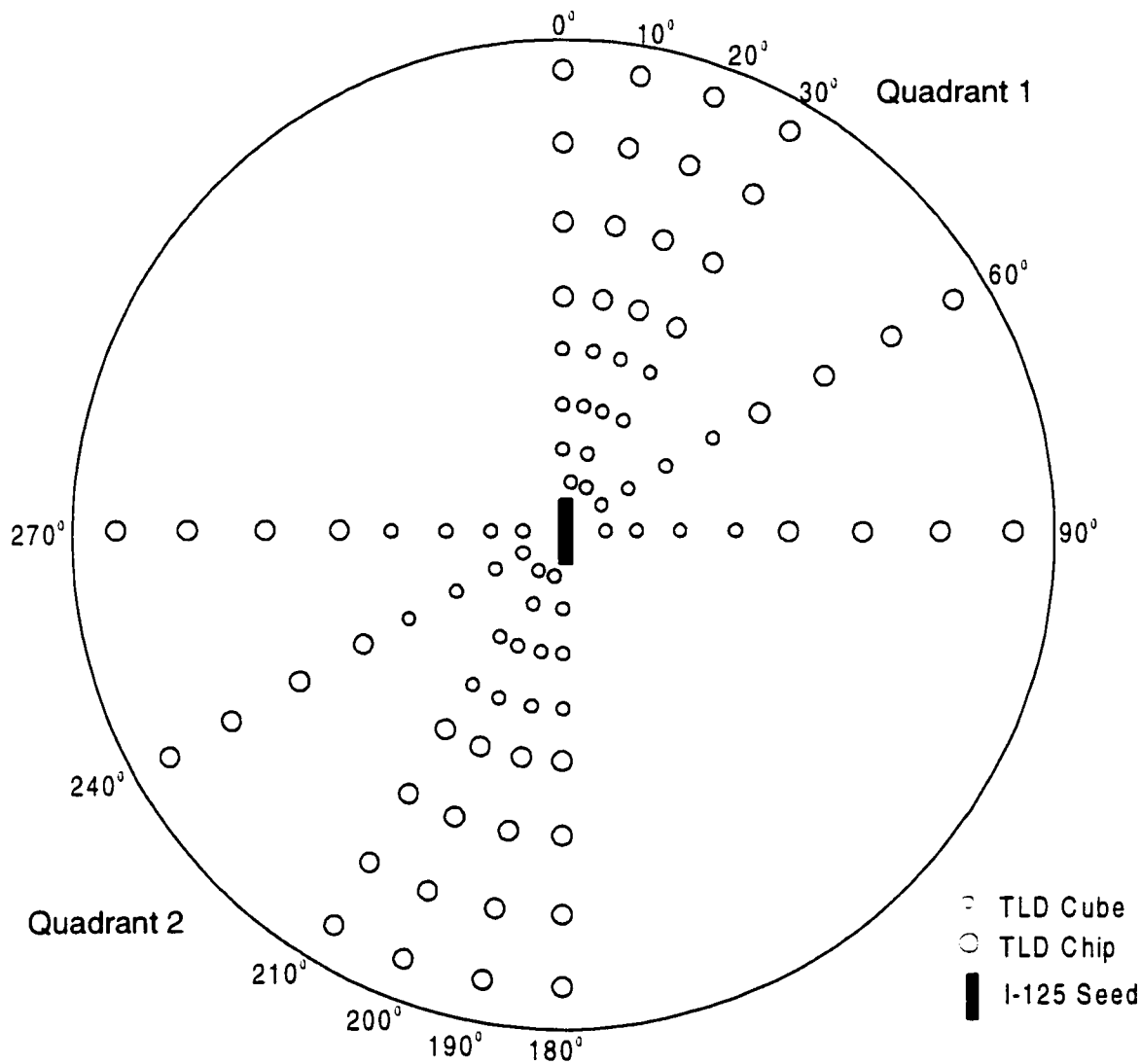


**Figure 3.5 Solid Water Phantom Design**

### 3.2.4 Dosimetry System Performance

The effect of annealing and cooling on the thermoluminescence of LiF TLD 100 is very crucial. The sensitivity of the material changes with the different annealing procedures. This variation is due to the presence of certain lattice defects at the different temperatures. A number of annealing procedures were tested that were intended to restore the material to its initial characteristics and also to remove the low temperature peaks before reading. It is always desirable to obtain a glow curve having only the longer-lived high temperature peaks 4 and 5. Several investigations have concluded that peaks 2 and 5 are involved with a dipole type defect and peak 4 is caused by a dipole complex [Dhar *et al.*, 1973]. The high temperature traps are said to result from an aggregation of the low temperature traps. The TL signal is therefore usually integrated between peaks 3 and 5 so as to include the whole of the main peak. A post-irradiation or a pre-read anneal can help erase peak 2. An ideal annealing procedure that accentuates peak 5 was obtained and is referred to as the pre-read anneal method in all the further experiments.

#### 3.2.4.1 Pre-read anneal Method

A single 6.24 mCi seed (calibration strength) was used in these experiments.

The following protocol was selected to process the TLDs:

- i. The TLDs are arranged on an aluminum annealing tray, which has holes to accommodate them, and then placed in a Model 168 TLD annealing furnace manufactured by the Radiation Products Design Inc, Albertville, MN. The TLDs are then baked at 400°C for 1.5 hours. This helps to restore the TLDs to their virgin characteristics by emptying all the electron and hole traps and dispersing the impurity ions to their original

states. The annealing tray for the cubes is covered with an aluminum lid, as the cubes were found to be more sensitive to changes in the hot air stream in the oven.

- ii. The annealing tray is then air cooled on a brass block for half an hour. Air-cooling maximizes peak 5, showing that it may be identified with the first cluster of dipoles which probably forms the dimer or trimer [Horowitz, 1984]. Optimum cooling rates are obtained by the transfer of the TLD annealing tray from the oven onto the metal block.
- iii. The TLDs are then exposed to ionizing radiation.
- iv. An ensuing short anneal at 100°C is performed for 15 minutes in the Single-wall transite oven manufactured by the Blue M Electrical Company, Illinois. This pre-readout annealing of the TLDs helps to empty the unstable low temperature traps with low potential depth so that they make a very small contribution to the read-out. These are the traps having peaks with a high fading rate at room temperature [Schmuhl, 1997]. The pre-read anneal empties completely the traps leading to peaks 1 and 2, and partly some of peak 3. Trials with different temperatures and times showed that an anneal at 100°C for 15 minutes emptied peaks 1 and 2 and had a very negligible effect on the sensitivity of peak 5.
- v. The thermoluminescence in the TLDs is determined using a TLD reader. A post-read anneal on the reader was avoided.
- vi. The absorbed dose is calculated from the acquired data.

The need for a low-temperature anneal following the high-temperature anneal at 400°C was studied, however the results neither seemed to enhance peak 5 nor decrease peaks 1 and 2. Hence this step was not performed again. The read-out cycle was accomplished using a Harshaw Model 5500 automatic TL reader<sup>†</sup>. It performs very accurately the various operating cycles

---

<sup>†</sup> Harshaw-Bicron, Solon, Ohio

to record the TL content emitted by the dosimeter on heating it with hot nitrogen gas. Some of the steps include – pre-heating the dosimeters, reading the dosimeters, annealing the dosimeters, photomultiplier noise reading and test light reading. The pre-heat by the reader, done in addition to the post-irradiation anneal, raises the temperature of a dosimeter to that of peak 3 (~125°C) in 15 secs so as to further empty the peaks below. This does not affect peaks 4 and 5. After the pre-heat, the temperature rises linearly at a rate of  $15^{\circ} \text{C s}^{-1}$  to the final acquire temperature of 325°C in about 16 secs, so that peaks 4 and 5 are completely emptied (see Figure 2.5). It is seen that the performance is linear for a range of delivered doses from 10  $\mu\text{Gy}$  (1 mrad) to 1 Gy (100 rads) and supralinear from 1 Gy to 20 Gy (2000 rads).

The heating rate of the TL read-out process is to be set with care. To minimize read-out variations arising from the heating rate, it is better to measure the integral signal rather than the peak height. The non-radiative transitions have been found to increase with heating rate, while the luminescent emission is independent of the heating rate. The non-radiative transitions decrease the TL efficiency, which thus happens with increasing heating rates. This is known as thermal quenching. The glow peaks then get shifted to higher temperatures with increased heating rates. These high temperature peaks have a tendency to be supralinear.

### **3.2.4.2 Glow-Curve Deconvolution Method**

A single 6.3 mCi seed (calibration strength) was used in these experiments. In the glow curve deconvolution technique, the only difference with respect to the above technique was that the pre-read anneal was not



performed in step iv. Alternatively, the individual peaks were separated and integrated using Visual Basic programs operating on an Excel spreadsheet<sup>†</sup>.

The macro programs eliminate peaks 1 and 2 and curve fit the leading edge of peak 3 [Pla & Podgorsak, 1983]. In the case of glow-curve deconvolution, the pre-heat by the TLD reader was done at 40°C for 5 sec. The acquire temperature was set to rise linearly at a rate of 10°C s<sup>-1</sup> to 340°C in 30 sec.

### 3.2.4.3 Sensitization

Before the TLDs can be used in any measurements, they have to be annealed and sensitized [McGhee *et al.*, 1993]. Since two techniques were studied, the pre-read anneal and glow curve deconvolution, two groups of TLD cubes and chips each were chosen.

Number of chips: (a) for pre-read = 43 (b) for glow curve deconvolution = 21

Number of cubes: (a) for pre-read = 38 (b) for glow curve deconvolution = 24

They were annealed as stated before at a temperature of 400 °C for 1.5 hours. After cooling, the cubes were arranged in a square matrix of holes machined in a 10 x 10 cm<sup>2</sup> lucite block of thickness 0.5 cm with a lid of the same thickness. The holder had a 25 x 25 cm collar of the same material. The chips were kept for irradiation on a circular tray, of thickness 0.5 cm and diameter 10 cm, on its periphery. This holder too was provided with a lid and collar as in the previous case. The lid brings the depth of the TLDs to be at the depth of dose maximum for a Co-60 beam. Since lucite was used as a buildup material, it was necessary to determine the water equivalent thickness of the lucite holder and collar. The buildup layer thickness was hence to be varied and the difference in the dose recordings noted. The Protea electrometer<sup>‡</sup> used for the measurements was always kept at a fixed

---

<sup>†</sup> Microsoft Corp., Redmond, WA

<sup>‡</sup> Protea Systems Corporation, Benicia, CA

distance of 81 cm from the Co-60 source. The source-to-surface distance was kept at 80 cm, which included 1 cm of solid water above the detectors.

The raw electrometer reading for various buildup thickness' was noted following irradiation under the cobalt beam, and it showed that a thickness of 13 mm of water was equivalent to 11 mm of perspex or lucite.

Enough material (solid water) was placed under the tray to provide full backscattering. The TLDs were exposed to 100 cGy from a Theratron 780 Co-60 therapy machine<sup>†</sup>. Ideally, the TLDs belonging to the same batch should give the same response when exposed to the same amount of radiation. Analysis revealed that the irradiated TLDs showed variations in reading for the same dose received from one TLD to another. This could be attributed to their physical properties that include slight differences in mass and size. To account for this, the response of each individual chip was compared with the average response of the entire batch to determine an element correction coefficient (Equation 2.25). A set of calibration values was then generated for the cubes and the chips.

The mean displacement of the ECC values from the average of five measurements was calculated. Those TLD chips showing large variation (>2%) from the acceptable calibration range were discarded. The selected TLDs took their ECC values from the average of three measurements. The TLD measurements made in this work were always corrected using the individual ECC values. The identity of each TLD is maintained for every experiment, as the value of the ECCs are to be incorporated in the measurements.

---

<sup>†</sup> Theratronics, Kanata, Ontario

### 3.2.4.4 Linearity

LiF TLD 100 is linear with applied dose up to about 1 Gy and then becomes supralinear, which leads to an increase in TL response (Figure 2.4). The linearity of the TLD cubes and chips was studied by irradiating them with increasing amounts of radiation from a Co-60 therapy unit. Doses varying from 10 cGy to 22 Gy and 100 cGy to 20 Gy were given to the cubes and chips respectively and the linearity in response of the TLDs analyzed.

If  $D$  is the dose given to the TLDs, then the reading obtained from them must be corrected for supralinearity using a correction factor. Hence, the uncorrected dose,

$$TL_{corr} = TL_{uncorr} \times C_{supralin}, \quad (3.1)$$

where, using a polynomial representation for the dose response,

$$TL_{uncorr} = aD + bD^2 + cD^3,$$

$$TL_{corr} = aD,$$

and

$$\begin{aligned} C_{supralin} &= \frac{TL_{corr}}{TL_{uncorr}} \\ &= \frac{aD}{aD + bD^2 + cD^3}. \end{aligned} \quad (3.2)$$

The supralinearity correction factor is then

$$C_{supralin} = [1 + \alpha D + \beta D^2]^{-1}, \quad (3.3)$$

where

$$\alpha = b/a \quad \text{and} \quad \beta = c/a.$$

### 3.2.5 I-125 Seed Anisotropy

The dose measurements were done using the solid water phantom described in section 3.2.3. For each measurement, a single radial distance was selected and all the holes drilled along that distance on the twelve diverging lines from the seed were populated. This method was adopted to avoid the inter-chip effect as in this case there were no chips to block the irradiation of the experimental thermoluminescent dosimeter. All the empty chip and cube holes were filled with solid water plugs and water drops respectively. The seed was placed in the central jig for a pre-determined time and the slab was sandwiched on either side by the other circular slabs of solid water. The setup was left undisturbed in a room with negligible background for the required time. After irradiation, the TLDs were treated as explained in section 3.2.4.1. For the farther distances from 4 to 10 cm, TLD chips were used and for distances up to 3 cm, cubes were employed.

The TG-43 report [Nath *et al.*, 1995] recommends an air kerma strength conversion factor ( $S_k$  / quantity) for I-125 seeds of  $1.270 \text{ U mCi}^{-1}$  and a dose rate constant,  $\Lambda$ , of  $0.88 \text{ cGy hr}^{-1} \text{ U}^{-1}$ . Hence, the dose rate at a distance of 1 cm from the source axis is obtained as the product of the air kerma strength and the dose rate constant for a certain activity of the source (from Equation 2.4). The dose rate from an  $M \text{ mCi}$  source equals  $1.270 \times 0.88 \times M \text{ cGy hr}^{-1}$ . The dose rate at any distance can then be calculated approximately using the inverse square law

$$\dot{D}(r) = \dot{D}(1) \left( \frac{1}{r^2} \right), \quad (3.4)$$

where  $r$  is the radius chosen. Doses of 30 cGy were given to distances up to 3 cm and beyond that the dose was decreased due to the increase in time of irradiation. A dose of 15 cGy was given to the dosimeters when placed at 4 cm, 10 cGy at 6 cm and 6 cGy each at 8 and 10 cms. As the dose to be given

## Materials and Methods

is fixed, the time of irradiation is found (neglecting source decay) as the ratio of the dose to the dose rate at that particular radial distance.

The anisotropy function was calculated using the data obtained from reading the processed TLDs in the Harshaw TLD reader by employing Equation 1.7.

## References

1. Butson M.J., Yu P.K.N., Metcalfe P.E., Effects of readout light sources and ambient light on radiochromic film, *Physics in Medicine and Biology*, 43, 2407-2412, (1998)
2. Constantinou C., Attix F.H., Paliwal B.H., A solid water phantom material for radiotherapy x-ray and  $\gamma$ -ray beam calibrations, *Medical Physics*, 9(3), 436-441, (1982)
3. Dhar A., DeWerd A.L., Stoebe T.G., Effects of annealing and cooling processes on thermoluminescence of LiF (TLD 100), *Health Physics*, 25(Oct), 427-433, (1973)
4. Horowitz Y.S., "Thermoluminescence and thermoluminescent dosimetry", CRC Press Inc., Florida, (1984)
5. McGhee P., Humphreys S., Dunscombe P., An efficient approach to routine TL dosimetry, *Medical Dosimetry*, 18, 187-191, (1993)
6. Nath R., Melillo A., Dosimetric characteristics of a double wall  $^{125}\text{I}$  source for interstitial brachytherapy, *Medical Physics*, 20(5), 1475-1483, (1993)
7. Niroomand-Rad A., Blackwell C.R., Coursey B.M., Gall K.P., Galvin J.M., McLaughlin W.L., Meigooni A.S., Nath R., James E.R., Soares C.G., Radiochromic film dosimetry: Recommendations of AAPM Radiation Therapy Committee Task Group 55, *Medical Physics*, 25(1), 2093-2115 (1998)
8. Pla C., Podgorsak E.B., A computerized TLD system, *Medical Physics*, 10(4), 462-466, (1983)
9. Schmuhl T., Schmidt R., Ludemann L., Temperature profiles of an annealing oven and effects on TL signals, *Radiation Protection Dosimetry*, 71(2), 147-151, (1997)
10. Stevens M.A., Turner J.R., Hugtenburg R.P., Butler P.H., High-resolution dosimetry using radiochromic film and a document scanner, *Physics in Medicine and Biology*, 41, 2357-2365 (1996)

## **CHAPTER 4**

### **4 EXPERIMENTAL RESULTS**

This chapter will present in detail the results obtained in the experiments with the Sr-90 ophthalmic applicators and the I-125 model 6711 seed.

To use Sr-90 applicators in therapy, it is necessary to know the surface and the depth doses. The calibration of the Sr-90 applicators was done using radiochromic film and supplemented using thermoluminescent dosimeters. The precision with which the films are measured is dependent on the instrumentation used, which in this case is a document scanner. Calibration curves for the horizontal and vertical irradiation of the radiochromic films were made by relating the optical density (derived from the scanner signal) to the surface dose. The validity of the document scanner as an instrument for reading radiochromic film was investigated. Exposures from the Sr-90 applicators were compared to get relative output values using both radiochromic film and thermoluminescent detectors. A depth dose curve was made from a vertical film irradiation of the Sr-90 SIA 20 applicator. In addition, the response of a horizontally irradiated cut film with respect to an uncut one was examined.

The I-125 seed was used to study the anisotropy of the dose distribution around it. An account of the preparation of the TLDs for the experiments is given. Calibration curves of the dose response of the TLDs were obtained which allow for the determination of any dose depending on the TL output. Since the experiments were conducted with two sizes of TLDs, chips and the cubes, two calibration curves were obtained. Measurements of the anisotropy function were done using the pre-read anneal and the glow

curve deconvolution techniques. Our results are compared with previously published data from the AAPM TG 43 report [Nath *et al.*, 1995] and Monte Carlo calculations by Weaver [Weaver, 1998].

### 4.1 Radiochromic Film Calibration

The optical density was calculated by applying Equation 1.5. The average of the transmittance values from the control films, which were unirradiated and stored along with the irradiated ones, was used for the background subtraction as the initial intensity  $I_0$  in the above equation.

To check the temporal stability of the reader, the mean optical density was determined from a matrix of 14x14 pixels taken at the center of sequentially scanned images of a film strip irradiated to 30 Gy (Figure 4.2). The optical was found to vary by about 2% from the initial scan (Table 4.1).

To find suitable locations on the scanner bed for placing the irradiated films for the sensitivity study, various spatial positions were examined. It was observed that there was a variation of approximately 4% in the values of the optical density of the same film when placed at the corners (especially at the two corners near the hinge) with respect to the other positions. The readings from all the other positions were within 1% (Figure 4.1). Hence when the experiments were conducted, care was taken to arrange the films to be around the center of the scanner bed.

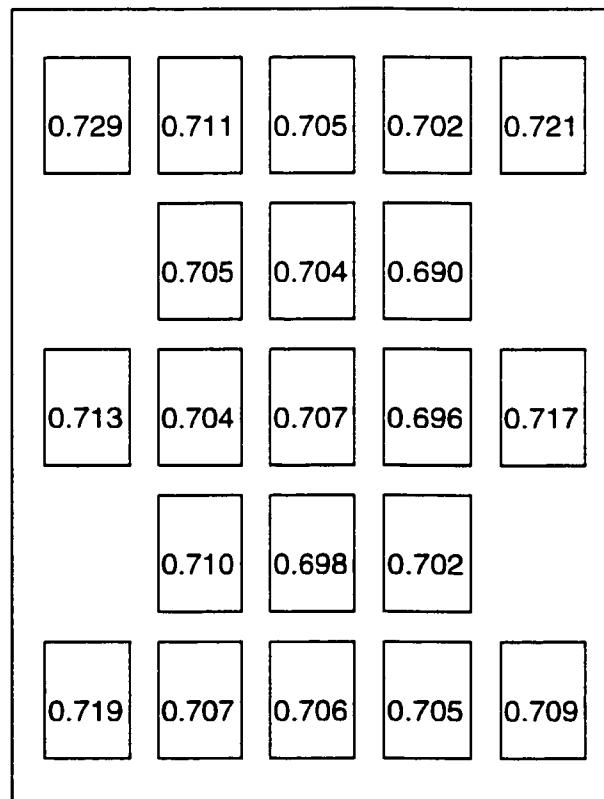
The MD-55-2 radiochromic film is available with a cut right corner for orientation purposes. The long side of the clipped corner is parallel to the direction of the coating application [Niroomand-Rad *et al.*, 1998]. However, being doubly coated, it is expected that both sides would respond similarly to irradiation. When both the sides were treated with doses of 20 and 45 Gy, it was found that the difference between the readings was less than 2%.



**Table 4.1:** Temporal variations in optical density of a film irradiated to 30 Gy

Reading Date	Optical Density
20/5/98	0.704
21/5/98	0.702
22/5/98	0.707
25/5/98	0.715
26/5/98	0.714
27/5/98	0.715
28/5/98	0.715
29/5/98	0.714

Hinge →

**Figure 4.1:** Optical density from a single film irradiated to 30 Gy and positioned at different locations using the template on the scanner

#### 4.1.1 Dose Response Curve

The radiochromic film can be irradiated either horizontally (face-on) or vertically (edge-on). The results obtained on image processing are given in the following two sections.

##### 4.1.1.1 Horizontal calibration

The filmstrips irradiated horizontally (Figure 4.2) on the lucite block using the Sr-90 SIA 20 applicator were studied after two days. The absorbed dose response is shown in Figure 4.3. The net optical density increases with increasing dose. A plot of the natural logarithms of the optical density and the absorbed dose shows the linearity. The dose is related to the optical density by the formula given in Equation 2.30,

$$D = \left[ \frac{1}{a} \log_{10} \left( \frac{I_0}{I} \right) \right]^{\frac{1}{\alpha}}. \quad (2.30)$$

When a least square linear fit is applied to the calibration data, the regression value of " $\alpha$ " gives the slope and " $\ln(a)$ " gives the intercept. It was determined that there is need for two linear fits, one in the range between 10 - 20 Gy and the other from 20 - 50 Gy. Non-linearity was seen to set in beyond 50 Gy and hence the upper value of the calibration curve was fixed at this dose. The values of the exponent, " $\alpha$ " in the power function and that of the parameter, " $a$ " are 0.628 and 0.086 for the 10-20 Gy range and 0.534 and 0.114 in the range from 20-50 Gy respectively. The maximum error in the dose calculation with these values is 0.3%. The need for such a "bi-linear" fit has also recently been reported by the AAPM TG No. 55 [Niroomand-Rad, 1998].

## Results

The effect of cutting the GafChromic film was studied by horizontally irradiating a film cut in the middle with the SIA 20 applicator (Figure 4.4). A comparison was made with an undamaged film by averaging a cross-section containing four pixels across the cut to eliminate any noise. The cut was found to create an effect on a width of 12 pixels as shown in Figure 4.5 and 4.6 are compared. Since there are eight pixels in a millimeter, the width of the affected area was estimated to be 0.51 mm.

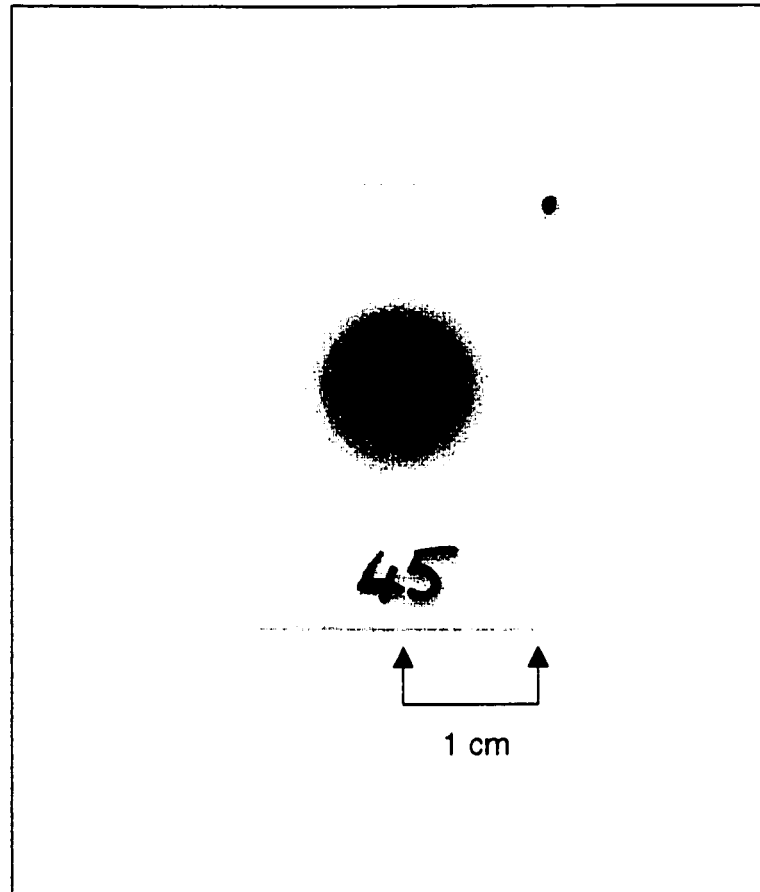


**Figure 4.2:** A horizontally irradiated filmstrip (2 x 3 cm) irradiated to 45 Gy using the SIA 20 applicator.

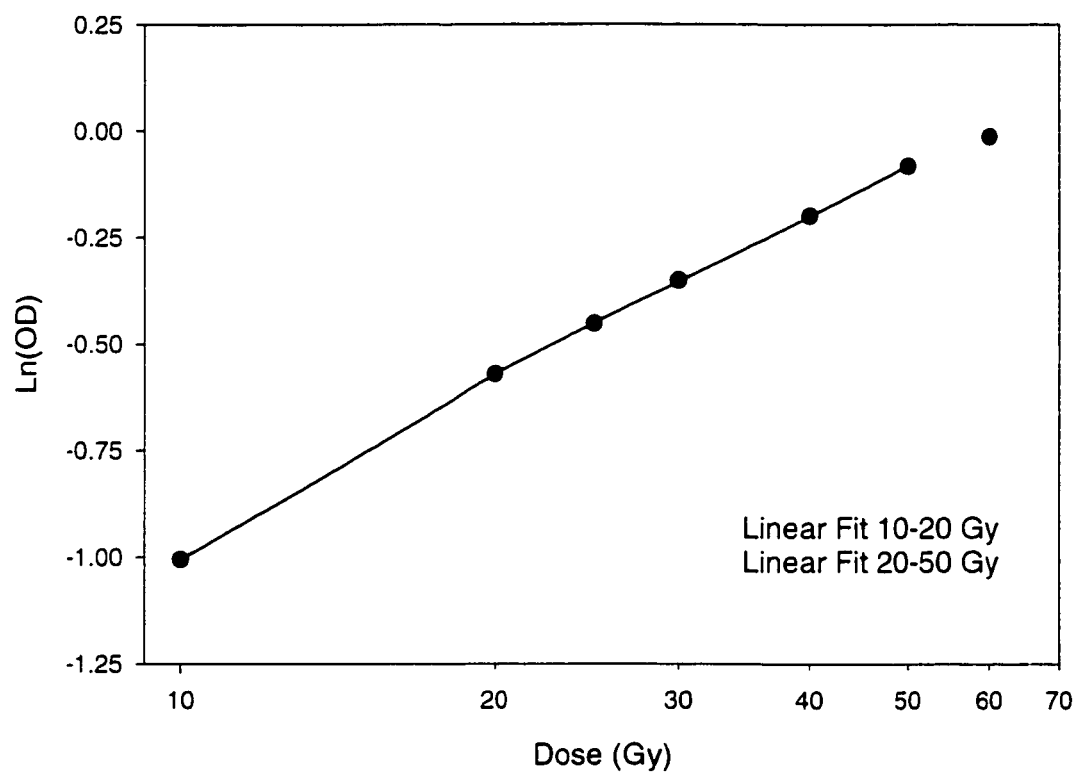


**Figure 4.3:** Film calibration curve (Horizontal)

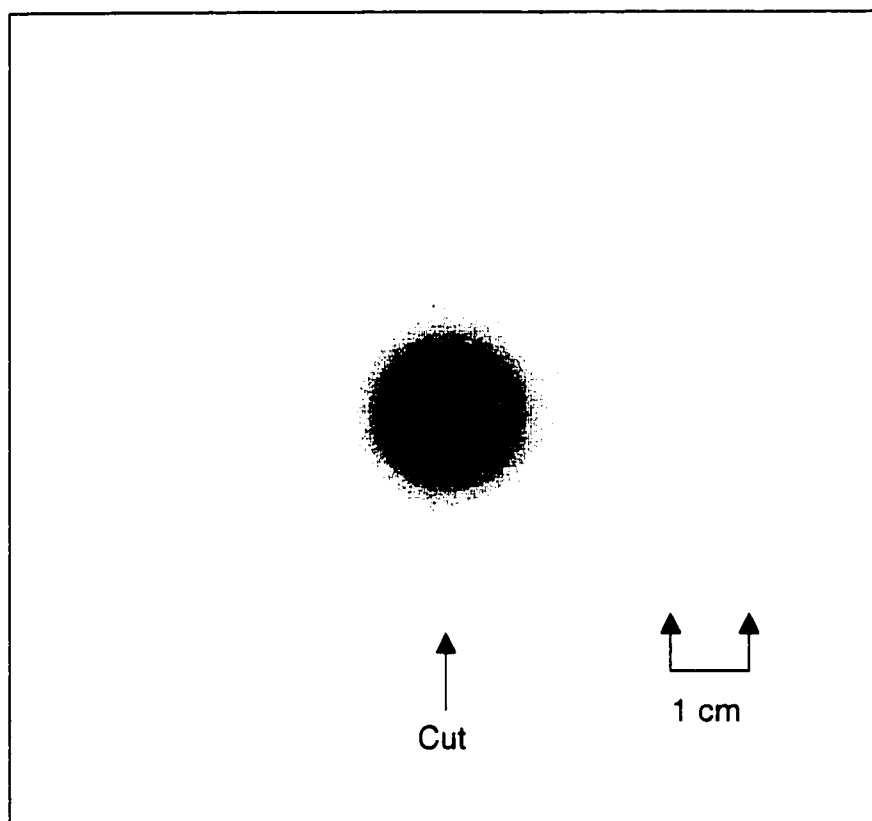


**Figure 4.4:** Film cut through the middle and irradiated to 45 Gy using the SIA 20 applicator.

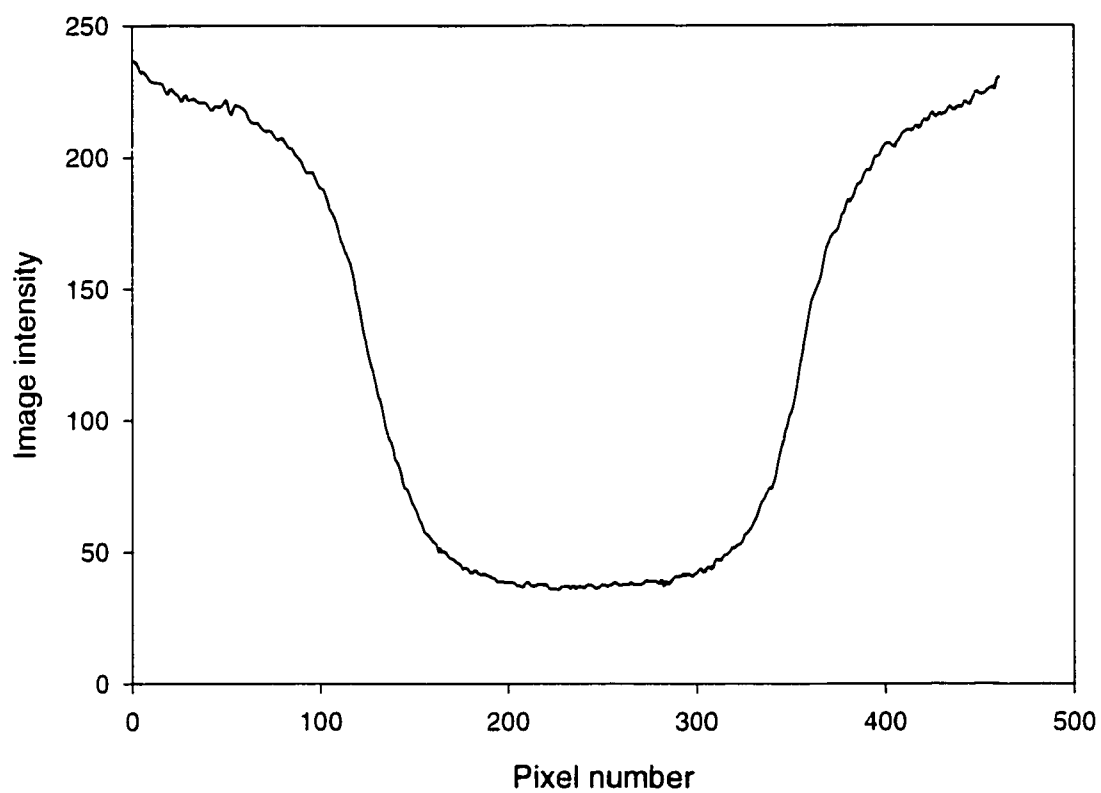


**Figure 4.5:** Cross-section of an uncut film given a dose of 45 Gy using the SIA 20 applicator.

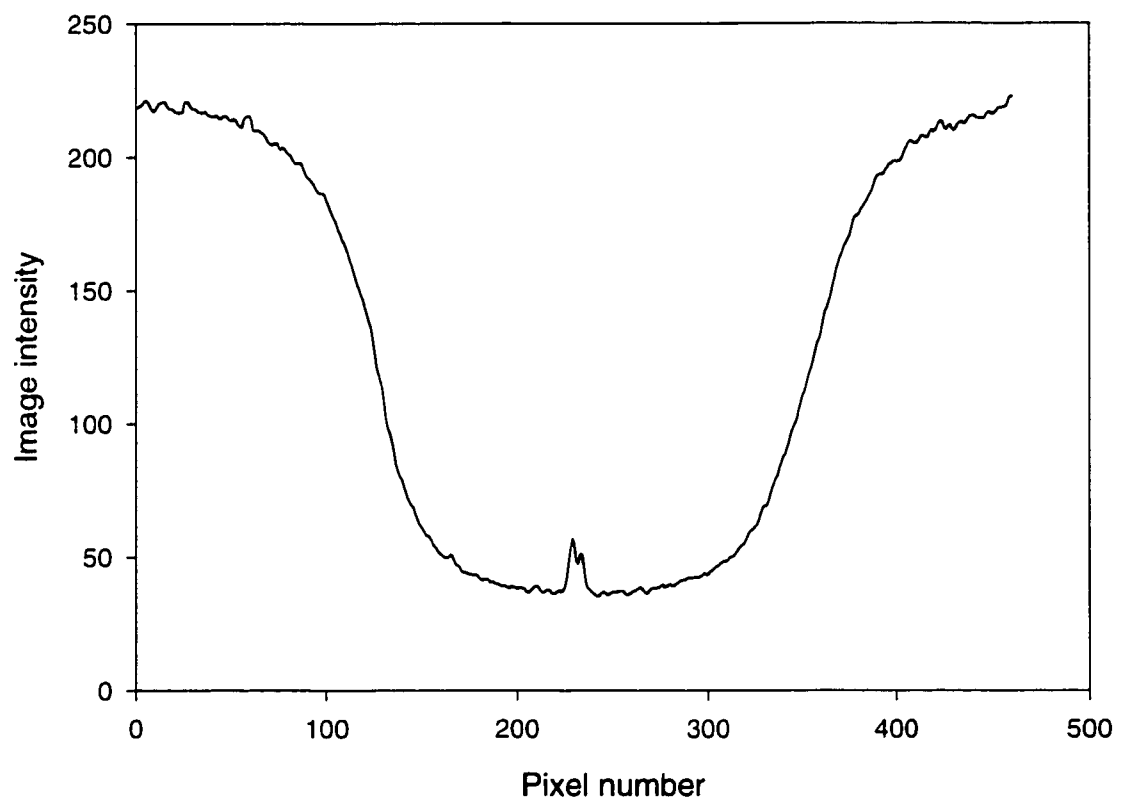


**Figure 4.6:** Cross-section of a cut film given a dose of 45 Gy using the SIA 20 applicator.



### 4.1.1.2 Vertical calibration

The filmstrips were held between the lucite blocks in the vertical position and irradiated using the SIA 20 Sr-90 applicator (Figure 4.7). The strips were then handled exactly the same way as for horizontal irradiation. Before the experiment was conducted, the distance to the dose maximum from the edge was determined. The number of pixels from the cut edge to the dose maximum was found to be eight and hence the distance is about 0.3 mm. Next a horizontal irradiation was done with and without 0.3 mm of plastic spacer between the source and the film. A difference in dose of 22% was found due to the presence of the spacer. Hence, the dose at apparent dose maximum is about 22% less than the given (surface) dose in the case of vertical irradiation. This could be attributed to the fact that, on cutting the film, the sensitive layer at the edge may be becoming damaged. This causes the surface dose to be less than that recorded below. The calibration curve relating the optical density to the radiation dose for vertical irradiation is given in Figure 4.8. This plot is also divided into two parts, with " $\alpha$ " and " $a$ " taking the values of 0.650 and 0.049 in the range of surface doses from 10-20 Gy and 0.768 and 0.036 in the range from 20-45 Gy.

### 4.1.1.3 Central axis depth dose of SIA 20

The percent depth dose was plotted (Figure 4.9) using the average data from a column of five pixels along the central axis of a film irradiated vertically to a dose of 40 Gy. As the maximum occurs at a depth of 0.3 mm due to the edge effect (see section 4.1.1.2), the data is shown extrapolated to the surface. The depth dose obtained alternatively by face-on irradiation of film positioned horizontally between solid water slabs of thickness 1 mm is also shown. Depth dose values given by the manufacturer are presented for comparison.

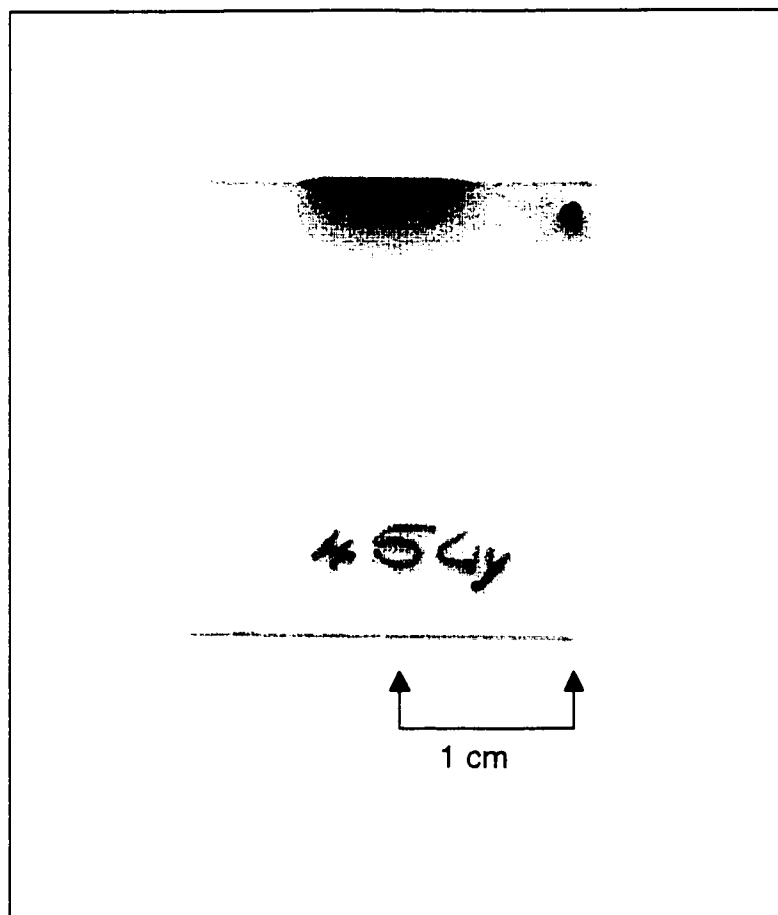


**Figure 4.7:** A vertically irradiated filmstrip (2 x 3 cm) irradiated to 45 Gy using the SIA 20 applicator.

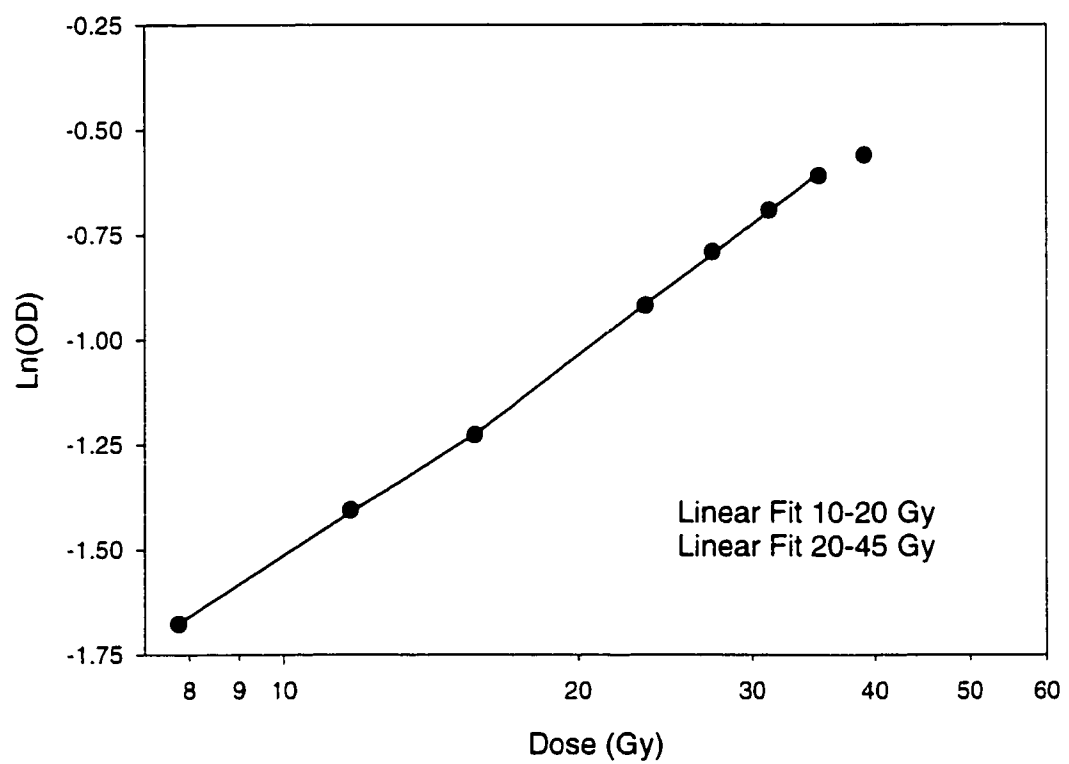


**Figure 4.8:** Film calibration curve (Vertical)

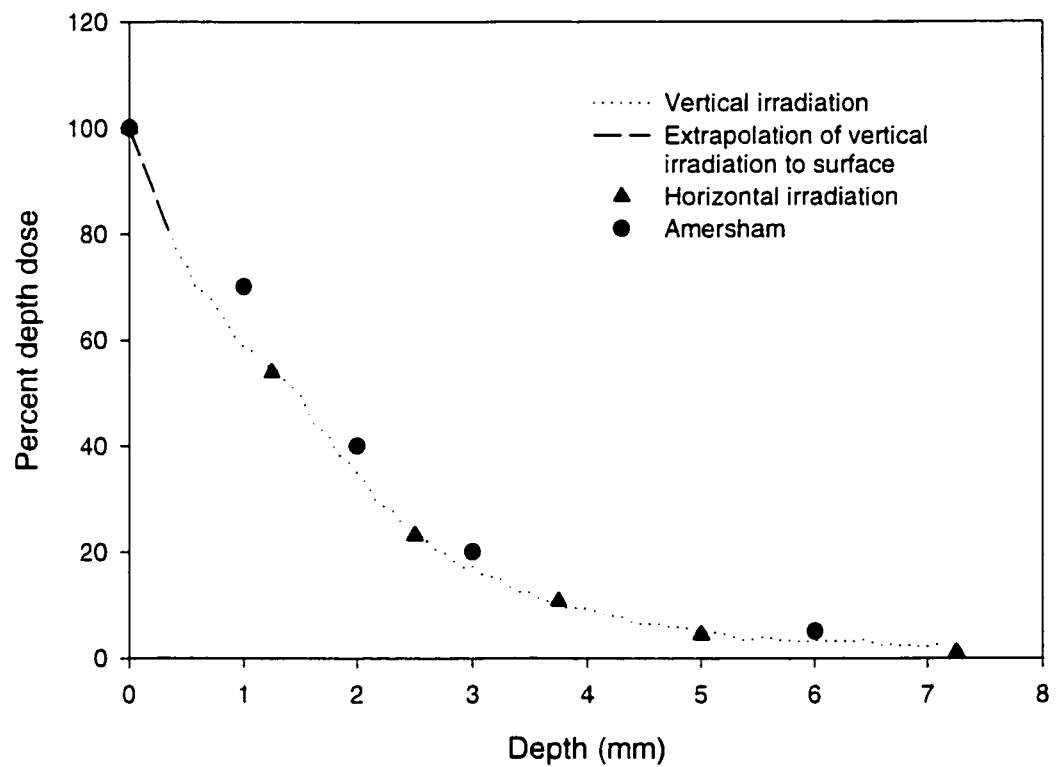


**Figure 4.9:** Central axis depth dose obtained by the vertical and horizontal irradiation of the film.

## **4.2 Relative output of Sr-90 applicators**

To maintain accuracy and consistency in dose delivery and prevent clinical predicaments, it is necessary to establish the relative surface dose rates of the old and new ophthalmic applicators.

### **4.2.1 Measurements using radiochromic films**

The four applicators at the Cross Cancer Institute (SIA K610, SIA K965, SIA K964, SIA 20) involved in the relative measurements study were used to irradiate the radiochromic films to doses of 20 and 45 Gy. The relative dose rates of the applicators should be known to within  $\pm 20\%$  for the consistency of the treatment. Calibration of each of the four applicators was performed with respect to the SIA K610. The results obtained for each calibration are given in Tables 4.2a and b. The error in the manufacturer's dose rates are not included because of the coherence in the errors which would in that case disappear on taking the ratios. All dose rates in these tables have been corrected for decay to the time of study.

In the case of the SIA K965, the difference between the experimental and the manufacturer's estimates of relative dose rate is about 2%, and for the other two applicators, it varies from 2-6%.

**Table 4.2a: Relative dose rates of the Sr-90 Applicators**  
**(Given Dose = 20 Gy)**

Applicator	Mfr. DR <sup>†</sup>	Given Dose (Gy)	Irradiation Time (sec)	Film Optical Density	Exp. DR <sup>‡</sup>	DR Diff* (%)
SIA K610 (12 mm)	1.00	20.0	156±0.5	0.532±0.018	1.00±0.04	0±4.8
SIA K965 (18 mm)	0.85	20.0	183±0.5	0.546±0.018	0.87±0.04	2.4±4.9
SIA K964 (7x4 mm)	1.31	20.0	119±0.5	0.500±0.018	1.23±0.06	-6.1±4.7
SIA 20 (9 mm)	4.72	20.0	33±0.5	0.564±0.018	5.01±0.25	6.1±5.2

† Dose rate specified by manufacturer with respect to SIA K610

‡ Experimental dose rate with respect to SIA K610

\* Difference in manufacturer and experimental dose rate

**Table 4.2b: Relative dose rates of the Sr-90 Applicators**  
**(Given Dose = 45 Gy)**

Applicator	Mfr. DR <sup>†</sup>	Given Dose (Gy)	Irradiation Time (sec)	Film Optical Density	Exp. DR <sup>‡</sup>	DR Diff* (%)
SIA K610 (12 mm)	1.00	45.0	352±0.5	0.847±0.007	1.00±0.01	0±1.2
SIA K965 (18 mm)	0.85	45.0	412±0.5	0.835±0.007	0.84±0.01	-1.2±1.1
SIA K964 (7x4 mm)	1.31	45.0	268±0.5	0.833±0.007	1.29±0.02	-1.5±1.2
SIA 20 (9 mm)	4.72	45.0	75±0.5	0.836±0.007	4.64±0.06	-1.7±1.3

† Dose rate specified by manufacturer with respect to SIA K610

‡ Experimental dose rate with respect to SIA K610

\* Difference in manufacturer and experimental dose rate

#### 4.2.2 Measurements using thermoluminescent dosimeters

The above mentioned relative output measurements were again done using thermoluminescent dosimeters in cube form as the detector medium. A dose of 12.7 Gy was delivered with the SIA 20 applicator and doses of 10 Gy each with the other three applicators. The reading of each dosimeter was corrected using their respective ECC. The ECC values were found to vary about 2% with time. As the doses given are in the supralinear region, the readings were corrected with the supralinearity factor (see Section 4.3.2).

$$C_{\text{supralin}} = [1 + 0.0324D - 0.000526D^2]^{-1} \quad (4.1)$$

Four TLDs were irradiated with each applicator. The reading from the four are averaged and the results are displayed in Table 4.3.

**Table 4.3: Relative dose rates of the Sr-90 Applicators  
(Using TLDs)**

Applicator	Mfr. DR <sup>†</sup>	Given Dose (Gy)	Irradiation Time (sec)	TL Q <sup>★</sup> (μC)	Exp. DR <sup>‡</sup>	DR Diff <sup>*</sup> (%)
SIA K610 (12 mm)	1.00	10.0	75±0.5	17.0±1.4	1.00±0.11	0±11.3
SIA K965 (18 mm)	0.85	10.0	88±0.5	16.3±1.4	0.82±0.09	-3.5±11.1
SIA K964 (7x4 mm)	1.31	10.0	57±0.5	16.9±1.4	1.31±0.15	-0.3±11.3
SIA 20 (9 mm)	4.72	12.7	20±0.5	23.4±1.4	5.15±0.52	9.1±11.1

† Dose rate specified by manufacturer with respect to SIA K610

★ Charge collected in the thermoluminescent detector (Supralinearity corrected)

‡ Experimental dose rate with respect to SIA K610

\* Difference in manufacturer and experimental dose rate

The percentage change in dose rate is found to be comparable while using the thermoluminescent detectors. The advantage of using the radiochromic film for these measurements is its high spatial resolution. The relative outputs of the applicators are quite consistent considering the fact that a 20% variation is acceptable clinically.

### **4.3 I-125 Model 6711 Seed Dosimetry**

A major drawback in the use of I-125 seeds in interstitial brachytherapy is their highly anisotropic photon emission. The need for an anisotropy correction becomes evident when the sources are regularly arranged as in catheters. The thermoluminescent dosimeters, prior to their use in making anisotropy measurements, had to be prepared in order to optimize their performance.

#### **4.3.1 ECC Determination**

The investigations used LiF thermoluminescent dosimeters in the form of chips and minicubes. Each dosimeter was assigned a particular number so as to make it individually identifiable by placing it in a unique spot marked on an annealing tray. A record was maintained throughout the period of study to note the history of dose received by each TLD on irradiation. The dosimeters had to be compensated for the variations in sensitivity amongst themselves due to differences in physical properties by the determination of their individual element correction coefficient (ECC). The photon beam from a Theratron 780 Co-60 unit was used for this purpose. The ECCs determined for the separate groups of chips and cubes by the pre-read anneal and the glow curve deconvolution methods are given in Tables 4.4 to 4.7. The average ECC, its standard deviation, and the maximum and minimum percent changes are shown in the tables.



**Table 4.4:** ECC of chips by pre-read anneal method

CHIPS	ECC 1	ECC 2	ECC 3	AV. ECC	Std Dev	% Max diff	% Min diff
A1	1.015	1.003	1.004	1.007	0.007	0.7	-0.4
A2	0.992	0.984	0.986	0.987	0.004	0.5	-0.3
A3	0.982	0.976	0.980	0.979	0.003	0.3	-0.3
A4	0.957	0.955	0.955	0.956	0.002	-0.1	-0.1
A5	0.909	0.912	0.907	0.909	0.002	0.3	-0.1
A6	1.019	0.997	1.002	1.006	0.011	1.3	-0.9
A7	1.022	1.015	1.018	1.018	0.004	0.4	-0.3
A8	1.002	1.009	1.007	1.006	0.004	0.1	-0.4
A9	1.021	1.013	1.047	1.027	0.017	1.9	-1.3
A10	0.975	0.962	0.978	0.972	0.009	0.6	-1.0
A11	0.976	0.974	0.973	0.974	0.001	-0.1	0.0
A12	1.008	1.009	1.007	1.008	0.001	-0.1	0.0
A13	1.008	1.005	1.004	1.006	0.002	-0.2	0.0
A14	1.010	1.002	1.005	1.006	0.004	0.4	-0.4
A15	0.986	0.982	0.988	0.985	0.003	0.3	-0.4
A16	0.983	0.988	0.994	0.988	0.005	0.5	-0.5
A17	0.951	0.954	0.957	0.954	0.003	0.3	-0.3
A18	0.994	0.987	0.980	0.987	0.007	0.7	-0.7
A19	1.030	1.035	1.031	1.032	0.002	-0.1	-0.1
A20	1.010	0.999	1.001	1.003	0.006	0.6	-0.4
A21	1.005	1.004	0.987	0.999	0.010	0.6	-1.2
A22	0.953	0.951	0.945	0.950	0.004	0.3	-0.4
A23	1.011	1.003	1.004	1.006	0.005	0.5	-0.3
A24	1.040	1.044	1.047	1.044	0.004	0.3	-0.4
A25	1.026	1.025	1.021	1.024	0.003	0.2	0.1
A26	1.072	1.087	1.082	1.080	0.007	0.6	-0.7
A27	1.017	1.027	1.023	1.022	0.005	0.5	-0.5
A28	1.012	1.020	1.004	1.012	0.008	0.8	-0.8
A29	1.019	1.016	0.998	1.011	0.011	0.8	-1.3
A30	0.986	0.978	0.984	0.983	0.004	0.2	-0.5
A31	1.019	1.011	1.011	1.014	0.005	0.5	-0.3
A32	1.024	1.031	1.037	1.031	0.007	0.6	-0.7
A33	1.027	1.027	1.025	1.026	0.001	-0.1	0.1
A34	0.998	0.998	1.002	0.999	0.003	0.3	-0.2
A35	1.014	1.006	1.003	1.008	0.006	0.6	-0.2
A36	0.994	0.997	0.995	0.996	0.002	-0.1	0.0
A37	0.992	1.002	1.007	1.000	0.007	0.7	-0.8
A38	0.950	0.968	0.960	0.959	0.009	0.9	-0.9
A39	1.032	1.053	1.034	1.040	0.012	1.3	-0.8
A40	0.998	1.004	1.006	1.003	0.004	0.4	-0.5
A41	1.007	1.017	1.034	1.020	0.014	1.5	-1.2
A42	1.007	1.014	1.016	1.012	0.005	0.3	-0.5
A43	0.976	0.993	0.991	0.987	0.009	0.4	-1.1

**Table 4.5: ECC of cubes by pre-read anneal method**

<b>CUBES</b>	<b>ECC 1</b>	<b>ECC 2</b>	<b>ECC 3</b>	<b>AV. ECC</b>	<b>Std Dev</b>	<b>% Max diff</b>	<b>% Min diff</b>
B1	0.980	1.027	1.033	1.013	0.03	2.0	-3.3
B2	1.017	1.007	0.970	0.998	0.02	1.9	-2.8
B3	0.958	0.959	0.901	0.939	0.03	2.1	-4.1
B4	1.002	1.058	1.111	1.057	0.05	0.1	-5.2
B5	1.030	1.087	1.075	1.064	0.03	2.1	-3.2
B6	1.004	0.952	0.957	0.971	0.03	3.4	-1.9
B7	1.007	0.951	1.022	0.993	0.04	2.9	-4.2
B8	1.002	1.037	1.014	1.018	0.02	1.9	-1.5
B9	1.021	1.013	0.988	1.007	0.02	1.3	-1.9
B10	1.009	0.971	0.946	0.975	0.03	3.4	-3.0
B11	0.988	0.949	0.958	0.965	0.02	2.4	-1.6
B12	0.993	0.985	0.995	0.991	0.01	0.4	-0.6
B13	0.947	0.944	0.982	0.957	0.02	2.5	-1.4
B14	0.970	0.984	0.928	0.961	0.03	2.5	-3.4
B15	0.977	1.061	0.989	1.009	0.05	5.1	-3.2
B16	0.997	1.021	0.943	0.987	0.04	3.5	-4.4
B17	1.027	1.060	1.009	1.032	0.03	2.7	-2.2
B18	1.004	0.959	1.022	0.995	0.03	2.7	-3.6
B19	0.998	0.956	0.993	0.982	0.02	1.0	-2.7
B20	1.016	1.031	0.998	1.015	0.02	1.6	-1.6
B21	1.159	1.138	1.127	1.141	0.02	1.5	-1.2
B22	0.966	0.999	1.037	1.001	0.04	3.6	-3.5
B23	1.058	1.069	1.106	1.078	0.02	2.6	-1.8
B24	0.956	0.940	0.992	0.962	0.03	3.0	-2.3
B25	0.966	0.981	1.012	0.986	0.02	2.7	-2.1
B26	1.029	1.036	0.987	1.017	0.03	1.9	-3.0
B27	1.015	1.009	1.026	1.016	0.01	0.9	-0.8
B28	1.053	1.041	1.065	1.053	0.01	1.1	-1.1
B29	0.933	0.955	0.865	0.918	0.05	4.0	-5.8
B30	1.063	1.025	1.016	1.035	0.02	2.7	-1.8
B31	0.988	0.937	0.960	0.961	0.03	2.7	-2.5
B32	0.985	0.971	1.053	1.003	0.04	5.0	-3.2
B33	0.965	0.966	1.022	0.984	0.03	3.8	-2.0
B34	0.927	1.022	1.015	0.988	0.05	3.4	-6.2
B35	1.026	1.003	0.980	1.003	0.02	2.3	-2.3
B36	1.002	0.981	0.975	0.986	0.01	1.6	-1.1
B37	0.939	0.972	0.963	0.958	0.02	1.5	-2.0
B38	1.098	1.024	1.078	1.067	0.04	2.9	-4.0

**Table 4.6:** ECC of chips by glow curve deconvolution method

Chip #	ECC1	ECC2	ECC3	AV. ECC	Std Dev	% Max diff	% Min diff
C1	0.919	0.943	0.934	0.932	0.012	1.2	-1.4
C2	0.931	0.954	0.951	0.945	0.013	0.9	-1.5
C3	0.979	1.028	1.019	1.009	0.026	1.9	-2.9
C4	0.915	0.943	0.938	0.932	0.015	1.2	-1.8
C5	1.017	1.029	1.029	1.025	0.007	0.4	-0.8
C6	1.002	1.004	1.004	1.003	0.001	0.1	-0.1
C7	0.950	0.947	0.939	0.945	0.006	0.5	-0.7
C8	1.069	1.051	1.051	1.057	0.011	1.2	-0.6
C9	1.033	1.022	1.039	1.031	0.008	0.7	-0.9
C10	0.978	0.992	0.996	0.989	0.009	0.7	-1.1
C11	0.978	0.980	0.978	0.978	0.001	0.1	0.0
C12	1.008	1.004	1.018	1.010	0.007	0.8	-0.6
C13	1.028	1.010	1.005	1.014	0.013	1.4	-1.0
C14	1.026	1.018	1.020	1.022	0.004	0.5	-0.3
C15	1.011	1.004	1.015	1.010	0.006	0.5	-0.6
C16	1.031	1.021	1.027	1.026	0.005	0.4	-0.5
C17	1.037	1.026	1.018	1.027	0.010	1.0	-0.9
C18	1.038	1.005	1.005	1.016	0.019	2.2	-1.1
C19	1.055	1.054	1.032	1.047	0.013	0.8	-1.4
C20	1.026	1.000	1.023	1.016	0.014	0.9	0.9
C21	1.008	0.985	0.983	0.992	0.014	1.7	-0.9

**Table 4.7:** ECC of cubes by glow curve deconvolution method

CUBES	ECC1	ECC2	ECC3	AV.ECC	Std Dev	% Max diff	% Min diff
D1	0.919	0.908	0.900	0.909	0.010	-1.0	-1.0
D2	1.015	1.064	1.048	1.043	0.025	2.1	-2.6
D3	1.086	1.005	0.987	1.026	0.053	5.9	-3.8
D4	0.964	0.951	0.950	0.955	0.007	0.9	-0.5
D5	1.082	1.088	1.098	1.089	0.008	-0.2	-0.6
D6	0.954	0.979	1.052	0.995	0.051	5.8	-4.1
D7	1.017	1.013	1.026	1.019	0.007	0.7	-0.6
D8	1.072	0.993	1.004	1.023	0.043	4.8	-2.9
D9	0.920	0.974	0.956	0.950	0.027	2.5	-3.1
D10	0.969	0.975	0.992	0.979	0.012	1.4	-1.0
D11	0.994	0.967	1.020	0.994	0.026	2.6	-2.7
D12	0.958	1.055	1.061	1.025	0.058	3.5	-6.5
D13	1.084	1.091	1.076	1.084	0.008	0.7	-0.7
D14	0.996	0.995	0.956	0.982	0.023	1.3	-2.7
D15	1.007	0.920	0.953	0.960	0.044	4.9	-4.2
D16	0.959	0.919	0.912	0.930	0.026	3.1	-1.9
D17	1.012	1.027	1.087	1.042	0.040	4.3	-2.9
D18	0.963	0.981	0.944	0.963	0.019	1.9	-1.9
D19	0.978	1.058	1.032	1.023	0.041	3.5	-4.3
D20	0.997	0.971	0.985	0.985	0.013	1.3	-1.3
D21	1.040	1.067	1.018	1.042	0.024	2.4	-2.2
D22	0.993	0.997	0.978	0.989	0.010	0.8	-1.1
D23	1.075	1.066	1.029	1.057	0.025	0.9	-2.7
D24	1.124	1.223	1.166	1.171	0.049	4.4	-4.0

#### 4.3.2 Dose Response

The dose response of the TLDs was measured in a series of experiments for delivered doses ranging from 1-20 Gy. The linearity in the corrected response of the chips and cubes with respect to the absorbed dose is represented in Figures 4.10 and 4.11.

In both cases, each point on the graph depicts the average response from a group of six TLDs (either chips or cubes) which has been corrected for individual detector response and supralinearity. The supralinearity factor is given by equation 3.5 as

$$C_{\text{supralin}} = [1 + \alpha D + \beta D^2]^{-1} . \quad (3.3)$$

The values for the parameters  $\alpha$  and  $\beta$  obtained from regression statistics are  $\alpha = 0.0156 \text{ Gy}^{-1}$  and  $\beta = -0.000068 \text{ Gy}^{-2}$  for the chips and  $\alpha = 0.0324 \text{ Gy}^{-1}$  and  $\beta = -0.000526 \text{ Gy}^{-2}$  for the cubes. The calibration curves are important for knowing the supralinearity region as all TLDs of a particular size, composition, and manufacture are observed to respond similarly [Williams and Thwaites, 1993].

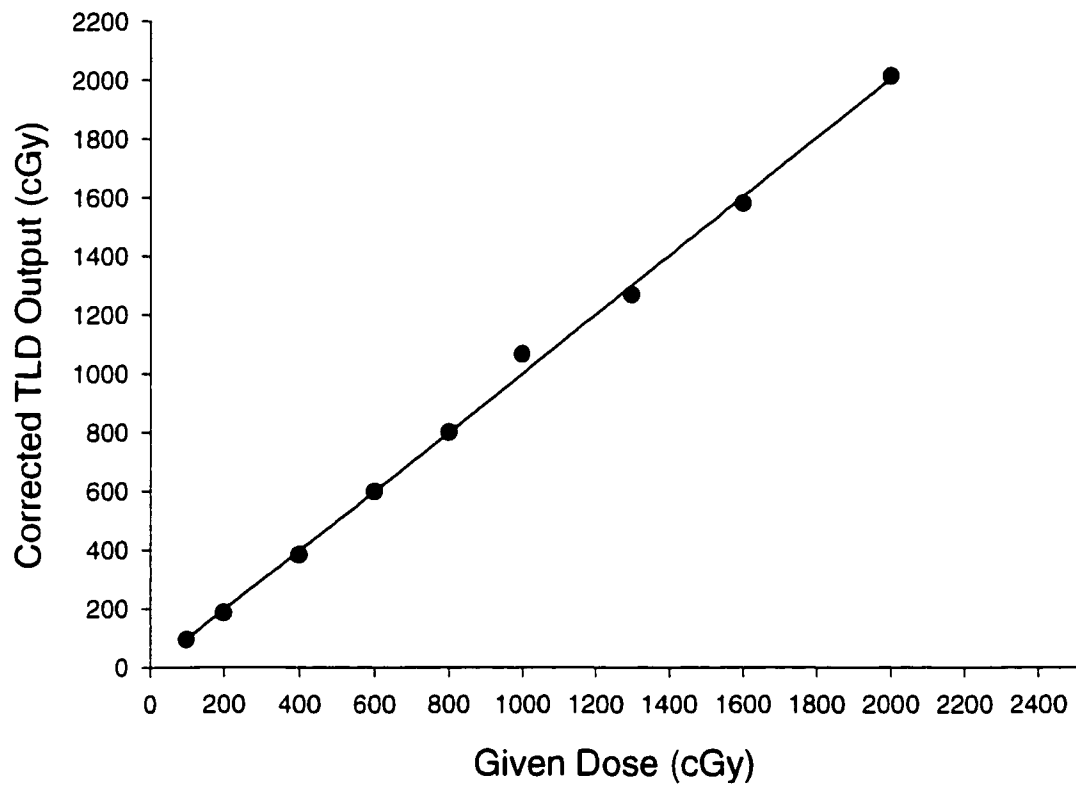


**Figure 4.10:** Linearity of the corrected dose response of the LiF TLD chips.

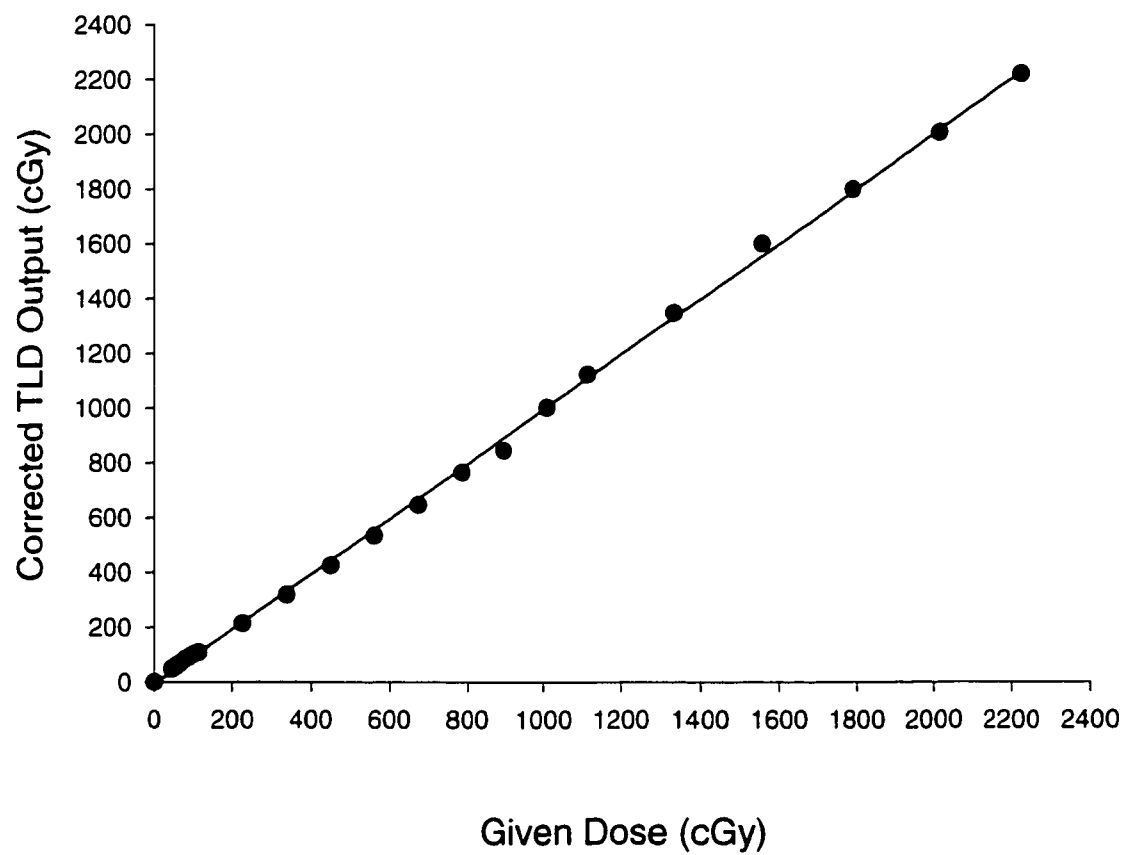


**Figure 4.11:** Linearity of the corrected dose response of the LiF TLD cubes.

### 4.3.3 I-125 model 6711 seed anisotropy

The anisotropy function was experimentally determined to find the dose variation away from the radial axis due to attenuation and scatter, and normalized to one at  $\theta_0=90^\circ$  for all radii. It was hence obtained from the ratio of the dose at angle  $\theta$  to that at angle  $\theta_0$  for the same radial distance, similarly to Equation 1.7.

#### 4.3.3.1 Pre-read anneal technique

Selected thermoluminescent chips and cubes were processed according to the pre-read anneal method. After the high temperature anneal, the dosimeters were arranged along one particular radius for irradiation with the I-125 seed. There are two opposite quadrants and each has six angles. The readings from the two quadrants were averaged during evaluation (Figure 3.5). For the phantom measurements, doses in the range from 6 to 30 cGy were used. In this range  $C_{\text{supralin}} = 1$ . The glow curve displayed for one particular dosimeter using this method is shown in Figure 4.12. Each experiment was repeated twice to improve the statistical quality of the data. The charge obtained after the irradiation was corrected with the element correction coefficient to get the dose

$$D_i = \frac{Q_i \times \text{ECC}_i}{\text{RCF} \times k}, \quad (2.28)$$

where RCF is the reader calibration factor that has dimensions of nC cGy<sup>-1</sup> and k is the proportionality factor. The anisotropy function could then be calculated using



$$F(r, \theta) = \frac{D(r, \theta)G(r, \pi/2)}{D(r, \pi/2)G(r, \theta)}, \quad (4.2)$$

where  $D(r, \theta)$  and  $G(r, \theta)$  are the dose and geometry factor at angle  $\theta$  and radius  $r$  respectively. Since RCF is a constant as the doses are recorded in the same reading cycle, it does not appear in the final result.

Values for the anisotropy function were calculated as a function of polar angles ranging from  $0^\circ$  to  $90^\circ$  (quadrant 1) and  $180^\circ$  to  $270^\circ$  (quadrant 2) and radii extending from 1 to 10 cm. The data from polar quadrant 1 was averaged with that from quadrant 2 for the calculations. The data at short distances were combined with the geometry factors given in Table 4.8 below as prescribed by Equation 1.7.

**Table 4.8<sup>†</sup>:** The geometry factor,  $G(r, \theta)$  times  $r^2$ , for a seed approximated by a 3.0 mm line source as calculated with Equation 2.7.

$\theta$ (deg)	$r=1.0$ cm	$r=2.0$ cm	$r=5.0$ cm
0	1.023	1.006	1.001
10	1.022	1.006	1.001
20	1.019	1.005	1.001
30	1.015	1.004	1.001
60	0.9999	1.000	1.000
90	0.9926	0.9980	1.000

<sup>†</sup>[Nath *et al.*, 1995]

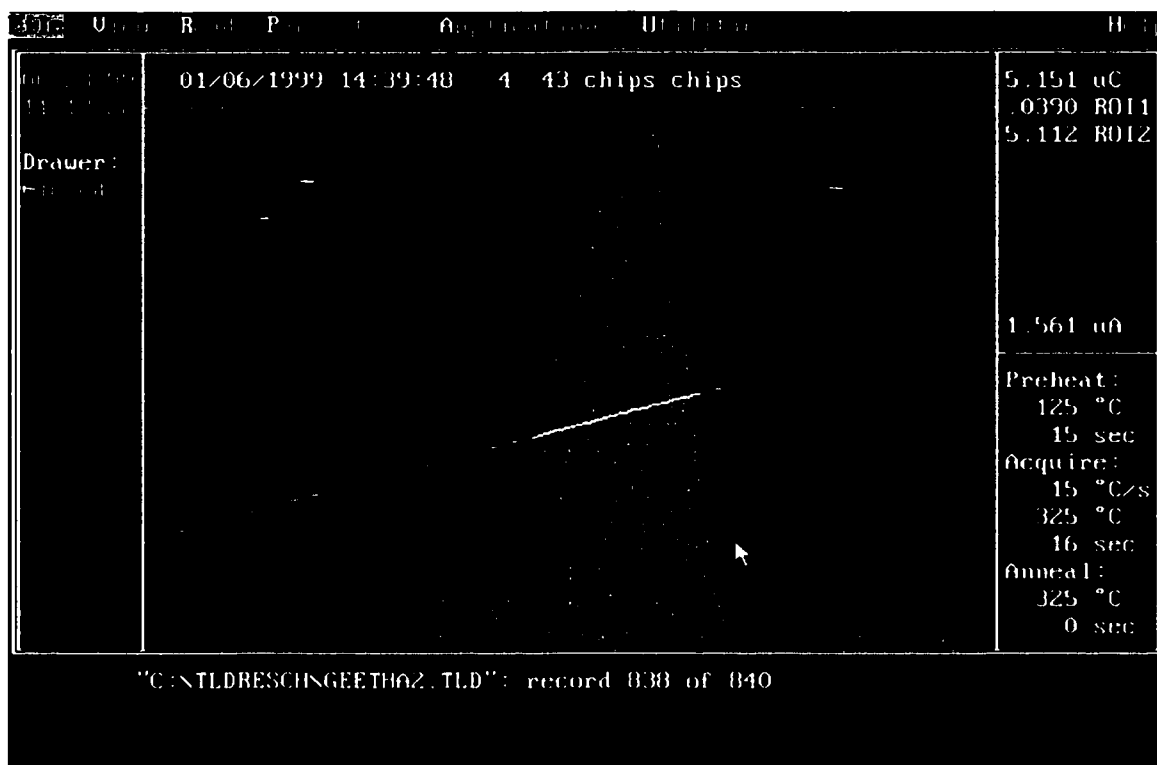


**Figure 4.12:** Glow curve displayed by the Harshaw 5500 TLD reader using the pre-read anneal method.

**Table 4.9:** Experimentally obtained values of the anisotropy function  $F(r,\theta)$  for the I-125 model 6711 seed using pre-read anneal technique. The estimated uncertainties (1 s.d.) are  $\pm 0.05$  for  $r \leq 3$  cm and  $\pm 0.02$  for  $r > 3$  cm.

$\theta$ (deg) $r$ (cm)	0.0	10.0	20.0	30.0	60.0	90.0
1.0	0.35	-	0.63	-	0.99	1.00
2.0	0.43	0.52	0.71	0.76	0.95	1.00
3.0	0.44	0.52	0.70	0.75	0.94	1.00
4.0	0.51	0.59	0.74	0.82	0.98	1.00
6.0	0.55	0.61	0.74	0.85	0.98	1.00
8.0	0.58	0.66	0.78	0.84	0.98	1.00
10.0	0.61	0.68	0.78	0.86	0.98	1.00

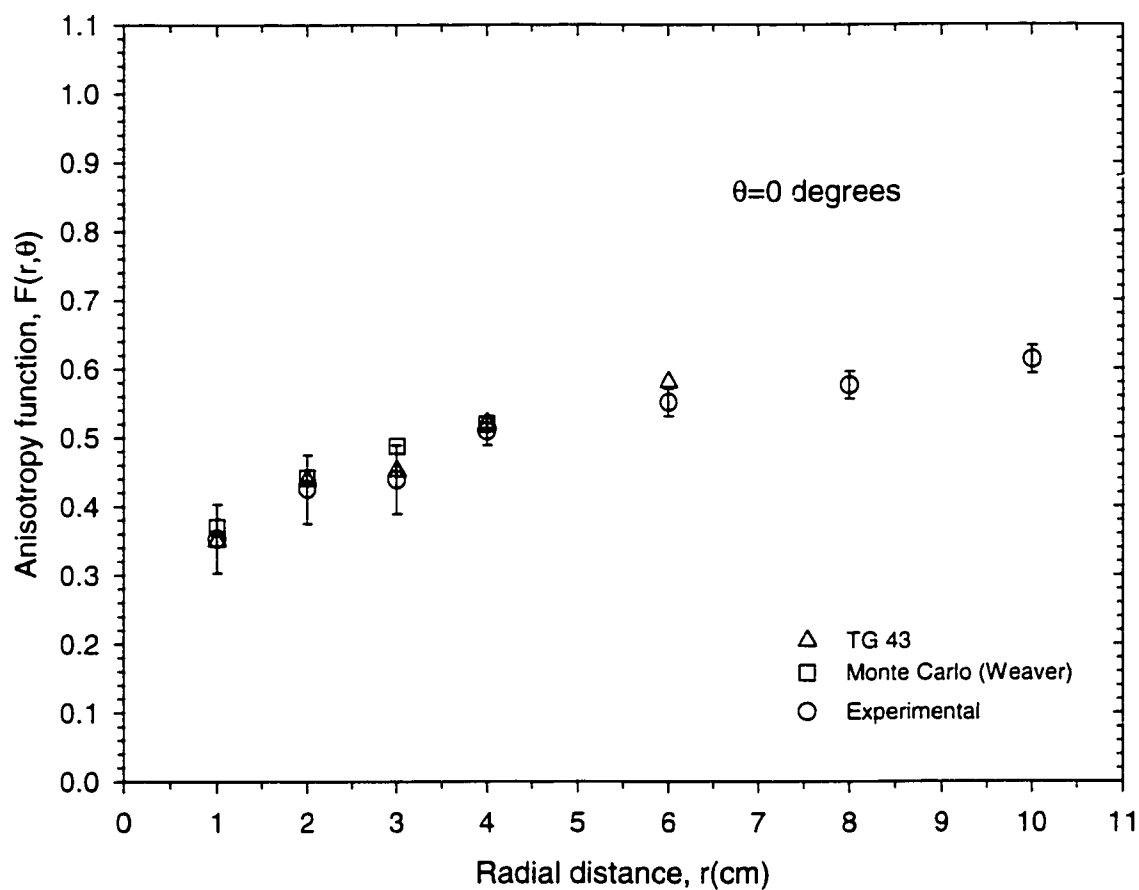


**Figure 4.13:** Plot of the anisotropy function for I-125 model 6711 seed measured at radial distances ranging from 1 cm - 10 cm for a polar angle of  $0^\circ$  using the pre-read anneal technique.

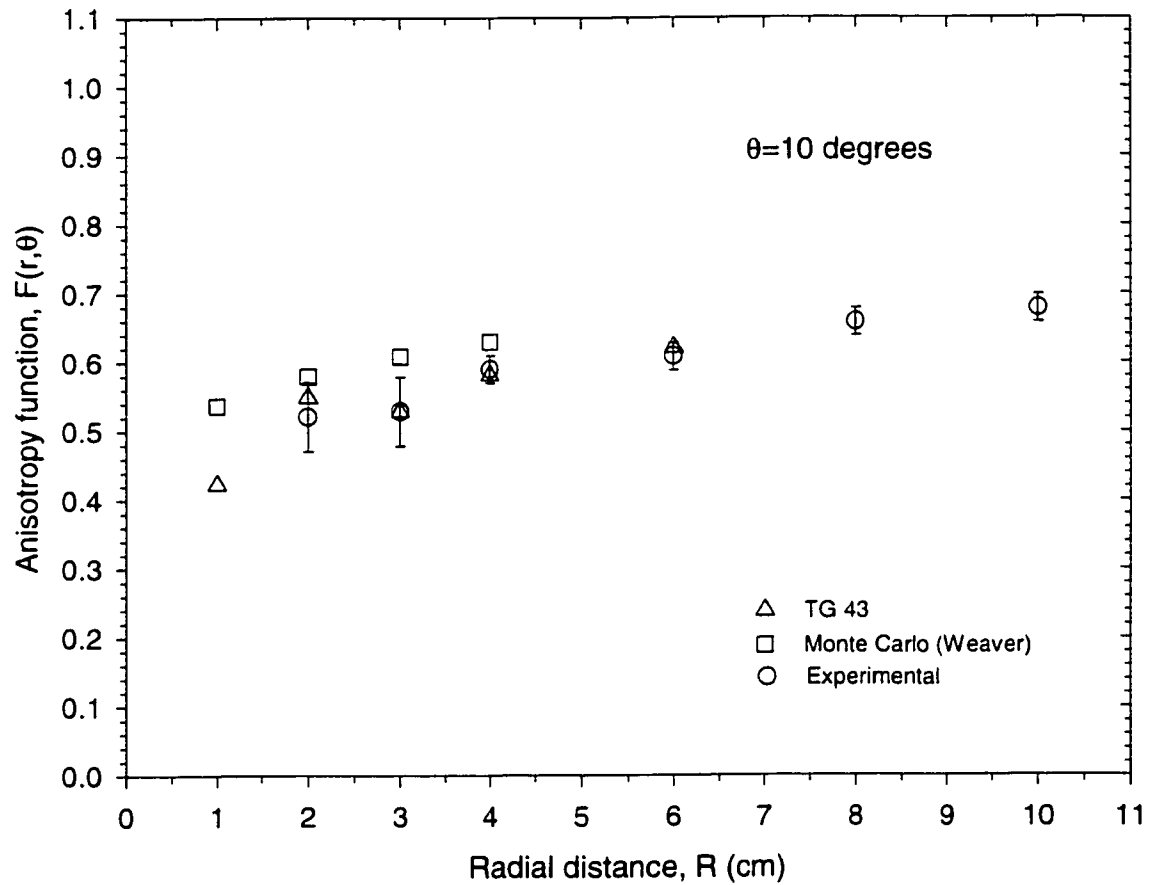


**Figure 4.14:** Plot of the anisotropy function for I-125 model 6711 seed measured at radial distances ranging from 2 cm - 10 cm for a polar angle of  $10^\circ$  using the pre-read anneal technique.

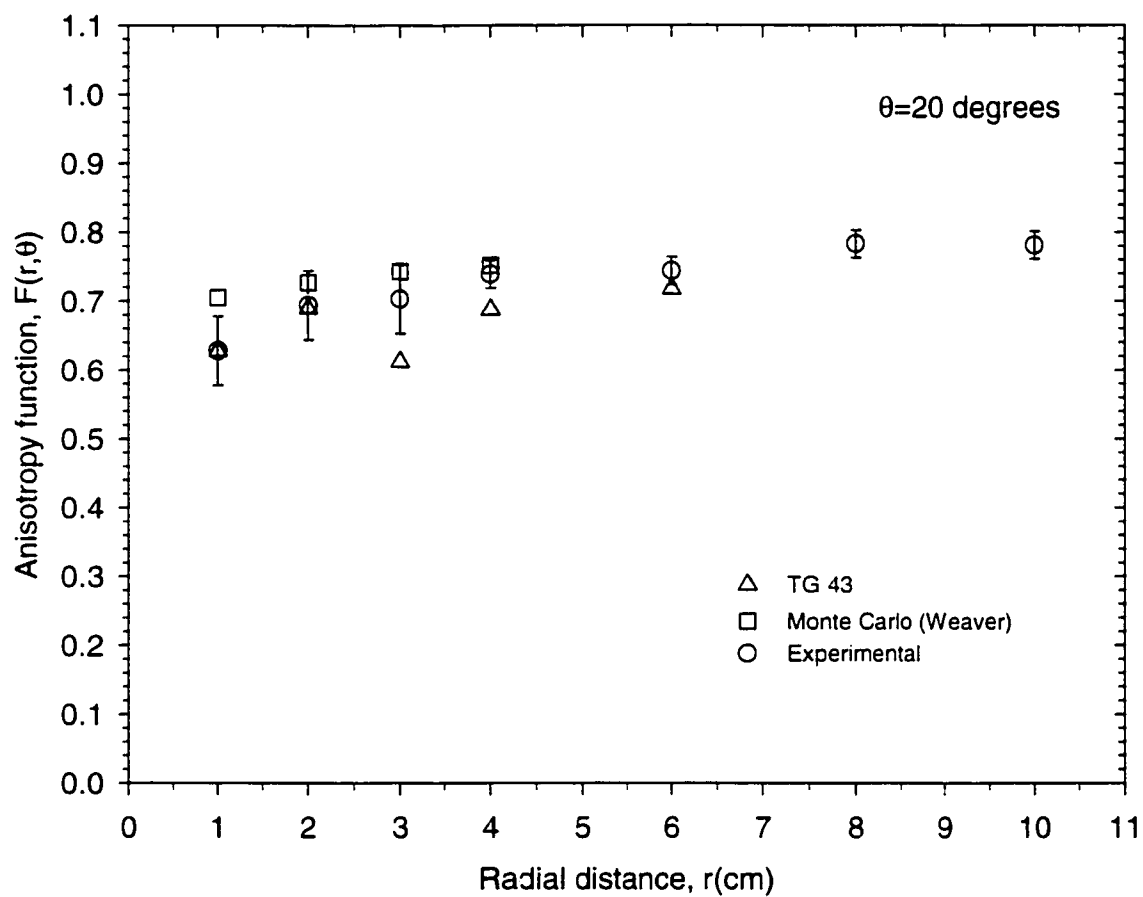


**Figure 4.15:** Plot of the anisotropy function for I-125 model 6711 seed measured at radial distances ranging from 1 cm - 10 cm for a polar angle of  $20^\circ$  using the pre-read anneal technique.

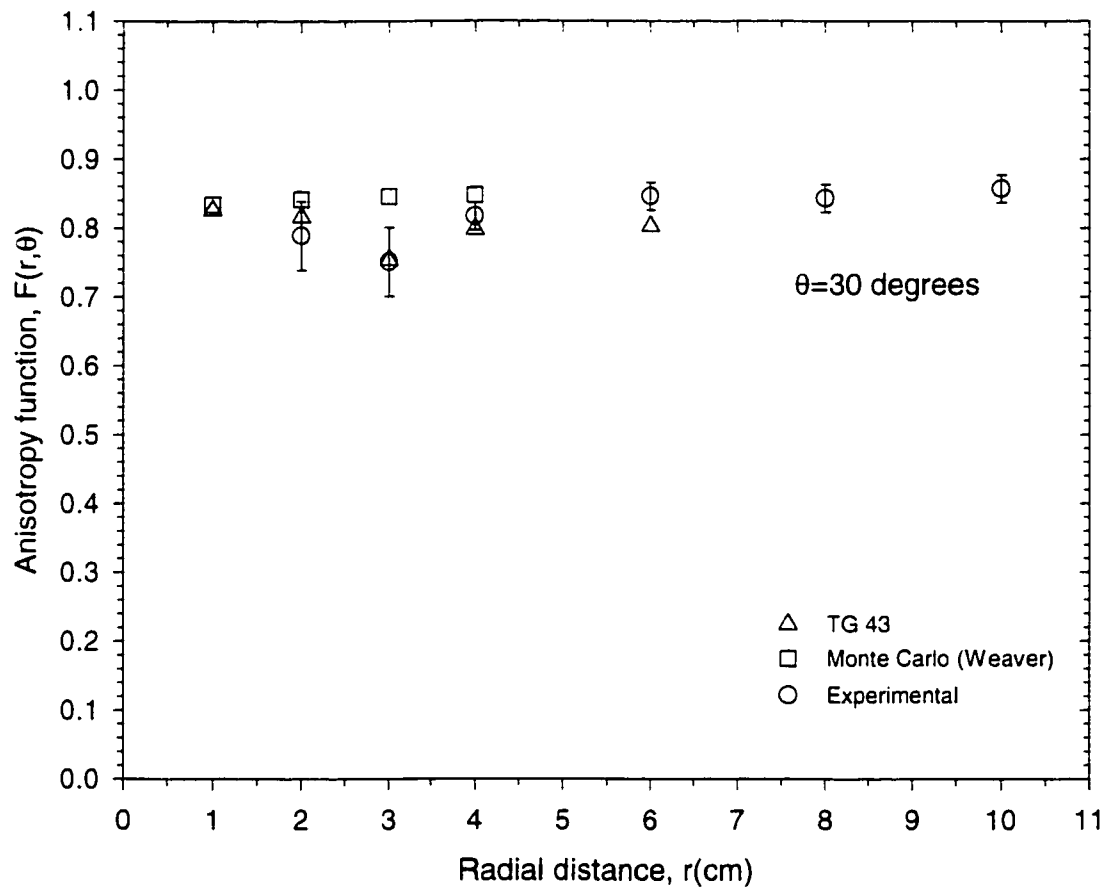


**Figure 4.16:** Plot of the anisotropy function for I-125 model 6711 seed measured at radial distances ranging from 2 cm - 10 cm for a polar angle of  $30^\circ$  using the pre-read anneal technique.

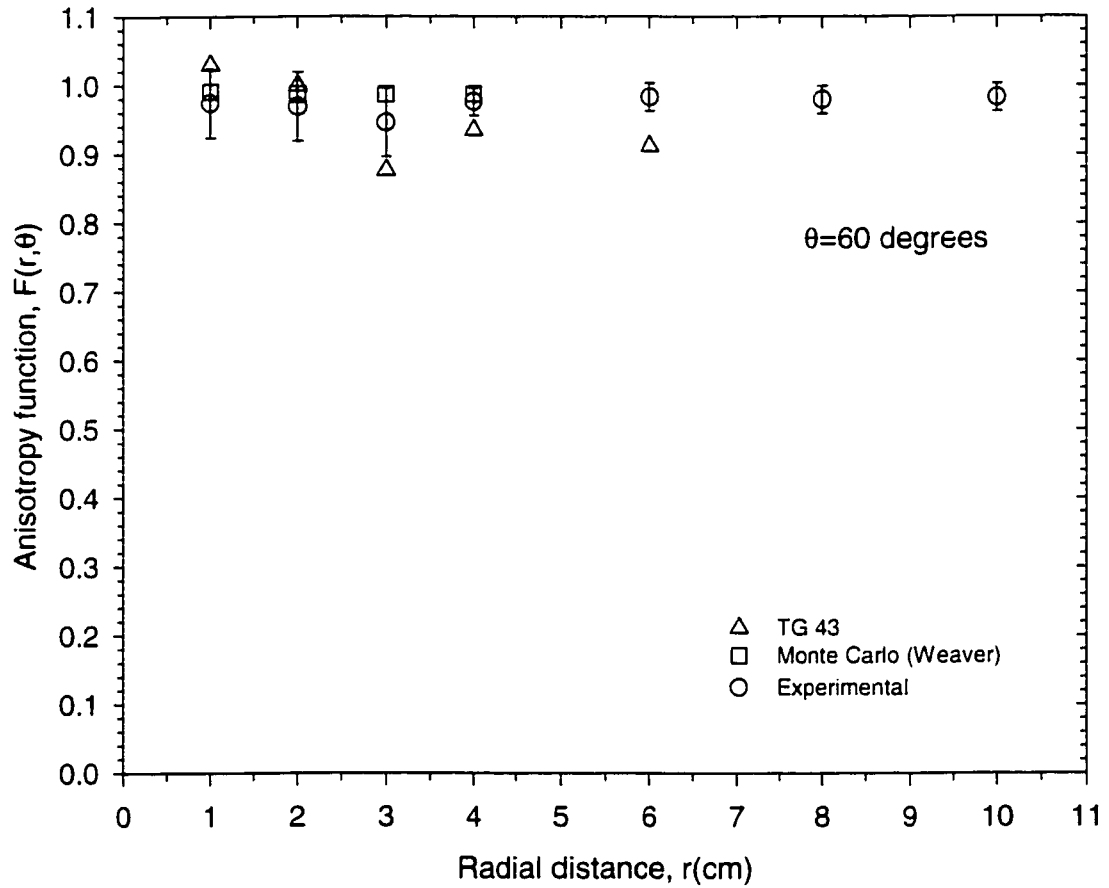


**Figure 4.17:** Plot of the anisotropy function for I-125 model 6711 seed measured at radial distances ranging from 1 cm - 10 cm for a polar angle of  $60^\circ$  using the pre-read anneal technique.



The uncertainties in the anisotropy values for the cubes and chips were estimated to be 0.05 and 0.02 respectively. From Table 4.9 and Figures 4.13 - 4.17, the anisotropy function is seen to increase as the radius increases. This phenomenon is attributed to the fact that at greater distances from the seed, scattering increases and this conceals the angular variation in the dose associated with the differential photon absorption in the source and its titanium capsule. The anisotropy function is also seen to increase with polar angle and approaches unity at  $90^\circ$ . Since this function is a ratio of two dose rates and corresponding geometry factors, some of the systematic experimental errors will cancel out. The trends in the experimental data obtained here are compared with previously published data obtained from the AAPM TG-43 report and Monte Carlo calculations performed by Weaver. The analysis shows a mild discontinuity in the results at the 3 cm distance that is also evident in the AAPM TG-43 data. The reason for this feature is unclear at the present time.

### **4.3.3.2 Glow Curve Deconvolution Technique**

As there was no pre-read anneal conducted for this technique, the low temperature peaks are present in the glow curve obtained during readout (Figure 4.18). The macro program was used to eliminate peaks 1 and 2 and fit the leading edge of peak 3 in the desired range prior to integration. The results are again plotted, as for the pre-read anneal method, in comparison with the AAPM TG 43 data and Monte Carlo estimates by Weaver in Figures 4.19 to 4.23. Though the results appear to be very similar to that by the pre-read anneal method, there are greater variations in the individual data values. The data at the 3 cm distance did not show the discontinuity seen with the previous technique. In this case the uncertainties were 0.07 for the cubes and 0.03 for the chips.



**Figure 4.18:** Glow curve displayed by the Harshaw 5500 TLD reader using the glow curve deconvolution method.

**Table 4.10:** Experimentally obtained values of the anisotropy function  $F(r,\theta)$  for the I-125 model 6711 seed using glow curve deconvolution technique. The estimated uncertainties (1 s.d.) are  $\pm 0.07$  for  $r \leq 3$  cm and  $\pm 0.03$  for  $r > 3$  cm.

$\theta$ (deg) $r$ (cm)	0.0	10.0	20.0	30.0	60.0	90.0
1.0	0.29	-	0.55	-	0.93	1.00
2.0	0.44	0.53	0.65	0.72	0.94	1.00
3.0	0.44	0.54	0.67	0.82	0.97	1.00
4.0	0.45	0.53	0.67	0.78	0.93	1.00
6.0	0.52	0.57	0.69	0.78	0.93	1.00
8.0	0.55	0.60	0.71	0.80	0.98	1.00
10.0	0.54	0.64	0.73	0.82	0.95	1.00

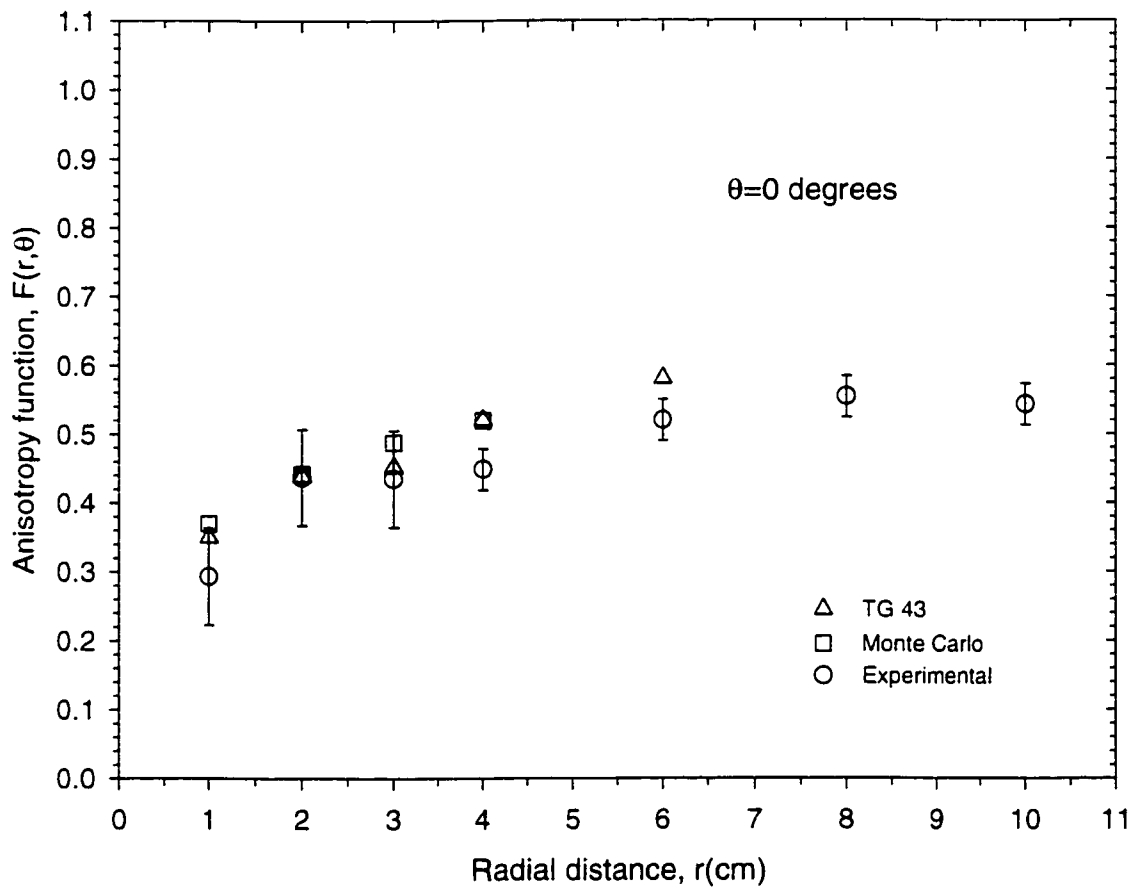


**Figure 4.19:** Plot of the anisotropy function for I-125 model 6711 seed measured at radial distances ranging from 1 cm - 10 cm for a polar angle of  $0^\circ$  using the glow curve deconvolution technique.

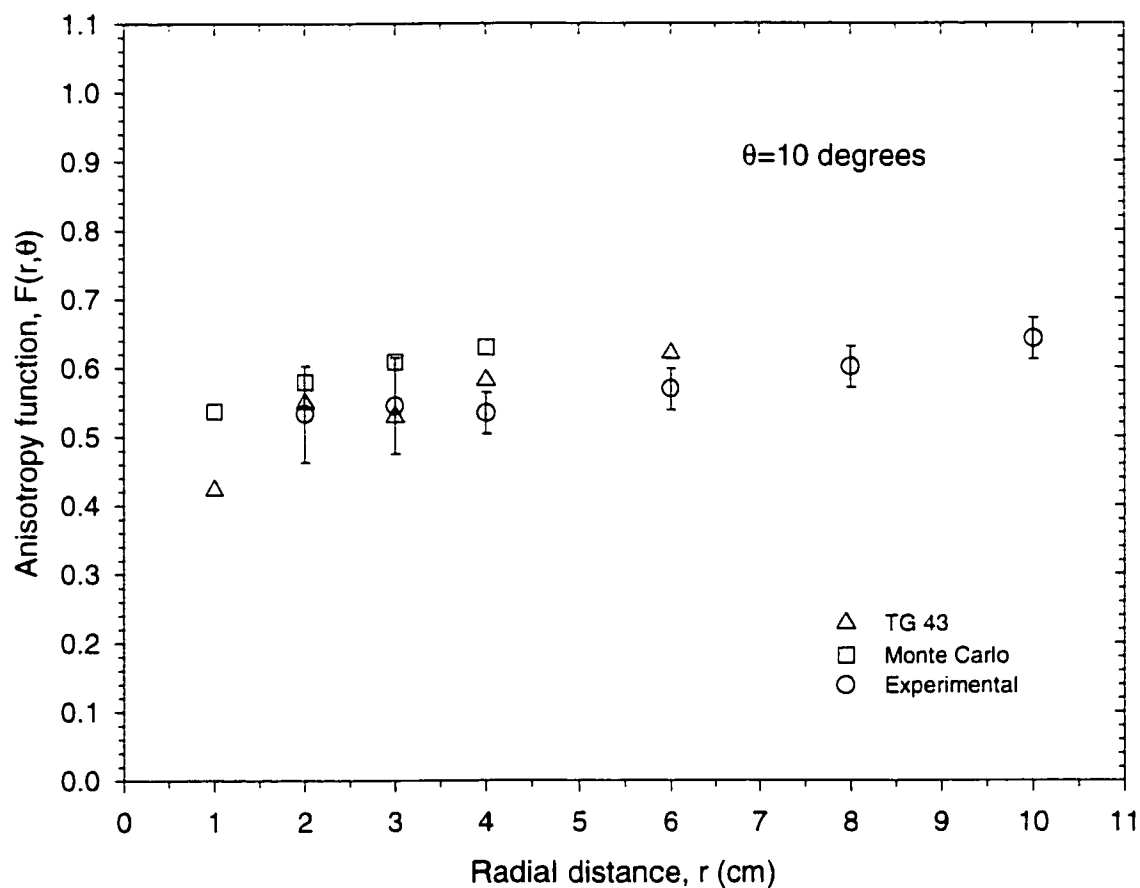


**Figure 4.20:** Plot of the anisotropy function for I-125 model 6711 seed measured at radial distances ranging from 2 cm - 10 cm for a polar angle of  $10^\circ$  using the glow curve deconvolution technique.

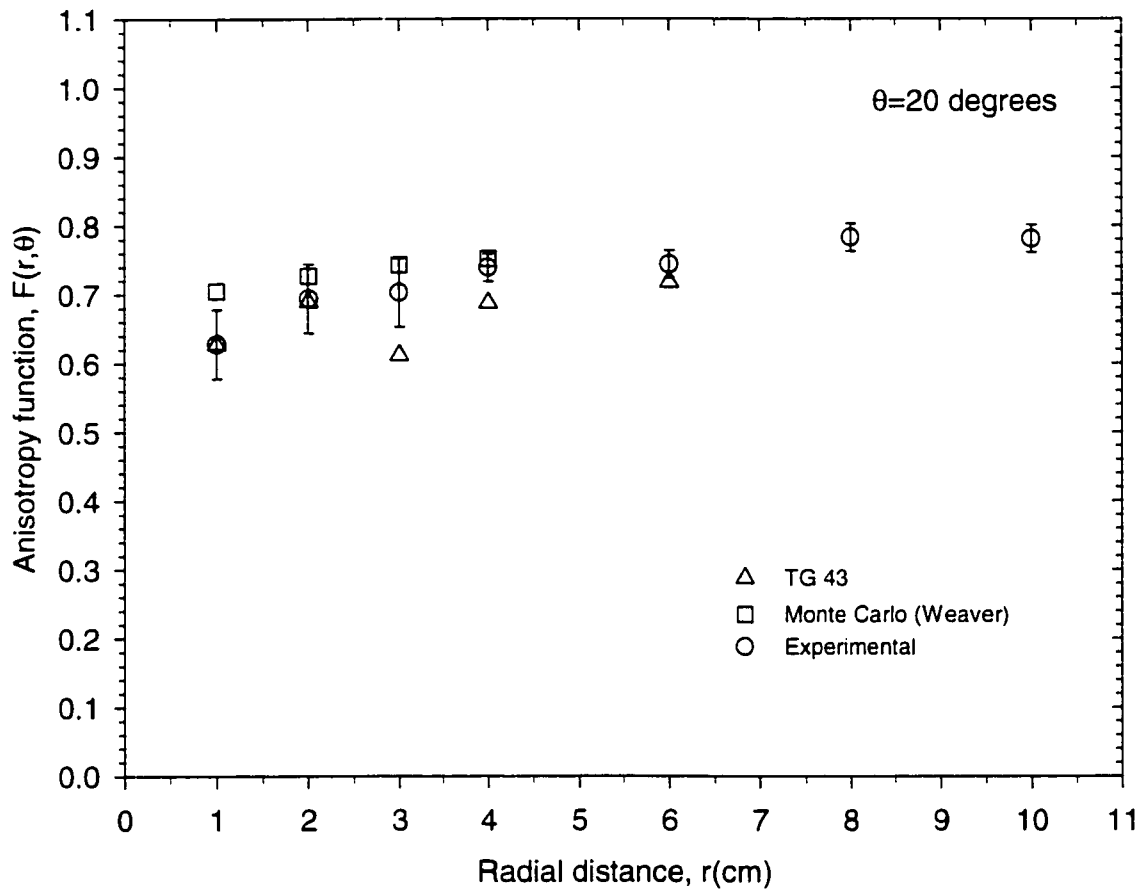


**Figure 4.21:** Plot of the anisotropy function for I-125 model 6711 seed measured at radial distances ranging from 1 cm - 10 cm for a polar angle of  $20^\circ$  using the glow curve deconvolution technique.

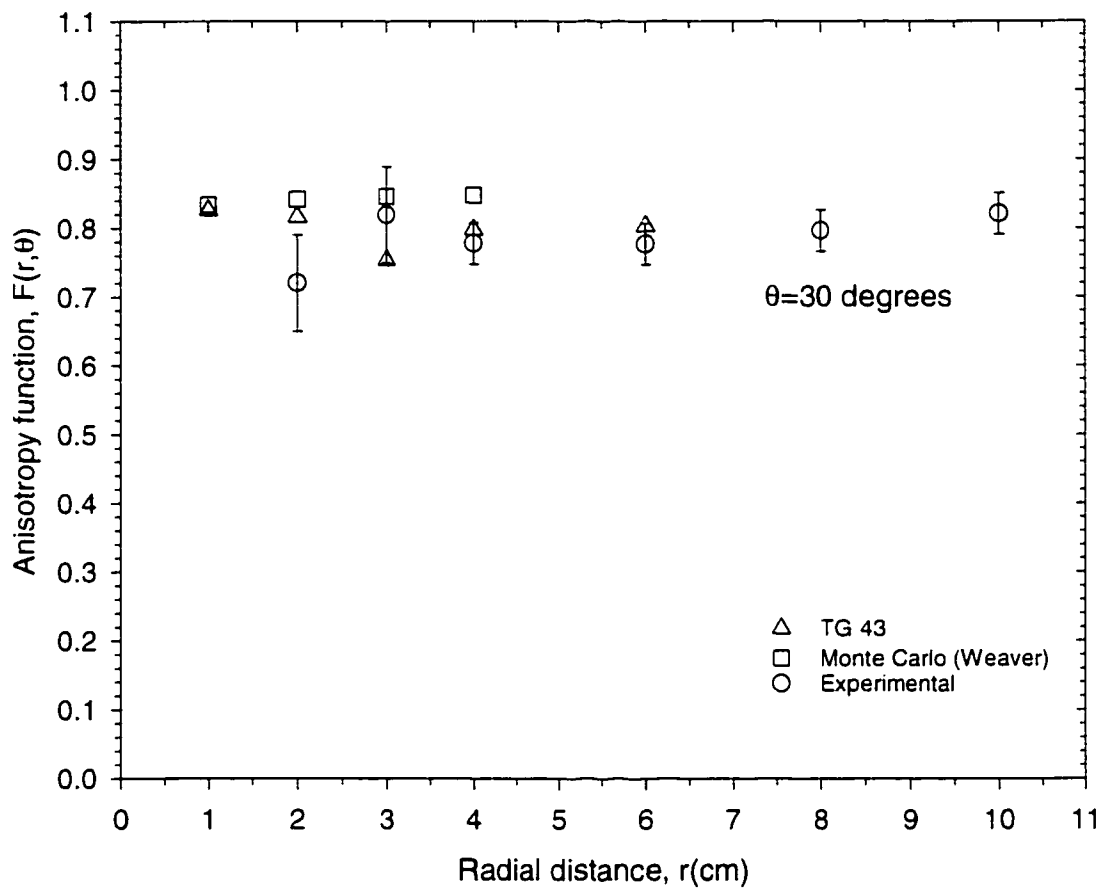


**Figure 4.22:** Plot of the anisotropy function for I-125 model 6711 seed measured at radial distances ranging from 2 cm - 10 cm for a polar angle of  $30^\circ$  using the glow curve deconvolution technique.

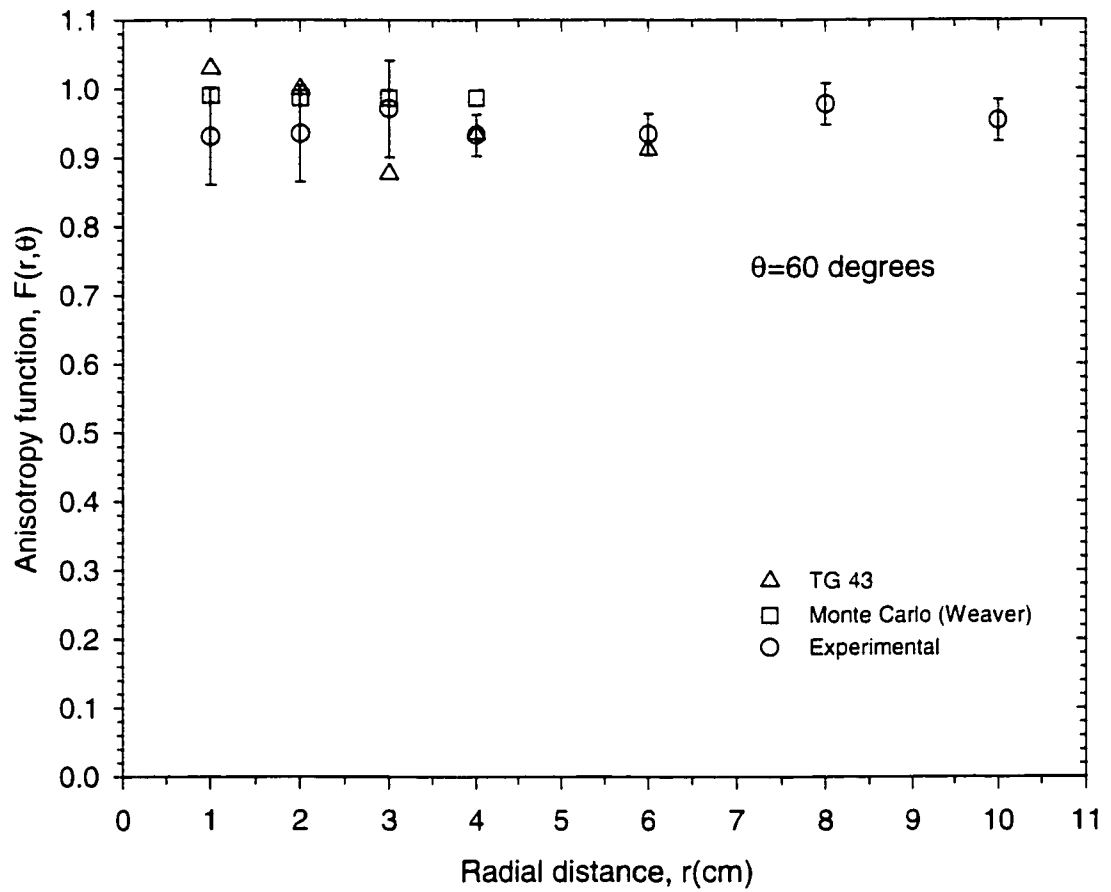


**Figure 4.23:** Plot of the anisotropy function for I-125 model 6711 seed measured at radial distances ranging from 1 cm - 10 cm for a polar angle of  $60^\circ$  using the glow curve deconvolution technique.



## References

1. Nath R., Anderson L.L., Luxton G., Weaver K.A., Williamson J.F., Meigooni A.S., Dosimetry of interstitial brachytherapy sources: Recommendations of AAPM Radiation Therapy Committee Task Group No. 43, *Medical Physics*, 22(2), 209-234 (1995)
2. Niroomand-Rad A., Blackwell C.R., Coursey B.M., Gall K.P., Galvin J.M., McLaughlin W.L., Meigooni A.S., Nath R., James E.R., Soares C.G., Radiochromic film dosimetry: Recommendations of AAPM Radiation Therapy Committee Task Group 55, *Medical Physics*, 25(1), 2093-2115 (1998)
3. Weaver K., Anisotropy functions for I-125 and Pd-103 sources, *Medical Physics*, 25(12), 2271-2278 (1998)
4. Williams J.R., Thwaites D.I., "Radiotherapy Physics in Practice", Oxford Medical Publications, (1993)

## **CHAPTER 5**

### **5 SUMMARY**

In brachytherapy, measuring the dose rate around the source is important to ensure safe and effective patient treatment. A number of experiments were conducted in the course of this work to verify the dosimetry of two types of brachytherapy sources - Sr-90 ophthalmic applicators and the model 6711 I-125 seed.

When a new ophthalmic applicator is purchased, the old applicators have to be re-calibrated to assess their relative outputs. This is done to ensure that the patient dosimetry will be consistent, regardless of which applicator is selected for treatment. Of the four applicators at the Cross Cancer Institute, three are about twenty eight years old and one, the SIA 20, is new. Radiochromic film was used for these measurements and was read using a document scanner. The validity of radiochromic film in this application was evaluated by investigating its reproducibility and uniformity. It was found that GaFChromic film varied only 2% from an initial scan when scanned daily for a period of two weeks. The spatial variation in reading at different locations on the scanner bed was found to be less than 1%.

The GaFChromic film was calibrated in the horizontal (face-on) and vertical (edge-on) planes. It was seen in both cases that a bi-linear log-log dose response provided a good description of the measured data as suggested in the work of TG 55 [Nirroomand-Rad, 1998]. The reasons for the differences in the horizontal and vertical calibration curves (Figures 4.3 and 4.8) are not known at the present time. A significant deviation from linearity after a dose of 50 Gy was seen in the case of horizontal irradiation.

For horizontal irradiation, the dose to optical density relation in the 10-20 Gy range was found to be

$$D = \left[ 25 \log_{10} \left( \frac{I_0}{I} \right) \right]^{1.15}, \quad (5.1)$$

and in the dose range between 20-50 Gy the relation was

$$D = \left[ 8.33 \log_{10} \left( \frac{I_0}{I} \right) \right]^{2.04}. \quad (5.2)$$

The error in this representation was less than 2%. Similarly in the case of the vertical calibration, non-linearity was seen to set in beyond a dose of 45 Gy. The dose to optical density relation in the 10-20 Gy range was

$$D = \left[ 25 \log_{10} \left( \frac{I_0}{I} \right) \right]^{1.54}, \quad (5.3)$$

and for the range from 20-45 it was

$$D = \left[ 31.25 \log_{10} \left( \frac{I_0}{I} \right) \right]^{1.3}. \quad (5.4)$$

Depth dose plots for the SIA 20 applicator were made by the two different modes of irradiation -vertical and horizontal. Both curves were found to be consistent with the manufacturer's data. These results confirm the applicability of a document scanner as a reader for GafChromic film.

The relative outputs of the four ophthalmic applicators when studied with the radiochromic films were seen to show variations of up to 6%. These differences are not statistically significant, and are well within the uncertainty of  $\pm 20\%$  (3 s.d.) assigned by the manufacturer to their calibration.

When the same relative exposures were measured using thermoluminescent dosimeters, the experimental and manufacturer's relative dose rates showed differences up to 9%, however these were not statistically significant. The credibility of using radiochromic film for measuring the relative output of ophthalmic applicators and the document scanner as a film reader has hence been further verified by this study.

The photon emission distribution from the model 6711 I-125 seed is significantly anisotropic leading to uncertainties in clinical dosimetry. The recommended dosimetric data available are those from a single laboratory [Nath *et al.*, 1995]. In preparing TLDs (chips and cubes) for the anisotropy measurements, they underwent a primary sensitization routine. Separate dose response curves were created for these detectors from which a supralinearity correction was determined as:

$$C_{\text{supralin}} = [1 + 0.0156 D - 0.000068 D^2]^{-1} \quad \text{[FOR CHIPS]} \quad (5.3)$$

$$C_{\text{supralin}} = [1 + 0.0324 D - 0.000526 D^2]^{-1} \quad \text{[FOR CUBES]} \quad (5.4)$$

The anisotropy function for the model 6711 seed was determined using the pre-read anneal and the glow curve deconvolution methods. Figures 5.1 and 5.2 represent the corresponding polar plots for selected distances of 2, 3, and 4 cm, along with previously published data. Our experimental results are seen to vary somewhat from the values recommended by TG-43, which were obtained using an older TLD reader having less precision than the Harshaw 5500, but are not significantly different in a statistical sense.

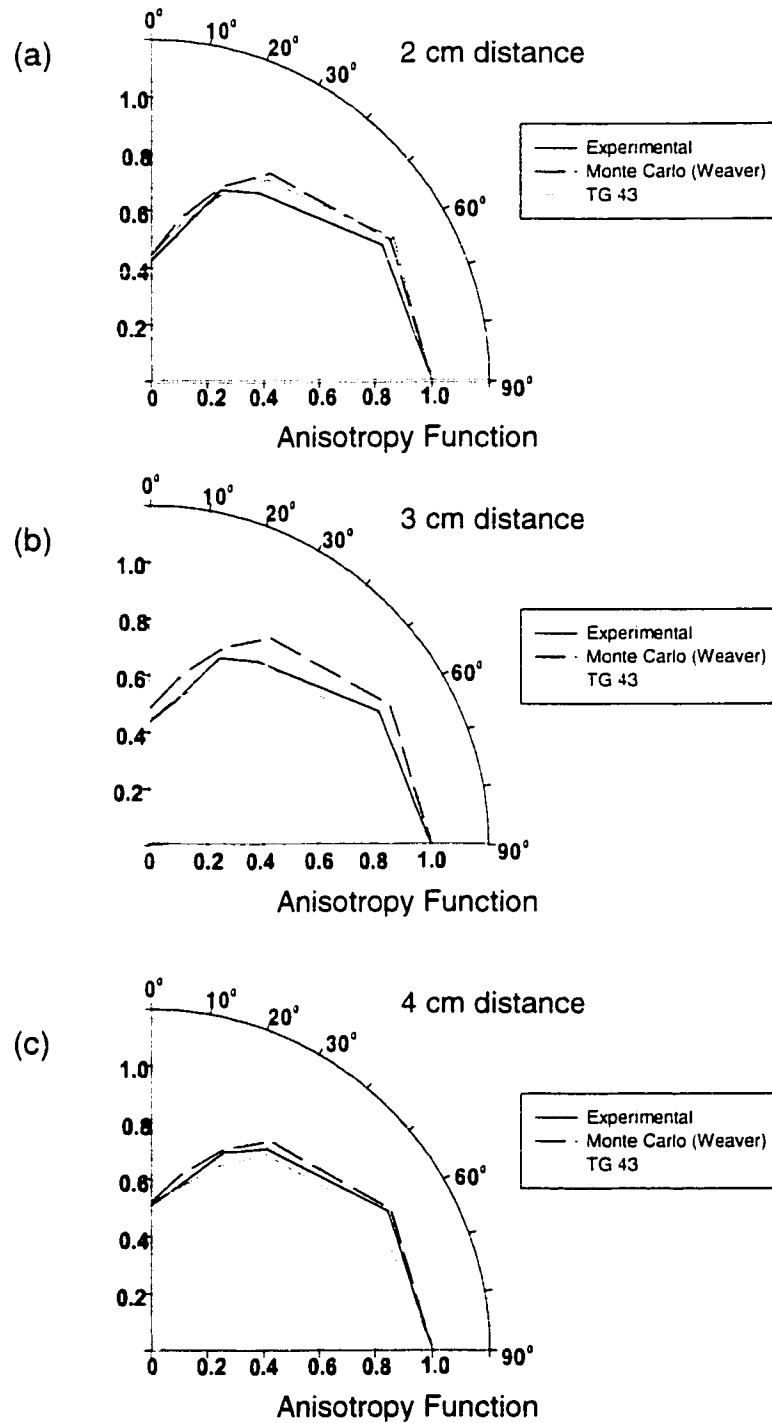


**Figure 5.1:** Polar plots of the anisotropy function using the pre-read anneal technique for an I-125 model 6711 seed for distances of (a) 2 cm, (b) 3 cm, (c) 4 cm. Data obtained experimentally are shown along with Monte Carlo calculations [Weaver, 1998] and TG 43 measurements [Nath *et al.*, 1995].

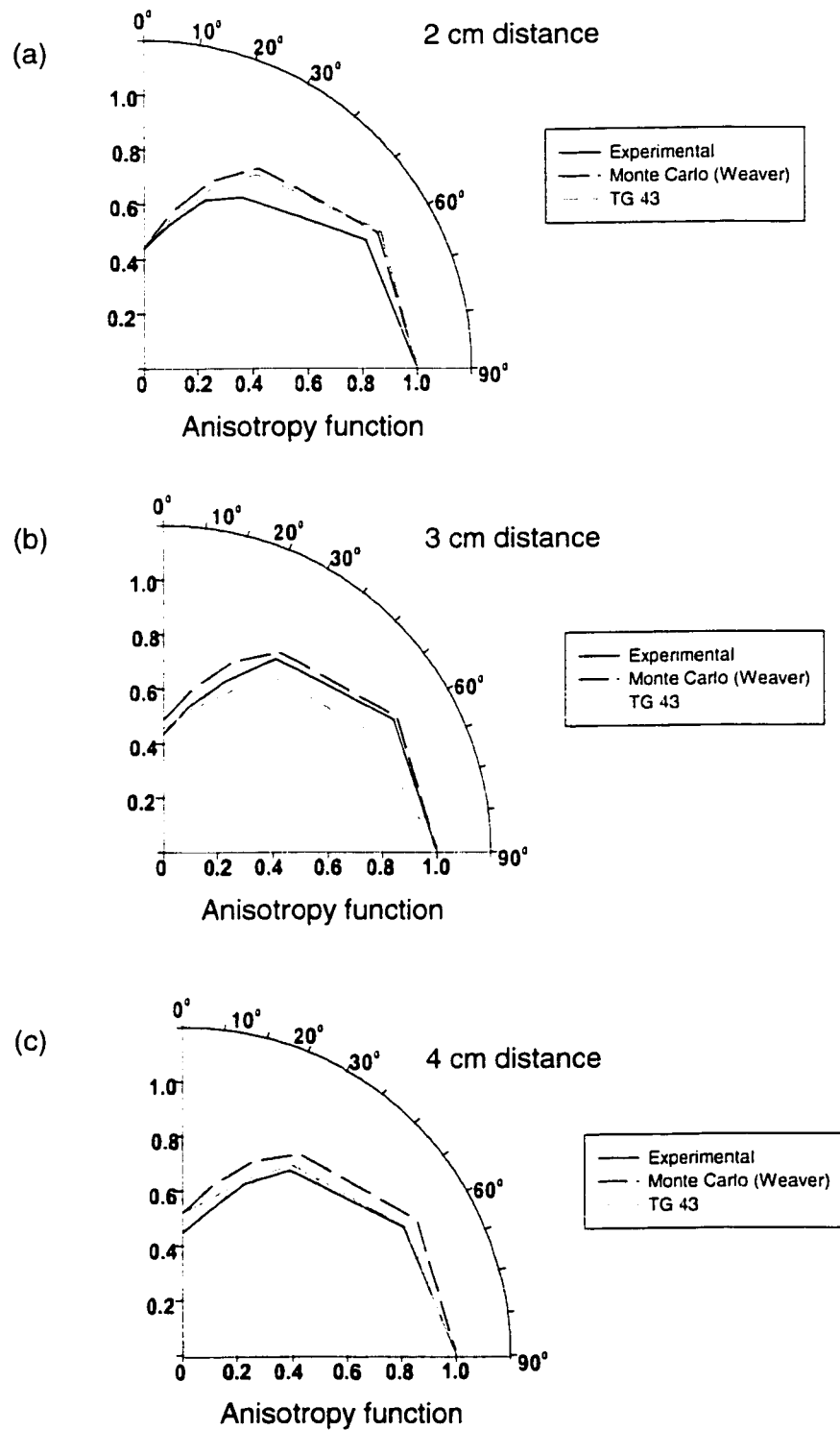


**Figure 5.2:** Polar plots of the anisotropy function using the glow curve deconvolution technique for an I-125 model 6711 seed for distances of, (a) 2 cm, (b) 3 cm, (c) 4 cm. Data obtained experimentally are shown along with Monte Carlo calculations [Weaver, 1998] and TG 43 measurements [Nath *et al.*, 1995].

In conclusion, the accuracy of the manufacturer's relative output values for four Sr-90 ophthalmic applicators manufactured over a span of twenty eight years has been verified, and published values of the anisotropy function for the model 6711 I-125 seed have been confirmed. As regards the applicators, the observed consistency in output calibration implies that a new applicator, the SIA 20, can be placed into clinical service without modifying the historical treatment protocol that has been used for the others. As regards the I-125 seed, confirmation of the published anisotropy function values means that pre- and post- implant dosimetry for treatments based upon these sources, which includes permanent prostate implants, does not require revision.

## References

1. Nath R., Anderson L.L., Luxton G., Weaver K.A., Williamson J.F., Meigooni A.S., Dosimetry of interstitial brachytherapy sources: Recommendations of AAPM Radiation Therapy Committee Task Group No. 43, *Medical Physics*, 22(2), 209-234 (1995)
2. Niroomand-Rad A., Blackwell C.R., Coursey B.M., Gall K.P., Galvin J.M., McLaughlin W.L., Meigooni A.S., Nath R., James E.R., Soares C.G., Radiochromic film dosimetry: Recommendations of AAPM Radiation Therapy Committee Task Group 55, *Medical Physics*, 25(1), 2093-2115 (1998)
3. Weaver K., Anisotropy functions for I-125 and Pd-103 sources, *Medical Physics*, 25(12), 2271-2278 (1998)